A Study of Different Modeling Approaches for Model-Based Building Thermal Control

Ali Saberi Derakhtenjani

A Thesis

In the Department

of

Building, Civil and Environmental Engineering

Presented in Partial Fulfillment of the Requirements

for the Degree of Master of Applied Science (Building Engineering) at

Concordia University

Montreal, Québec, Canada

September 2014

CONCORDIA UNIVERSITY
School of Graduate Studies

This is to certify that the thesis prepared

By: Ali Saberi Derakhtenjani

Entitled: A study of different modeling approaches for model-based building thermal control

and submitted in partial fulfillment of the requirements for the degree of

Master of Applied Science (Building Engineering)

complies with the regulations of the University and meets the accepted standards with respect to originality and quality.

Signed by the final examining committee:

Dr. L. Wang Chair

Dr. G. Vatistas (External) Examiner

Dr. R. Zmeureanu Examiner

Dr. A. Athienitis Supervisor

Approved by _____
Chair of Department or Graduate Program Director

_____
Dean of Faculty

Date _____

ABSTRACT

A study of different modeling approaches for model-based building thermal control

Ali Saberi Derakhtenjani

This thesis presents an assessment of different modeling methodologies for developing dynamic thermal models for buildings and discusses the benefits of each for model-based thermal control in buildings. The modeling section consists of two main parts: (1) the development of a detailed dynamic thermal model by means of frequency domain techniques and transfer functions (2) the development of low-order, grey-box, RC (resistance-capacitance) thermal network models with parameter optimization. The models are verified with experimental data from the Environmental Chamber (EC) test facility at Concordia University. Environmental Chamber is an experimental facility that is designed to test and calibrate building dynamic thermal models and technologies. The advantages of each of the modeling approaches for understanding the thermal behavior of the Environmental Chamber are discussed.

A detailed frequency domain model is developed from the application of first-principle heat transfer equations to study the thermal characteristics of the system. A detailed lumped parameter finite difference model (LPFD) is used as a tool to calculate required data for the frequency domain model that was not available through experiment. LPFD model also provides significant insight into the actual behavior of the chamber under transient conditions.

Then, the creation of low-order, grey-box, RC circuit model for the Environmental Chamber is explained, as well as a methodology for optimizing the circuit parameters to find the "effective" resistances and capacitances for a defined objective which is the fit between measured and simulated air temperature. The challenges encountered while using experimental data to perform optimization for the low-order RC circuits are discussed. Such low-order models that capture the important physics of the problem are best suited to real time MPC in building automation systems in which they can be actually implemented.

Finally, an analytical frequency domain model is developed for a thermal zone in an experimental facility (one of Hydro-Québec's Twin Houses in Shawinigan). The effect of different floor coverings on the thermal response of the zone is investigated by means of the frequency domain model. Also, using the frequency domain model, the effect of increasing the thermal mass and thermal conductivity of the materials used in the zone on the thermal response of the zone is investigated. The importance of studying the magnitude of the zone transfer function for effective thermal storage in the zone in an important certain frequency range is demonstrated. The key advantage of frequency domain modeling for evaluating design options without any need to perform simulation is presented.

ACKNOWLEDGEMENTS

I would like to express my gratitude to my supervisor, Dr. Andreas K. Athienitis, for his expert guidance and support for my research and providing the opportunity for me to pursue my Master's studies in the Solar Laboratory at Concordia University. I have always appreciated his enthusiasm for this interesting research field and this is a great motivation for me.

I am especially thankful to my co-advisors, Dr. José A. Candanedo and Dr. Vahid R. Dehkordi, at Natural Resources Canada, CanmetENERGY, for providing the opportunity for me to work with them in such interesting research field and for their eager support in all parts of the project. I would like to thank Dr. Candanedo for giving me invaluable guidance, advice and comments on my work, on the quality of presentation and writing. I always appreciate things I learned from him not only in research but also in languages, art, and life. I would like to thank Dr. Dehkordi for his expert guidance in using MATLAB in my project and topics related to control engineering.

I want to thank my colleagues in Solar Laboratory at Concordia University for their help in my work and their friendship, including Costa Kapsis, Sam Yip, Edvinas Bigaila, Dr. Yuxiang Chen, Tingting Yang and especially Jennifer Date for carefully proof-reading my thesis.

I would like to thank Dr. Jiwu Rao for his help on the experimental part of my work and his valuable comments on the results. Also, I want to thank Josef Ayoub, Gerald Parnis and Lyne Dee for their administrative assistance.

I would like to thank all the staff in building research group at CanmetENERGY-Varennes, especially Dr. Sophie Hosatte, Dr. Jacques Martel, Justin Tamasauskas and Sylvie Lavoie.

I would like to thank all the staff in building research group at Hydro-Québec LTE Shawinigan, including Éric Dumont, Ahmed Daoud, Jonathan Bouchard and Karine Lavigne.

I would like to thank some of my best friends in Montreal with whom I shared valuable moments and experiences, including Ali Karimli, Costa Kapsis, Andreea Mihai, Mathieu Le Cam, Dimitris Ladas, Anthony Rey, Nicholas Zibin and Eric McDonald.

My special thanks go to my dear cousin, Dr. Yassamin Khosravisaeid, for her constant moral support, her care and her encouragements.

And finally I would like to thank my family, my mom, Nooshin Amirpoorsaid, my dad, Mohammadjavad Saberi Derakhtenjani and my sister, Rana Saberi Derakhtenjani for their love and continuous moral and financial support. I would like to dedicate this work to them.

I would like to acknowledge the financial support though NSERC/ Hydro-Québec industrial research Chair held by Dr. Athienitis and Graduate Student Support Program (GSSP) from the faculty of Engineering and Computer Science of Concordia University. Also, in-kind support from CanmetENERGY-Varennes, a partner in the Chair, is acknowledged with thanks.

TABLE OF CONTENTS

LIST OF FIGURES

LIST OF TABLES

NOMENCLATURE

Symbols

A_i	Area of surface represented by node i (m^2)
C_i	Thermal capacitance of node i (J/K)
C_a	Thermal capacitance of air (J/K)
e_i	Error between setpoint and air temperature at time step i (ºC)
E	Error function presented in complex curve fitting
$F(i,j)$	View factor between surfaces i and j
$F_{i,j}^*$	Radiant exchange factor between surfaces i and j
j	Node j, or the imaginary unit, $j=\sqrt{-1}$
J	Objective function used for optimization
k	Thermal conductivity of materials (W/m.k)
l_i	Thickness of surface i (m)
n	Harmonics
NTS	Total number of time steps in the discrete Fourier transform
p	Period of time (seconds)
Q_{eq}	Equivalent source (W)
$\mathbf{Q}$	Source vector
Q_{aux}	Auxiliary(heating/cooling) source (W)
Q_i	Source entering node i (W)

Q_{sg}	Solar gains (W)
$R_{i,j}$	Thermal resistance between nodes i and j (K/W)
S	Laplace variable
t	Time
$\mathbf{T}$	Temperature vector (ºC)
$T_{setpoint}$	Air setpoint temperature (ºC)
T_i	Temperature of node i (ºC)
T_o	Outdoor temperature (ºC)
U_{inf}	Infiltration U-value (W/K)
U_{win}	Window U-value (W/m^{2}K)
$\mathbf{u}$	Input vector
$U_{i,j}$	Thermal radiation U-value between surface i and j (W/K)
$\mathbf{x}$	State vector
$\mathbf{y}$	Output vector
$\mathbf{Y}$	Admittance matrix
$Y_{self,i}$	Self-admittance for surface i
$Y_{transfer,i}$	Transfer-admittance for node i
$\mathbf{Z}$	Impedance matrix
$Z_{i,j}$	Transfer function between nodes temperature of i and source entering node j
Z_f	Fitted transfer function

Greek Letters

α_i	Thermal diffusivity of surface equal to $\sqrt{k / \rho c_p}$
γ	$\sqrt{s / \alpha}$
ω	angular frequency
σ	Stefan-Boltzman constant equal to $\approx 5.67\times10^{-8}$ W/m^{2}K^4
ε	Emissivity
Δt	Time step
$\Delta\theta(t)$	temperature rise at time t (ºC)
$\Delta\theta_{total}$	Total temperature rise (ºC)
κ	Curvature of exponential curves
ρ	(1) Density (Kg/m^3), (2) reflectivity

1 INTRODUCTION

1.1 Background and Motivation

Buildings consume 53% of the electricity produced in Canada. In Quebec, 94% of generated electricity comes from hydroelectric plants. Due to its cold winter weather, Quebec has a high heating demand. In January 2013 there was a peak demand of 39.1 GW reported by Hydro-Québec (Hydro-Québec 2013). Finding ways to reduce the peak demand and energy consumption of buildings, and consideration of energy efficiency measures in buildings is a necessity.

There has been a transformation in commercial and institutional buildings design from smaller window area (1950s) to air-conditioned, "glass towers" with large windows (Athienitis and O'Brien 2014). This evolution was mainly due to the development of the sealed double-glazed windows with high level of insulation or use of special coatings to reduce heat transfer through the windows and optimized transmission of solar radiation. Larger window area means more daylight, but also, higher cooling and heating demands. Thus, more efficient building envelopes and passive solar techniques must be employed (Athienitis and O'Brien 2014).

Considering the potential of incident solar radiation on building surfaces to provide the energy demand of buildings, the concept of net-zero energy buildings was introduced. According to the definition by Athienitis and O'Brien (2014), the net-zero energy building (NZEB) is a building that produces as much as energy as it consumes in an average year. This idea has been widely accepted as a feasible, long-term goal (Marszal et al. 2011).

Majority of the solar radiation can be transformed to useful heat to be used in different parts of the building such as domestic hot water (DHW) or cloth dryers (Gordon 2001) . Also there has been a sharp drop in the price of solar photovoltaics (PV) that converts solar radiation into electricity (90% cost-reduction per watt generating capacity in the last 10 years) (Athienitis and O'Brien 2014).

The main motivation of the present thesis is to evaluate the benefits of different modeling approaches for understanding building thermal behavior of buildings and energy management in buildings. There is a need for rapid feedback on cost and performance of alternative design approaches in buildings and building simulation has emerged as a practical method to evaluate the options in terms of relevant design issues. Building simulation models allow us to make a quick and inexpensive evaluation of the building performance under different circumstances. Also, the effect of employing different control strategies on building performance can be investigated by using energy models developed for the buildings. For example by taking advantage of frequency domain techniques, different variables are studied under a range of dominant harmonics and thus, it is important to develop reduced order thermal networks that accurately predicts building transient dynamic response in these important frequency ranges. Also low-order models are well-suited for the application of model predictive control (MPC) strategies in which models can be actually implemented into the building automation system.

The main case study here is Environmental Chamber (EC) which is introduced in the next section.

1.2 Solar Simulator Environmental Chamber

The following text is based on the description provided by the manufacturer of the test facility (PSE 2009). The Solar Simulator-Environmental Chamber (SSEC) laboratory is an experimental facility located at Concordia University in downtown Montreal, Canada. This facility allows accurate and repeatable testing of solar systems and advanced building envelopes under standard test conditions with well-simulated solar radiation and indoor and outdoor conditions. It consists of two major systems:

1. A large scale solar simulator (Figure 1.1) designed to emulate solar radiation to test solar systems such as PV and PV/T modules, solar air collectors, solar water collectors and building-integrated solar systems. It consists of eight metal halide lamps with an artificial sky to remove infrared radiation from lamps. The solar simulator meets the standards EN 12975:2006 and ISO 9806-1:1994. The test specimen size can be up to 2.4 m × 3.2 m.

2. A two-storey environmental chamber with a mobile solar simulator (Figure 1.1).This component, which is the main focus of this thesis, is used to test building technologies under controlled environmental conditions, by simulating exterior, interior climates (from arctic to desert). Here is a list of some of its specifications and capabilities:

- Testing building envelope components, such as advanced wall systems that may include solar energy utilization components, under a range of conditions from arctic to desert.

- Developing test methods and design standards for predictable, relative hygrothermal performance and durability of different building envelope systems under various climatic conditions.
- Testing wall systems and rooms up to 7m high, for hygrothermal and energy performance, including solar electricity and useful heat generation.
- Thermal control studies to improve building operation and reduce peak demand such as model predictive control.
- Temperature test range: -40°C to 50°C.

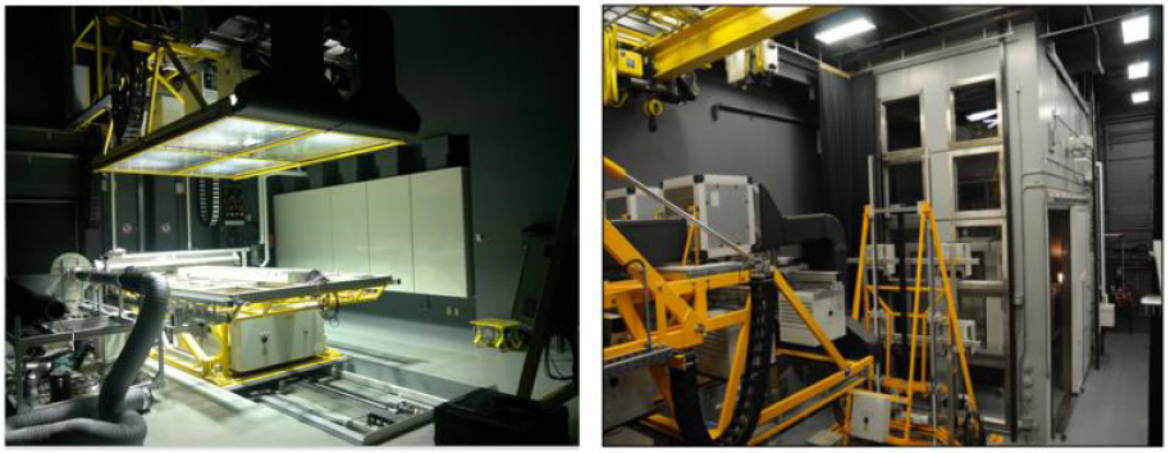

Figure 1.1. Solar Simulator (left), Environmental Chamber (right)

Figure 1.2 shows a schematic for the environmental chamber with a test room inside and mobile solar simulator:

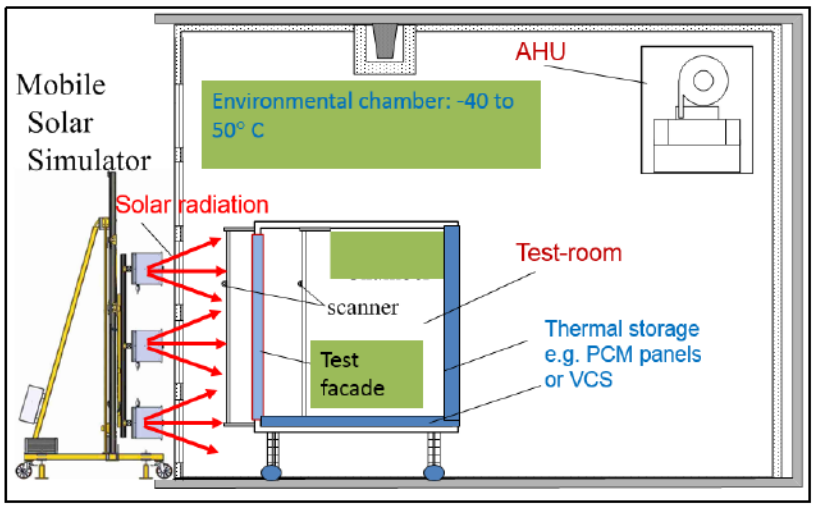

Figure 1.2. Schematic of the Environmental Chamber with mobile solar simulator

1.3 Objectives

The main objectives of this thesis are:

1. To develop and compare control-oriented models for buildings that are particularly frequency domain models of appropriate resolution and low-order grey-box RC network models.

2. Apply the models to two case studies: Environmental Chamber and EHBE (Experimentation Houses for Building Energetics) experimental test facilities.

3. To study the benefits of each model for the application of control strategies in buildings.

1.4 Scope and Outline of the Thesis

This thesis covers theoretical background for each of the modeling approaches, discusses on the advantages and disadvantages of each modeling approach and their application to case studies. Also discussed are the benefits of each model for the purpose of building control and finally, an application of low-order RC model for a temperature setpoint study is presented.

This thesis does not cover designing control strategies or model predictive control (MPC) studies. However, design of control strategies is stated and emphasized as a future extension of this research. The knowledge developed in this thesis is expected to be useful for MPC studies.

The following list summarizes the content of each chapter in this thesis:

- Chapter 1: *Introduction*. Presents the motivation and objectives of the work done and presented as well as the thesis outline. Describes the Solar Simulator Environmental Chamber Laboratory at Concordia University. Environmental Chamber is the main case study in this thesis.

- Chapter 2: *Literature review*. Presents a review of related literature and previous works in the field of energy modeling and model-based control for buildings.

- Chapter 3: *Theoretical background*. Presents theoretical background behind the frequency domain model and the time domain models (finite-difference model

and low-order RC circuit model). Describes the mathematical structures of each of the two modeling approaches and shows the path for creating each model.

- Chapter 4: *Case Studies*. (1) Presents the application of methodologies presented in chapter 3 for the Environmental Chamber. Results obtained from analysis of building transfer functions derived from frequency domain model are presented. Using a detailed finite-difference model as a tool to estimate some data not empirically available and required for the frequency domain model is presented. Also, three low-order RC circuits developed for the Environmental Chamber are presented. Results obtained for each of the three RC circuit models by running an optimization routine are presented. Then, the application of different temperature setpoint strategies along with a PI controller to reduce the peak demand of the building during the temperature transition time is discussed. (2) Chapter 4 also presents the application of frequency domain model to a thermal zone in an experimental facility (one of Hydro-Québec's Twin Houses in Shawinigan) to study the effect of different floor coverings and wall materials on the thermal response of the zone. The significance of the magnitude of the zone transfer function in a certain frequency range for effective thermal storage in the zone is discussed. This facility is introduced in the same section.

- Chapter 5: *Conclusion*. Includes conclusions, a summary of the main contributions of the work and the recommendations for future work.

Under the work carried out in this thesis, two paper has been produced, first one was presented at esim 2014 conference and the second one (under a collaborative work) submitted to the journal of Energy and Buildings:

1. Saberi Derakhtenjani, Ali, Athienitis, Andreas K., Candanedo, José A., Dehkordi, Vahid R., "*Thermal Response Characterization of an Environmental Test Chamber by means of Dynamic Thermal Models*", esim 2014 conference, Ottawa, ON.

2. Candanedo, José A., Dehkordi, Vahid R., Saberi Derakhtenjani, Ali, Athienitis, Andreas K., "*Near-Optimal Transition between Temperature Setpoints for Peak Load Reduction in Small Buildings*". Submitted for Energy and Buildings.

Also, a poster was presented at SNEBRN[1] third annual general meeting, May 2014, Montreal, QC.

[1] Smart Net-Zero Energy Buildings Strategic Research Network

2 LITERATURE REVIEW

This chapter reviews relevant literature related to building energy models and their application for understanding the thermal behavior of buildings, as well as examples of work done related to designing control strategies for buildings. This review includes research on the utilization of frequency domain techniques in building thermal analysis and also the application of time domain modeling techniques, such as low-order, grey-box RC circuit models.

2.1 Modeling of building thermal dynamics

Appropriate modeling is the fundamental tool to study a system. It gives the ability to simulate design conditions for a building and to study its thermal response. Building models allow making right decisions on the design of strategies helping in optimal building performance, i.e., to minimize its energy consumption while maintaining occupant comfort. Simulation and analysis of thermal dynamics and energy fluxes in a building by means of a model aids at choosing appropriate building materials and energy systems considering the local climatic features and building functions. Therefore, there have been significant efforts in the building engineering field on developing models using experimental and theoretical simulation tools.

The characterization of dynamic thermal behavior of building components and systems has been an interesting research topic. This characterization is essential in the process of designing advanced strategies for buildings. Some of the most significant

thermal processes in the evaluation of building thermal behavior are (Athienitis and O'Brien 2014):

- Conduction heat transfer through the exterior and interior walls, roofs, ceilings and floors.
- Solar radiation through fenestration and transparent surfaces
- Internal heat gains generated by occupants, lighting systems and appliances
- Heat transfer through ventilation of outdoor air
- Infiltration and other miscellaneous heat gains.

When creating a model, all heat exchanges (conductive, convective and radiative) should be represented as accurately as possible considering reasonable assumptions. However, one should keep in mind that too much complexity can limit the applicability of the model in analysis and design. Also, some of the physical parameters may not be accurately known. Therefore, the level of complexity of the model must be carefully selected.

Generally, a model consists of a structure that receives input(s), i.e., known information, and produces "output(s)", i.e. the information we are looking for. Inputs of a model can be categorized as either controllable or non-controllable. Auxiliary heating/cooling can be considered as an example of controllable input while solar radiation is an uncontrollable one (Allard 2013).

There are currently several approaches for creating building energy models which can be categorized into two general methods: time domain modeling and frequency domain modeling. Each one has its own advantages and drawbacks. As mentioned earlier, a model

is created for a specific objective and therefore, the suitable modeling approach should be chosen based on the objective of the study.

According to the ASHRAE (2005), every modeling approach can be classified as either "forward" or "inverse". In a forward modeling approach all the parameters and properties of materials of the system are known or at least can be estimated to a good extent; using these values, the response of the system to certain inputs can be evaluated. Forward modeling approach is often used in the early stages of building design (Allard 2013). Most detailed building simulation programs are based on forward modeling approaches. All forward models are based on a certain number of assumptions that are not necessarily valid in a real building. Assumptions are made to facilitate dealing with complex heat transfer phenomena inside a building. Therefore, usually significant levels of calibration should be made on the model developed through forward modeling approach. Also the model may get too complex for the evaluation of design alternatives.

In contrast, in an inverse modelling approach, not much information about the structure of the system is available; that is, constitution of the system is partially or completely unknown. These models are also called "data-driven" or "empirical" as they are based on the measured data. Therefore, with inverse models, a mathematical model for the dynamic system will be identified using the measured data from the system (Ljung 1987).

2.1.1 Building simulation tools

Currently there are many building simulation software tools developed to study various aspects of building thermal dynamics. These software use specific mathematical

methods to deal with modeling details. Crawley et al. (2008) compared features and capabilities of twenty major building energy simulation programs. The conclusion was that choosing a suite of simulation tools that would support one's specific need is more productive than just relying on one tool.

One of the most utilized building simulation tools is EnergyPlus, developed by U.S. Department of Energy (EnergyPlus 2013). It is used to model energy in buildings, including heating, cooling, lighting, ventilation and other energy sources, as well as water use. It benefits from some add-ons tools like OpenStudio Plug-in for SketchUp. OpenStudio is a user-friendly 3-D drawing interface that can be used by architects and engineers for performing building energy simulations and also advanced daylight analysis (EnergyPlus 2013).

Another well-known tool in the building energy simulation field is TRNSYS, developed at the solar energy laboratory of University of Wisconsin (TRNSYS 2014). While its primary use is in the field of renewable energy engineering, passive and active solar design, it can be equally used to model dynamic systems such as traffic flow or biological processes (TRNSYS 2014). It has a relatively large library of components each of which contains a model simulating the performance of that component including HVAC equipment, pumps and multi-zone buildings.

Despite their benefits, detailed simulation tools like TRNSYS or EnergyPlus require many details and building information to create realistic models. This required detail can create complicated building models which may make it difficult to design and apply control strategies. Thus, developing a methodology to create simple, low-order

models that can simulate the actual performance of the building with enough accuracy for a specific objective seems essential for the study of control strategies.

2.2 Modeling Techniques

Thermal dynamic models of buildings can be classified into two general categories: time domain and frequency domain approaches. Some previously completed work related to each of these approaches are described and discussed in the following sections.

2.2.1 Time domain techniques

Time domain techniques are the most commonly used approaches in building energy simulation tools, in which the calculations are made from one time step to the next. One of these approaches is finite-difference technique.

Transient thermal analysis of buildings is often performed with two main objectives (Athienitis and Santamouris 2002): (1) peak auxiliary (cooling/heating) load calculation for proper sizing of the equipment, and (2) determination of dynamic temperature fluctuations within walls, considering solar effects, room temperature swings and condensation on wall interior surfaces. The finite-difference method is a suitable approach to study the transient response of a building. The main advantage of the finite difference approach is its ability to model non-linear phenomena in the system and the ease of its formulation (Incropera et al. 2006) . Thus, both linear and non-linear phenomena can be modeled using finite-difference approach. However, elements with considerable thermal mass need to be discretized into a number of lumped thermal capacitances. Increasing the number of lumped capacitances provides better accuracy, meaning that the

result will be closer to the exact thermal behavior of the element and in some cases, a large number of capacitances requires small time steps to avoid numerical instability. However, it should also be noted that very small time steps can lead to significant truncation error (Borresen 1981).

Athienitis (1997) developed an explicit finite-difference model to study the thermal performance of a passive solar building with radiant floor heating. By performing simulations with different amount of thermal mass under various control strategies, Athienitis determined an optimum thickness for the concrete based on the reduction of room temperature swings, energy savings and prevention of floor surface overheating. Athienitis and Chen (2000) studied the effect of solar radiation on floor heating system by means of a 3-D finite-difference model. Chen, Y. (2009) created a 3-D finite difference thermal model to simulate the thermal performance of the ventilated concrete slab in an energy efficient solar house, Ecoterra™, and verified his model with the full-scale monitored data. Chen concluded that his model has a good potential for completion of design and control strategy analysis. Chen also did thermal modeling for a ventilated structural component (Chen et al. 2012) using finite difference and frequency domain response methods and compared the results with experimental data.

2.2.2 Low-order, grey-box, RC circuit Models

Low-order, grey-box RC circuits are also used in building energy studies and simulation. In this approach, the system under study is shown by a low-order thermal network with the so-called "effective" R's (resistances) and C's (capacitances), obtained by adopting an optimization routine for a defined objective. Thus, a system identification technique for the RC circuit is applied.

The circuit provides a good physical interpretation of the system under study and it can be easily tailored to suit the needs of a given application. Candanedo et al. (2013) investigated a low-order grey-box modeling approach tailored to be used in control studies. The proposed approach by Candanedo et al. (2013) for developing the simplified, low-order RC model can be summarized as:

- Using "grey-box" thermal network models
- Determining equivalent (rather than strictly physical) parameters
- Finding the parameters through an optimization routine
- Using a standardized state-space formulation, as a link between modelling and control engineering
- Estimating uncertainty

Several other researchers have worked on the grey-box RC circuit models. Dewson et al. (1993) presented a methodology to identify reduced-order RC network model based on the observed time series measurements of the internal and external air temperatures and heat flux input into a building, over a four week period. They also presented a method to estimate the variance of the identified component values and discussed the pros and cons of this method. Antonopoulos and Koronaki (1998) proposed a methodology to calculate effective thermal capacitance of building elements. Fraisse et al. (2002) verified a simplified 3R4C building model based on electrical analogy. Gouda et al. (2002) presented an approach for the optimization of the reduced-order lumped capacity modelling of the dynamic thermal behavior of building spaces by means of a non-linear constrained optimization routine.

Wang and Xu (2006) used genetic algorithm to estimate parameters of building thermal network using on-site collected operation data. Xu et al. (2007) presented an alternative simplified building energy model by combining conduction transfer function (CTF) model of building envelopes and a grey-box, 2R2C thermal network model of building thermal mass. Bacher and Madsen (2011) suggested a procedure for identifying suitable RC models for thermal dynamics of buildings based on experimental data. Braun and Chaturvedi (2011) presented an inverse grey-box modeling approach using a transfer function with constrained parameters to represent the energy flow in building structure. They identified optimal parameters using a non-linear regression algorithm, tested this approach using the on-site data and found that one or two weeks of data are satisfactory to train the model for accurate future predictions. Lin et al. (2012) used a combination of analysis and experiments in commercial buildings to study the effect of various model structures and identification techniques on parameter estimates. They found that a second-order model can reproduce the input-output behavior of the full scale model (with 13 states) and reported that even a *single* state model has adequate capability to be sufficient for control purposes. Therefore, there is no need for complex models with high state dimension and large number of resistances/capacitances. Kim and Braun (2012) presented a method to develop reduced-order thermal model in which they employed net radiosity method for long-wave radiation interaction between the surfaces, one-D transient conduction through the walls and conductive and convective coupling between the zones. Also Cliff et al (2012) carried out a case study coupling a reduced-order CFD indoor air model with the reduced-order building envelope.

As it is shown, the use of low-order RC circuit models is highly beneficial in simplifying the study of building thermal dynamics and control applications. In this thesis low-order RC circuit models are developed for the Environmental Chamber and an application is studied by means of a developed model.

2.2.3 Frequency domain techniques and building transfer functions

An alternative approach in dynamic thermal modeling involves using frequency domain techniques. Steady-periodic models developed through this approach are often employed in passive solar analysis of buildings and building load calculations (Kimura 1977). Frequency domain approach has been shown to be efficient in building energy analysis in conjunction with network theory (Athienitis et al. 1990) . This method can facilitate the integration of design and control (Chen et al. 2013). Shou (1991) enumerated some potential advantages of frequency domain techniques over time domain techniques:

- Flexibility in their utilization for either simulation or analysis; in contrast, with time domain techniques, analysis requires running a simulation.
- More efficient and less expensive solutions than time domain due to the fact that there is no time step involved in calculations in frequency domain.
- No discretization for elements with thermal mass is needed. Instead, the exact solution obtained from solving the 1-D conduction heat transfer in Laplace domain is used.

The main disadvantage of frequency domain modeling is the difficulty of accommodating non-linearities. However, in practice, linearization of heat transfer phenomena is often an acceptable compromise (Shou 1991).

Athienitis et al. (1985) presented an efficient method for the frequency domain analysis of multi-zone passive solar buildings by employing multi-terminal representations and Y-diakoptics. In this method, nodes representing exterior surfaces are eliminated using the Norton theorem. Then, the resulting complex networks are split into subnetworks corresponding to rooms. Then, by means of nodal formulation, a solution for each subnetwork was found and these solutions were coupled to give the overall system solution without having to solve directly for the initial complex network.

Athienitis et al. (1986) presented an analytical method to determine room temperature swings in direct gain rooms. They used fundamental network concepts, such as delta to star transformations and Norton theorem to obtain solution for a representative room temperature. Diurnal (day-length) measure is used to determine the relative magnitude of harmonics of solar radiation absorbed in the room. They reported that the number of required harmonics in analysis needs to be increased with the decrease of the day-length. Also Athienitis et al. (1987) used discrete frequency domain methodology to determine auxiliary energy load in buildings. Flexible and efficient computer formulation techniques for nodal frequency domain equations is developed. This formulation is then used to model auxiliary heating/cooling source as a proportionally controlled heat source. Athienitis et al (1987) concluded that this methodology is suitable for passive solar analysis due to the fact that it allows complex heat transfer mechanism such as long-wave radiant exchanges between room surfaces to be directly included in the model and it is possible to model time varying conductances such as that for a window with night insulation. Haghighat and Athienitis (1988) compared two computer programs; one in a frequency domain and the other in time domain, and compared their result with the experimental data.

They reported that frequency domain approach was shown to be more computationally efficient and flexible.

Using the frequency domain model, the response of the system can be found at discrete frequencies over the frequency range of interest. These discrete frequency responses are the elements of building transfer functions. Studying building transfer functions gives substantial insight into building thermal behavior including the delay in the response of the zone to certain inputs.

Usually it is more practical to work with an equation that represents the response of the system with negligible error. Thus, it is required to create a polynomial s-transfer function from discrete frequency response of the system in complex, Laplace-domain. One of the existing method for this complex curve fitting was presented by Levy (1959) which consists of performing a least-squares complex interpolation on the discrete responses. Haghighat et al. (1988) presented an approach for experimental identification of time domain transfer functions coefficients. Wang and Chen (2002) developed a frequency-domain regression (FDR) method to calculate transient heat flow for multi-layer constructions, in which an s-transfer function of transient heat conduction in a building construction was estimated based on its theoretical frequency characteristics. Finally, response factors or CTFs were obtained by applying inverse Laplace transform on the polynomial s-transfer function. Also, Chen and Wang (2005), developed a procedure based on the FDR method to directly and accurately calculate outside, across and inside periodic response factors of a multilayer wall or roof from its geometric and thermal properties. However, the transfer functions of a building can be obtained through other approaches; for example, system identification techniques. Recently Allard (2013) used system

identification techniques to develop a data-driven simplified transfer function model for a solar house considering active/passive solar thermal storage (Ecoterra™), and studied BIPV/T design alternatives for the house using the developed model.

The frequency domain approach that is used in this thesis is based on the methodology presented by Athienitis et al. (1990).

2.3 Application of different modeling approaches in studies of model-based control for buildings

Building simulation tools are highly beneficial for the development and application of advanced control algorithms by giving the simulated response of the system before it is actually built. This way, the performance of a building can be evaluated under different operation alternatives. The main purposes for the development of most existing building simulation tools include: design of the building, HVAC system design and retrofit analysis. However, not a lot of attention has been directed to the study of building control strategies (Kim et al. 2013).

The objective of a smart controller is to save as much energy as possible while maintaining occupant comfort. Due to large level of thermal mass in some buildings and therefore large time constants in building response, the controller has to anticipate the internal and external disturbances (Kummert et al. 2001).

Athienitis et al. (1990) studied the transient thermal control by means of Laplace transfer functions obtained from a detailed thermal model in frequency domain. They concluded that for convective loads there is a separation between long-term and short-term

building thermal dynamics at frequencies about 35 cycles per day (period of 41 minutes) and the room air thermal capacitance is important for only high-frequency thermal dynamics.

Braun (1990) investigated the reduction in peak electrical demand and energy costs through optimal control of building thermal storage. Braun and Lee (2006) stated that the trajectory for changing temperature setpoint is extremely important during demand-limiting period in order to minimize the peak load while maintaining comfort. They derived an exponential air temperature setpoint trajectory based on the natural response of the building such that the cooling requirement is constant. Lee and Braun (2008a) worked further on this problem and presented three approaches to find a solution for demand-limiting setpoint trajectories. Two of these approaches use simplified inverse building model trained with short-term data, and analytical solutions obtained by the models are used to determine setpoint trajectories. The other approach is based on optimization of weighted-average loads. Lee and Braun (2008b) evaluated these methods for two different buildings through simulations and reported that for all 3 methods there were between 23 to 26% reduction in the simulated peak load. Recently, Fournier and Leduc (2014) studied the impact of multiple setpoint modulation strategies on the demand of a baseboard-heated cottage during peak periods .

Kummert et al. (2005) compared different heating controllers for passive solar buildings on two buildings based on a cost function combining the energy performance and thermal comfort. Candanedo and Athienitis (2010) developed simplified transfer functions models using system identification techniques to study the predictive control of solar homes with passive and active thermal storage. Also, Candanedo et al. (2011) used a simple

transfer function model for a synchronized control of radiant floor heating and a fenestration system with automatically controlled solar transmittance.

Kim et al. (2013) compared the results of two different models (TRNSYS and Modelica) for a case study considering the overall energy consumption, peak power demand, computing time and short term dynamics. A reduced-order model for building envelope coupled with Modelica is developed. The conclusion was that TRNSYS is more computationally fast compared to Modelica and therefore it is a powerful tool to design supervisory control strategies. However, the consistency of the inputs and outputs of Modelica with actual control systems means that, the control algorithms can be directly applied to a real building control system. Also, the relatively low computational speed of Modelica can be overcome by using a low-order model for building envelope instead of finite difference.

2.4 Conclusion

A great deal of effort has been made to develop suitable energy modeling approaches for buildings and study their thermal response by means of different mathematical and experimental techniques. Model-based thermal control studies have shown that control-oriented modeling is highly beneficial in evaluating different control algorithms and energy efficiency measures. Low-order models that are well-calibrated are especially beneficial in control studies and they are appropriate to be implemented into building automation system (BAS) to apply the designed control strategies. In this thesis, two different modeling approaches are applied to real case studies and benefits of each modeling approach for the application of control strategies in buildings are discussed.

3 BACKGROUND AND MODELING

This chapter presents the basic theory behind each modeling approach. The development of both frequency domain and time domain approaches (including finite-difference model and low-order grey-box RC circuit model) is explained.

To perform a building thermal simulation, the building is translated into mathematical expressions, usually consisting of a system of equations. Each of those equations describes a thermal process and interaction in the system. Then, these equations are solved together to give building's response over a period of time or a range of frequencies.

A thermal network representation of a building is analogous to an electrical circuit. Some of the basic principles of thermal networks are introduced in elementary heat transfer texts (Incropera et al. 2006). Often, building elements can be represented by a combination of lumped thermal capacitances, representing the energy storage capacity of these elements, and interconnected conductances, representing energy pathways between elements. Most of the time conductances are assumed to be constant; however, they can be modeled as a function of time or temperature differences.

Figure 3.1 illustrates time domain modeling vs. frequency domain modeling. In time domain modeling the variables are given or obtained as a vector vs. time. However, in frequency domain variables are given or obtained as a set of magnitudes and phase angles at different frequencies:

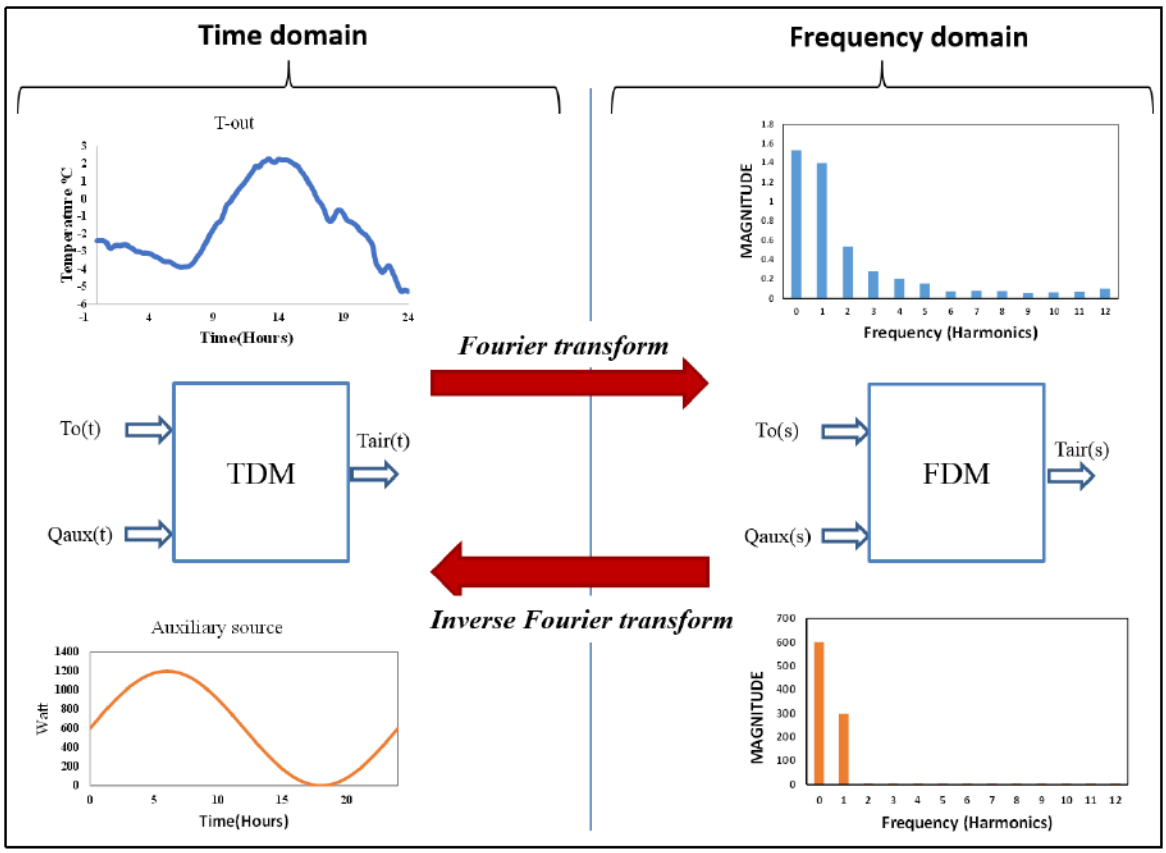

Figure 3.1. Comparison of time domain modeling vs. frequency domain modeling

One can switch between time domain and frequency domain using the discrete Fourier transform (DFT) or inverse discrete Fourier transform (IDFT) (see section 3.4).

3.1 Finite-difference technique

This section briefly describes the finite-difference modeling approach applied to thermal networks. In a finite-difference approach each of the walls and elements with thermal mass are discretized into a number of sub-layers. Each of those discretized areas is represented by a node and considered to be isothermal (Athienitis and Santamouris 2002). Each of the nodes associated with the thermal mass layers, has a lumped thermal capacitance connected to it and the conductances connect the node to the adjacent nodes.

Usually in the case of a thick wall with high level of thermal mass more than one capacitance is considered for the wall to increase the accuracy of the model. However, this is an approximation and not an exact solution.

Considering the time interval p, time step Δt, the general form of the explicit finite-difference model for the nodes with and without a lumped thermal capacitance can be stated as (Athienitis and Santamouris 2002):

$$T_{i,p+1} = T_{i,p} + \frac{\Delta t}{C_i}\left(Q_i + \sum_j \frac{T_{j,p} - T_{i,p}}{R_{i,j}} \right) \tag{3.1}$$

$$T_{i,p+1} = \frac{Q_i + \sum_j \frac{T_{j,p}}{R_{i,j}}}{\sum_j \frac{1}{R_{i,j}}} \tag{3.2}$$

where $T_{i,p}$ represents temperature of node "i" at time step "p", $T_{j,p}$ represents temperature of node "j" at time step "p", C_i is the thermal capacitance of node "i" and $R_{i,j}$ is the thermal resistance between nodes i and j.

The time step is selected based on the following condition (Athienitis 1994):

$$\Delta t \le \Delta t_{critical} \ , \qquad \Delta t_{critical} = \min\left(\frac{C_i}{\sum_j \frac{1}{R_{i,j}}} \right) \tag{3.3}$$

The finite-difference method has the advantage that it can accommodate non-linearities such as convection and radiation phenomena and it is relatively easy to apply control

strategies. However, usually initial conditions are not known and simulation should be repeated until a steady periodic solution is achieved (Athienitis and Santamouris 2002).

3.2 Frequency domain technique

3.2.1 Introduction

Frequency domain techniques and associated Fourier series methods have often been used in building energy analysis (Haghighat and Athienitis 1988). A key advantage of frequency domain techniques is that they take advantage of the inherent periodicity in the response of building. When a specific function such as solar radiation or outside temperature or setpoint profile over a few days is represented by a discrete Fourier series consisting of a mean and a few dominant harmonics (usually up to 12) we notice that some of the harmonics have a much higher amplitude than others. It is important to develop reduced order thermal networks that will accurately predict building dynamics in these important frequency ranges.

Frequency domain techniques are usually categorized into two groups: symbolic analysis and discrete frequency analysis (Shou 1991). Symbolic analysis is concerned with the case in which an analytical solution can be obtained which is usually the case of low-order models. This method is not practical when dealing with detailed, complex thermal circuits. In that case, the response of the system is found numerically at discrete frequencies.

In order to design a model-based control system for the building, relevant transfer functions of the building (or equivalent representations) can be used effectively. Thus, a

continuous form of a transfer function from discrete frequency response of the building is usually desired. A modified, least-squares fitting techniques is presented in section 3.2.4 and applied to the case studies on the next chapter to obtain building transfer functions.

3.2.2 Modeling Methodology

Thermal networks are analogous to electrical networks. That is to say, temperature is analogous to voltage and heat flow to current. The level of detail for thermal networks can vary based on how we model conduction, convection and radiation heat transfer. This is illustrated in Figure 3.2 and Figure 3.3 which are simplified and detailed thermal networks for a room. Traditionally, the two most common approaches for representation of convective and radiative heat exchanges in building simulation are:

1. Using combined radiative-convective heat transfer coefficients. This representation builds a star network as shown in example in Figure 3.2. This type of model is usually reasonable for small temperature differences between room air and surfaces. However, in the case of a room with high solar gains or with radiant heating this method is no longer accurate and produces significant errors.

2. Treating the radiative and convective heat exchanges separately as shown in Figure 3.3. This is the more accurate modeling approach.

Regarding conduction heat transfer, in Figure 3.2 and Figure 3.3, walls and surfaces with significant thermal mass are modeled with a two-port distributed element and the room air and light-weight room contents are modeled by a lumped thermal capacitance.

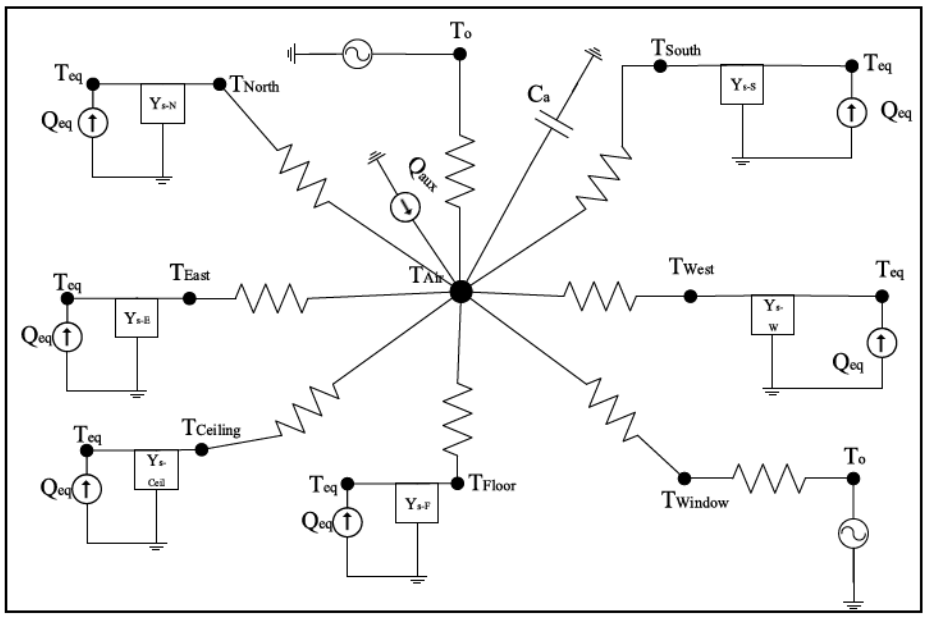

Figure 3.2. Simplified frequency domain thermal network with combined film coefficients

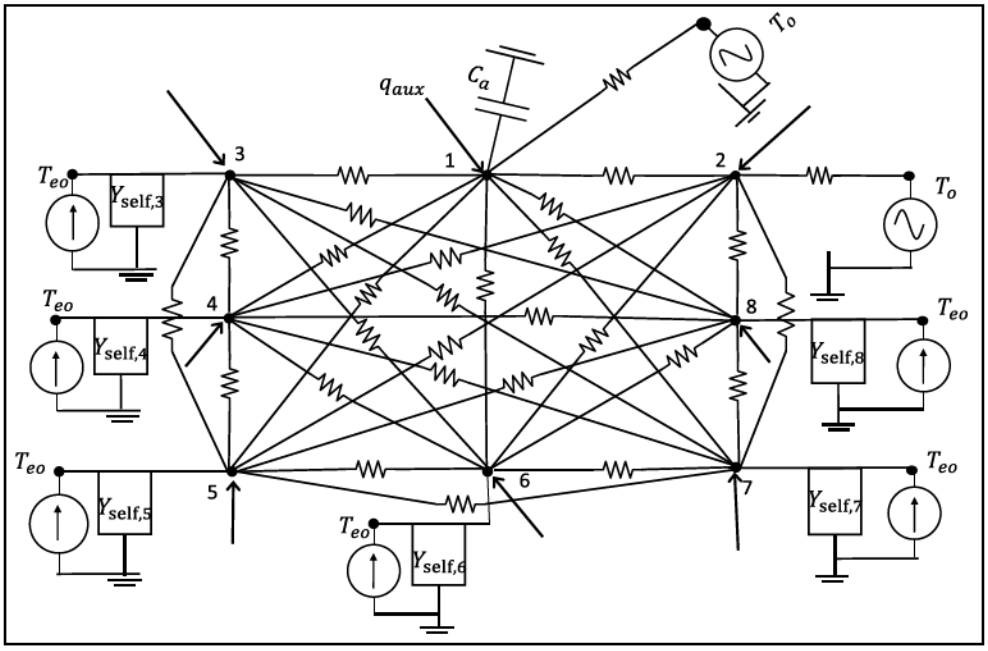

Figure 3.3. A detailed frequency domain thermal network

In Figure 3.3 the convective conductances, $U_{il} = A_i h_{c,i}$, connect the air node to the interior surfaces. The radiative conductances that interconnect the interior surfaces are given by, $U_{ij} = A_i F_{ij}^{*} \left(4\sigma T_m^3\right)$, where σ is the Stefan-Boltzman constant, $4T_m^3$ is the

linearization factor and F_{ij}^{*} is the radiative exchange factor between surfaces i and j (Edwards 1981). F_{ij}^{*} is function of view factor between the surfaces and their radiative properties and calculated as:

$$F_{ij}^{*} = \frac{m(i,j)\ \varepsilon_i \varepsilon_j}{\rho_j}$$

Where matrix $\mathbf{m} = \mathbf{M}^{-1}$, and elements of matrix $\mathbf{M}$ are calculated as: $\mathbf{M}(i,j) = \mathbf{I}(i,j) - \rho_i\ F(i,j)$. Here $\mathbf{I}(i,j)$ is the identity matrix so that $\mathbf{I}(i,j) = 1,\ \text{if } i = j$ otherwise, $\mathbf{I}(i,j) = 0$. $F(i,j)$ is the view factor between the two surfaces i and j .

The self-admittance and transfer-admittance for each of the walls and surfaces with thermal mass is calculated as (see Appendix C):

$$Y_{self} = \frac{U + Ak\gamma \tanh(\gamma l)}{\frac{U}{Ak\gamma}\tanh(\gamma l) + 1}\ , \qquad Y_{transfer} = \frac{-A}{\frac{A}{U}\cosh(\gamma l) + \frac{\sinh(\gamma l)}{k\gamma}} \tag{3.4}$$

And the equivalent heat source for each surface is calculated as:

$$Q_{eq} = -Y_{transfer} \cdot T_o \tag{3.5}$$

3.2.3 Analysis of the discrete frequency system response

The admittance transfer functions were presented in the previous section. Now, considering thermal network in Figure 3.3, an energy balance equation can be written for each one of the nodes in the network and by rearranging the equations, they can be written in a matrix form as:

$$\begin{bmatrix} sC_a + \sum_j U_{1,j} + U_{inf} & -U_{12} & -U_{13} & -U_{14} & -U_{15} & -U_{16} & -U_{17} & -U_{18} \\ -U_{12} & Y_{Self,2} + \sum_j U_{2j} & -U_{23} & -U_{24} & -U_{25} & -U_{26} & -U_{27} & -U_{28} \\ -U_{13} & -U_{23} & Y_{Self,3} + \sum_j U_{3,j} & -U_{34} & -U_{35} & -U_{36} & -U_{37} & -U_{38} \\ -U_{14} & -U_{24} & -U_{34} & Y_{Self,4} + \sum_j U_{4j} & -U_{45} & -U_{46} & -U_{47} & -U_{48} \\ -U_{15} & -U_{25} & -U_{35} & -U_{45} & Y_{Self,5} + \sum_j U_{5j} & -U_{56} & -U_{57} & -U_{58} \\ -U_{16} & -U_{26} & -U_{36} & -U_{46} & -U_{56} & Y_{Self,6} + \sum_j U_{6j} & -U_{67} & -U_{68} \\ -U_{17} & -U_{27} & -U_{37} & -U_{47} & -U_{57} & -U_{67} & Y_{Self,7} + \sum_j U_{7,j} & -U_{78} \\ -U_{18} & -U_{28} & -U_{38} & -U_{48} & -U_{58} & -U_{68} & -U_{78} & Y_{Self,8} + \sum_j U_{8,j} \end{bmatrix} \begin{bmatrix} T_1 \\ T_2 \\ T_3 \\ T_4 \\ T_5 \\ T_6 \\ T_7 \\ T_8 \end{bmatrix} = \begin{bmatrix} Q_1 \\ Q_2 \\ Q_3 \\ Q_4 \\ Q_5 \\ Q_6 \\ Q_7 \\ Q_8 \end{bmatrix}$$

The above system of equation can be summarized as:

$$\mathbf{YT} = \mathbf{Q} \tag{3.6}$$

In equation (3.6) **Y** is called the admittance matrix, **T** is the temperatures vector and **Q** is the source vector. The elements of matrix Y can be written by inspection (Vlach and Singhal 1983). It should be noted that that the thermal storage terms are all in the diagonal of admittance matrix because thermal storage is relative to a common reference temperature (Athienitis and O'Brien 2014). The temperatures are calculated by:

$$\mathbf{ZQ} = \mathbf{T} \tag{3.7}$$

where matrix $\mathbf{Z}=\mathbf{Y}^{-1}$ is called the impedance matrix. This matrix is a very important parameter and lots of insights about the thermal characteristics of the system can be obtained by studying this matrix, without any required simulations. Matrix **Z** contains the elements of building transfer functions at discrete frequencies and it represents the temperature change in node i due to heat input at node j for a frequency range. This type of transfer functions is studied for the Environmental Chamber in the next chapter.

As stated before, it is usually desirable to have a mathematical expression for building transfer functions. Therefore a fitting technique is required to obtain building transfer functions from discrete frequency responses.

There are currently several approaches to determine a continuous s-domain, Laplace transfer function from discrete frequency responses. One of the analytical methods presented by Levy (1959) is to perform a least squares complex interpolation on the discrete responses which is explained in the next section.

A modification made on the Levy method for the case of a known steady-state response is presented in the section 3.2.5.

3.2.4 Modified Least-squares fitting for building transfer functions

Consider transfer function $Z(j\omega)$ for which the values were obtained at discrete frequencies. The preferred form of the fitted polynomial may be expressed as:

$$Z_f(j\omega) = \frac{A_0 + A_1(j\omega) + A_2(j\omega)^2 + A_3(j\omega)^3 + \ldots}{B_0 + B_1(j\omega) + B_2(j\omega)^2 + B_3(j\omega)^3 + \ldots} \tag{3.8}$$

Now by separating the numerator and denominator into real and imaginary parts, equation (3.8) can be written as:

$$Z_f(j\omega) = \frac{\varepsilon + j\omega\beta}{\delta + j\omega\tau} = \frac{N(\omega)}{D(\omega)} \tag{3.9}$$

where:

$$\varepsilon = A_0 - A_2(j\omega)^2 + A_4(j\omega)^4 - \ldots \qquad \beta = A_1 - A_3(j\omega)^2 + A_5(j\omega)^4 - \ldots$$

$$\delta = 1 - B_2(\omega)^2 + B_4(\omega)^4 - \ldots \qquad \tau = B_1 - B_3(\omega)^3 + B_5(\omega)^4 - \ldots$$

then the fit error is defined as:

$$\varepsilon(\omega)=\left|Z(j\omega)-Z_f(j\omega)\right|=\left|Z(j\omega)-\frac{N(\omega)}{D(\omega)}\right| \tag{3.10}$$

now multiplying both sides by $D(\omega)$:

$$D(\omega)\varepsilon(\omega)=D(\omega)Z(j\omega)-N(\omega)=a(\omega)+jb(\omega)$$

where $a(\omega)$ and $b(\omega)$ are function of both frequency and unknown coefficients A_i and B_i. Then at any specific frequency:

$$|D(\omega)\varepsilon(\omega)|^2=a^2(\omega)+b^2(\omega)$$

Now E is defined as being the function that equals to $a^2(\omega)+b^2(\omega)$, summed over all m frequencies as (Levy 1959):

$$E=\sum_{n=0}^{m}\left[\left(r_n\delta_n-\omega_n\tau_nI_n-\varepsilon_n\right)^2+\left(\omega_n\tau_nr_n+\delta_nI_n-\omega_n\beta_n\right)^2\right] \tag{3.11}$$

where:

$$r_n=(Magnitude\ at\ \omega_n)\times\cos(phase\ angle\ at\ \omega_n)$$

$$I_n=(Magnitude\ at\ \omega_n)\times\sin(phase\ angle\ at\ \omega_n)$$

then, the error function E is minimized with respect to A_i and B_i, that is:

$\frac{\partial E}{\partial A_i}=0$, and $\frac{\partial E}{\partial B_i}=0$, which yield for A_i :

$$\frac{\partial E}{\partial A_0} = \sum_{n=0}^{m} -2(\delta_n r_n - \omega_n \tau_n I_n - \epsilon_n) = 0$$

$$\frac{\partial E}{\partial A_1} = \sum_{n=0}^{m} -2\omega_n(\omega_n \tau_n r_n + \delta_n I_n - \omega_n \beta_n) = 0$$

$$\frac{\partial E}{\partial A_2} = \sum_{n=0}^{m} 2\omega_n^2(\delta_n r_n - \omega_n \tau_n I_n - \epsilon_n) = 0 \qquad (3.12)$$

$$\vdots$$

$$\vdots$$

for B_i (it is assumed that $B_0 = 1$):

$$\frac{\partial E}{\partial B_1} = \sum_{n=0}^{m} -2\omega_n I_n(\delta_n r_n - \omega_n \tau_n I_n - \varepsilon_n) + 2\omega_n r_n(\omega_n \tau_n r_n + \delta_n I_n - \omega_n \beta_n) = 0$$

$$\frac{\partial E}{\partial B_2} = \sum_{n=0}^{m} -2\omega_n^2 r_n(\delta_n r_n - \omega_n \tau_n I_n - \varepsilon_n) - 2\omega_n^2 I_n(\omega_n \tau_n r_n + \delta_n I_n - \omega_n \beta_n) = 0$$

$$\frac{\partial E}{\partial B_3} = \sum_{n=0}^{m} 2\omega_n^3 I_n(\delta_n r_n - \omega_n \tau_n I_n - \varepsilon_n) - 2\omega_n^3 r_n(\omega_n \tau_n r_n + \delta_n I_n - \omega_n \beta_n) = 0 \qquad (3.13)$$

$$\vdots$$

$$\vdots$$

and so on.

Now let's define new variables λ, S, T, U , as :

$$\lambda_h = \sum_{n=0}^{m} \omega_n^h \ , \qquad S_h = \sum_{n=0}^{m} \omega_n^h r_n \ , \qquad T_h = \sum_{n=0}^{m} \omega_n^h I_n \ , \qquad U_h = \sum_{n=0}^{m} \omega_n^h \left(r_n^2 + \omega_n^2\right)$$

where parameter h depends on the desired order of the transfer function. By substituting the defined variables λ, S, T, U, equations (3.12) and (3.13) can be rearranged and written as:

$$
\begin{aligned}
&A_0\lambda_0 - A_2\lambda_2 + A_4\lambda_4 - A_6\lambda_6 + \ldots + B_1T_1 + B_2S_2 - B_3T_3 - B_4S_4 + B_5T_5 + \ldots = S_0 \\
&A_1\lambda_2 - A_3\lambda_4 + A_5\lambda_6 - A_7\lambda_8 + \ldots - B_1S_2 + B_2T_3 + B_3S_4 - B_4T_5 - B_5S_6 + \ldots = T_1 \\
&A_0\lambda_2 - A_2\lambda_4 + A_4\lambda_6 - A_6\lambda_8 + \ldots + B_1T_3 + B_2S_4 - B_3T_5 - B_4S_6 + B_5T_7 + \ldots = S_2 \\
&A_1\lambda_4 - A_3\lambda_6 + A_5\lambda_8 - A_7\lambda_{10} + \ldots - B_1S_4 + B_2T_5 + B_3S_6 - B_4T_7 - B_5S_8 + \ldots = T_3 \\
&\vdots \qquad\qquad \vdots \qquad\qquad \vdots \qquad\qquad \vdots \\
&A_0T_1 - A_1S_2 - A_2T_3 + A_3S_4 + A_4T_5 - \ldots + B_1U_2 - B_3U_4 + B_5U_6 - B_7U_8 + \ldots = 0 \\
&A_0S_2 + A_1T_3 - A_2S_4 - A_3T_5 + A_4S_6 - \ldots + B_2U_4 - B_4U_6 + B_6U_8 - B_8U_{10} + \ldots = U_2
\end{aligned}
\tag{3.14}
$$

Or in matrix form as equations (3.15) and (3.16):

$$
\mathbf{M} = \begin{Bmatrix}
\lambda 0 & 0 & -\lambda 2 & 0 & \lambda 4 & \cdots & T1 & S2 & -T3 & -S4 & T5 & \cdots \\
0 & \lambda 2 & 0 & -\lambda 4 & 0 & \cdots & -S2 & T_3 & S_4 & -T_5 & -S_6 & \cdots \\
\lambda_2 & 0 & -\lambda_4 & 0 & \lambda_6 & \cdots & T_3 & S_4 & -T_5 & -S_6 & T_7 & \cdots \\
0 & \lambda_4 & 0 & -\lambda_6 & 0 & \cdots & -S_4 & T_5 & S_6 & -T_7 & -S_8 & \cdots \\
\vdots & \vdots & \vdots & \vdots & \vdots & & \vdots & \vdots & \vdots & \vdots & \vdots & \\
T_1 & -S_2 & -T_3 & S_4 & T_5 & \cdots & U_2 & 0 & -U_4 & 0 & U_6 & \cdots \\
S_2 & T_3 & -S_4 & -T_5 & S_6 & \cdots & 0 & U_4 & 0 & -U_6 & 0 & \\
T_3 & -S_4 & -T_5 & S_6 & T_7 & \cdots & U_4 & 0 & -U_6 & 0 & U_8 & \cdots \\
\vdots & \vdots & \vdots & \vdots & \vdots & & \vdots & \vdots & \vdots & \vdots & \vdots &
\end{Bmatrix}
\tag{3.15}
$$

$$\mathbf{C}=\begin{Bmatrix} S_0 \\ T_1 \\ S_2 \\ T_2 \\ \vdots \\ 0 \\ U_2 \\ 0 \\ \vdots \end{Bmatrix}, \qquad \mathbf{N}=\mathbf{M}^{-1}\mathbf{C} \Rightarrow \mathbf{N}=\begin{Bmatrix} A_0 \\ A_1 \\ A_2 \\ A_3 \\ \vdots \\ B_1 \\ B_2 \\ B_3 \\ \vdots \end{Bmatrix} \tag{3.16}$$

Matrix **N** contains the coefficients of the fitted building transfer function.

3.2.5 Modification for a known steady-state transfer function value

In building modeling and studies, it is often the case that the steady-state value of a system's response is known. For example it can be measured from experimental data. The steady-state value of a transfer function is an important number. It shows the mean value of the transfer function while other frequencies show the deviation (dynamic values) from the mean value. While fitting a transfer function to system's discrete responses, it is desired to have that known steady-state value as the value of transfer function on the frequency of zero. To do that, the above-mentioned equations should be modified.

Consider transfer function Z for which the steady-state value is known. We can say $A_0 = Z(\omega = 0)$ then, $\partial E/\partial A_0 = 0$. Thus, the first equation on the equations (3.12) and (3.14) are eliminated and then the other equations should be arranged to find the new matrices **M** and **C** for the desired order of fit. The new derived formula for the matrices **M** and **C** is shown on equation (3.17). It should be noted that the matrices **M** and **C** can be created through inspection; that is as shown on equation (3.17), Matrix **M** is always a square matrix and its order equals to sum of the *number* of coefficients of transfer

function's denominator and numerator. Therefore, in matrix **M**, each row and column corresponds to denominator or numerator's coefficient:

$$\mathbf{M} = \begin{array}{c} \overbrace{}^{A_1\ A_2\ A_3\ A_4\ A_5} \quad \overbrace{}^{B_1\ B_2\ B_3\ B_4\ B_5} \\ \begin{bmatrix} \lambda_2 & 0 & -\lambda_4 & 0 & \lambda_6 & \cdots & -S_2 & T_2 & S_4 & -T_5 & -S_6 & \cdots \\ 0 & -\lambda_4 & 0 & \lambda_6 & 0 & \cdots & T_3 & S_4 & -T_5 & -S_6 & T_7 & \cdots \\ \lambda_4 & 0 & -\lambda_6 & 0 & \lambda_8 & \cdots & -S_4 & T_5 & S_6 & -T_7 & -S_8 & \cdots \\ 0 & -\lambda_6 & 0 & \lambda_8 & 0 & \cdots & T_5 & S_6 & -T_7 & -S_8 & T_9 & \cdots \\ \vdots & \vdots & \vdots & \vdots & \vdots & & \vdots & \vdots & \vdots & \vdots & \vdots & \\ -S_2 & -T_3 & S_4 & T_5 & -S_6 & \cdots & U_2 & 0 & -U_4 & 0 & U_6 & \cdots \\ T_3 & -S_4 & -T_5 & S_6 & T_7 & & 0 & U_4 & 0 & -U_6 & 0 & \cdots \\ -S_4 & -T_5 & S_6 & T_7 & -S_8 & \cdots & U_4 & 0 & -U_6 & 0 & U_8 & \cdots \\ \vdots & \vdots & \vdots & \vdots & \vdots & & \vdots & \vdots & \vdots & \vdots & \vdots & \end{bmatrix} \end{array}$$

$$C = \begin{bmatrix} T_1 \\ S_2 - A_0\lambda_2 \\ T_3 \\ S_4 \\ \vdots \\ -A_0T_1 \\ U_2 - A_0S_2 \\ -A_0T_3 \\ \vdots \end{bmatrix} \tag{3.17}$$

This approach is used to obtain building Laplace transfer functions from discrete frequency responses on the next chapter.

3.3 Low-order, grey-box RC circuit model

3.3.1 Introduction

This section describes the theory and methodology used to develop low-order, grey-box RC circuit models. This simplified modeling approach aims at facilitating further control studies in buildings. The circuit parameters (R and C values) obtained this way should be interpreted as "equivalent" numbers rather than "exact" physical parameters (Candanedo et al. 2013).

3.3.2 Modeling Methodology

The methodology used here is based on the work presented by Candanedo et al. (2013). As a first step, an RC circuit configuration for the building based on the physical properties and geometry of the building is proposed. Simulation results using this circuit is used as the initial conditions for the optimization problem. The variable (for example air temperature) for which the optimization is performed is usually measured by experiment or is calculated by using a detailed building simulation program. This optimization is done considering an objective function.

Let us assume a desired output variable y which is obtained from measurements or from detailed building simulation programs. Now, let us assume that $\hat{y}$ is value of the variable obtained from initial simulation of the low-order circuit. If there is "n" number of output variables, then the objective function here can be defined by using the Euclidian second norm (Candanedo et al. 2013). For example, in the case that only two outputs which are the temperature of two nodes in the circuit are taken into consideration, the objective function can be defined as:

$$J = \left\| T_1 - \hat{T}_1 \right\| + \left\| T_2 - \hat{T}_2 \right\| \tag{3.18}$$

where the Euclidian second norm is defined as:

$$\left\| y_i \right\| = \sqrt{(y_1)^2 + (y_2)^2 + \ldots + (y_n)^2} = \sqrt{\sum_{i=1}^{n} (y_i - \hat{y}_i)^2} \tag{3.19}$$

It should be pointed out that the objective function can be defined in infinite ways and the above equation is **not the only** objective function that can be defined to perform the optimization. However, since certain temperatures are relatively easy to measure, the objective function defined based on temperature for which the measured data is available can be a good choice.

3.3.3 State-space representation containing physical interpretation

A state-space representation is a mathematical description of a system in a compact manner consisting of a set of inputs, outputs and state variables that are related by first-order differential equations (Nise 2011). For linear and time-invariant systems, the differential and algebraic equations may be written in the matrix form that is a state vector $\mathbf{x}$ with n elements, an input vector $\mathbf{u}$ with m elements and an output vector $\mathbf{y}$ with L elements. Four matrices $\mathbf{A}_{n\times n}, \mathbf{B}_{n\times m}, \mathbf{C}_{L\times n}, \mathbf{D}_{L\times m}$, link the vectors $\mathbf{x}$, $\mathbf{u}$ and $\mathbf{y}$ together in the form:

$$\dot{\mathbf{x}} = \mathbf{A}\mathbf{x} + \mathbf{B}\mathbf{u} \tag{3.20}$$

$$\mathbf{y} = \mathbf{C}\mathbf{x} + \mathbf{D}\mathbf{u} \tag{3.21}$$

A detailed description of state-space modeling can be found in the control engineering text books [(Ogata 2009) and (Nise 2011)]. Technically, there are infinite ways to define the

states for a physical system depending on the desired objective (Candanedo et al. 2013). Here, temperatures of the nodes with thermal capacitance are considered as state variables *because these values have a certain physical meaning and they can be measured relatively easy*. Also this choice of states provides a well-ordered formulation of the state-space equations equivalent to the well-known finite-difference modeling formulation (Candanedo et al. 2013). For example, considering RC circuit shown on Figure 3.4, the matrices will be:

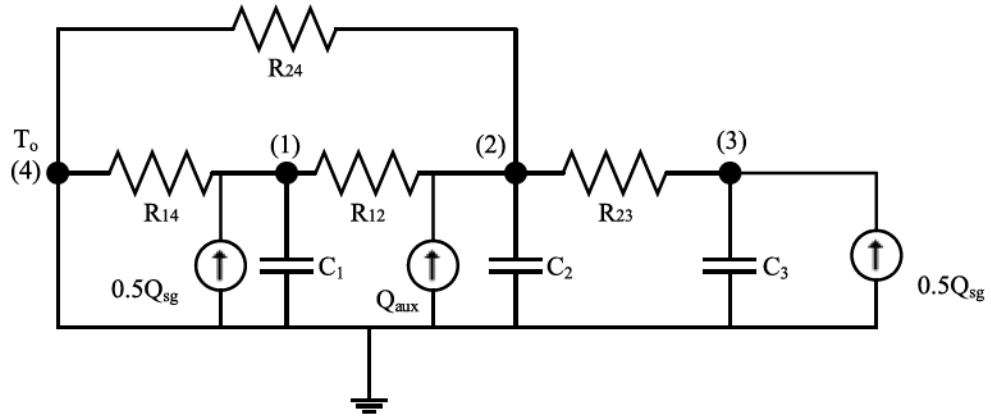

Figure 3.4.Example of a low-order, RC circuit model

$$\text{states:}\quad \mathbf{x}=\begin{bmatrix} T_1 \\ T_2 \\ T_3 \end{bmatrix} \qquad \text{inputs:}\quad \mathbf{u}=\begin{bmatrix} T_o \\ Q_{sg} \\ Q_{aux} \end{bmatrix} \qquad \text{desired output:}\quad \mathbf{y}=\begin{bmatrix} T_2 \end{bmatrix}$$

The matrices **A** and **B** can be found by writing energy balance equations for each node. By rearranging the equations for all the nodes into the form described in equations (3.20) and (3.21), matrices **A** and **B** are obtained as:

$$\mathbf{A}=\begin{bmatrix} -\left(\frac{U_{1,4}+U_{1,2}}{C_1}\right) & \frac{U_{1,2}}{C_1} & 0 \\ \frac{U_{1,2}}{C_2} & -\left(\frac{U_{2,4}+U_{1,2}+U_{3,2}}{C_2}\right) & \frac{U_{2,3}}{C_2} \\ 0 & \frac{U_{2,3}}{C_3} & \frac{U_{2,3}}{C_3} \end{bmatrix}, \quad \mathbf{B}=\begin{bmatrix} \frac{U_{1,4}}{C_1} & \frac{0.5}{C_1} & 0 \\ \frac{U_{2,4}}{C_2} & 0 & \frac{1}{C_2} \\ 0 & \frac{0.5}{C_3} & 0 \end{bmatrix} \tag{3.22}$$

The elements of A and B on the equation (3.22) can be found by inspection. General procedure to find matrices **A** and **B** for an RC thermal circuit presented by Candanedo et al. (2013) is explained here.

First let us define the capacitance matrix $\mathbf{M}_c$. Since all the capacitances in an RC thermal circuit are connected to the ground (which is the reference temperature, often considered as 0 °C), $\mathbf{M}_c$ is defined as a diagonal matrix.It can be seen that $\mathbf{M}_c$ is an invertible matrix,:

$$\mathbf{M}_c=\begin{bmatrix} C_1 & 0 & \cdots & 0 \\ 0 & C_2 & \ddots & \vdots \\ \vdots & \ddots & \ddots & 0 \\ 0 & \cdots & 0 & C_n \end{bmatrix}, \quad \mathbf{M}_c^{-1}=\begin{bmatrix} 1/C_1 & 0 & \cdots & 0 \\ 0 & 1/C_2 & \ddots & \vdots \\ \vdots & \ddots & \ddots & 0 \\ 0 & \cdots & 0 & 1/C_n \end{bmatrix} \tag{3.23}$$

the conductance matrix **U** is defined as:

$$\mathbf{U}=\begin{bmatrix} -\sum_j U_{1,j} & U_{1,2} & \cdots & U_{1,n} \\ U_{2,1} & -\sum_j U_{2,j} & \cdots & U_{2,n} \\ \vdots & \vdots & \ddots & \vdots \\ U_{n,1} & U_{n,2} & \cdots & -\sum_j U_{n,j} \end{bmatrix} \tag{3.24}$$

then matrix **A** is obtained as:

$$\mathbf{A} = \mathbf{M}_c^{-1}\mathbf{U} \tag{3.25}$$

and matrix **B** is defined as:

$$\mathbf{B} = \mathbf{M}_c^{-1}\mathbf{S} \tag{3.26}$$

Where **S** is the source matrix. Each element of **S**, shows the effect of source j, on the node i; that is for a power source it shows the fraction ($\alpha_{i,j}$) of the source *j* absorbed by node i:

$$s_{i,j} = \alpha_{i,j} Q_j \tag{3.27}$$

And for a temperature source which is connected to the node i by a conductance, $s_{i,j}$ is given by:

$$s_{i,j} = U_{i,j} T_j \tag{3.28}$$

The matrices C and D are written depending on the output of interest. In the example above the only output of interest is T_2 and there is no direct impact from the input variables on the outputs (no direct feedback):

$$\mathbf{C} = \begin{bmatrix} 0 & 1 & 0 \end{bmatrix} \qquad \mathbf{D} = \begin{bmatrix} 0 & 0 & 0 \end{bmatrix} \tag{3.29}$$

For example if the outputs of interest are T_2 and T_1, then matrices C and D will be:

$$\mathbf{C} = \begin{bmatrix} 1 & 0 & 0 \\ 0 & 1 & 0 \end{bmatrix} \qquad \mathbf{D} = \begin{bmatrix} 0 & 0 & 0 \\ 0 & 0 & 0 \end{bmatrix} \tag{3.30}$$

3.4 Final remarks and discussions

Chapter 3 presented theoretical background for each of the modeling approaches used in this thesis. In the next chapter, application of these approaches to case studies is discussed along with their advantages for further control studies.

It should be noted that to switch between time domain and frequency domain, the discrete Fourier transform can be used as explained below (Athienitis 1994).

Imagine the variable T (e.g. a room thermostat setpoint profile) is given in time domain as a vector of values versus time. In order to transfer T to frequency domain the discrete Fourier transform (DFT) is applied as follows (Athienitis 1994) :

$$T(n) = \sum_{i} (T_i \cdot \frac{\exp(-j \cdot \omega(n) \cdot t_i)}{NTS}) \tag{3.31}$$

where:

$i = i^{th}$ time step

$\omega(n) = \frac{2\pi n}{p}$, $n =$ harmonic number , $p =$ period

$NTS =$ (total number of data points)

and if T is given as a vector of magnitudes versus frequencies, to transfer it to time domain, the inverse discrete Fourier transform (IDFT) is applied as:

$$T_i = T(\omega(n=0)) + 2\sum_{n=1}^{nf} \mathrm{Re}[(T(\omega(n)) \cdot \exp(j \cdot \omega(n) \cdot t_i)] \tag{3.32}$$

where: nf = largest desired harmonic.

As an example, an outdoor air temperature profile with a 3-harmonic discrete Fourier series fit is shown in Figure 3.5.

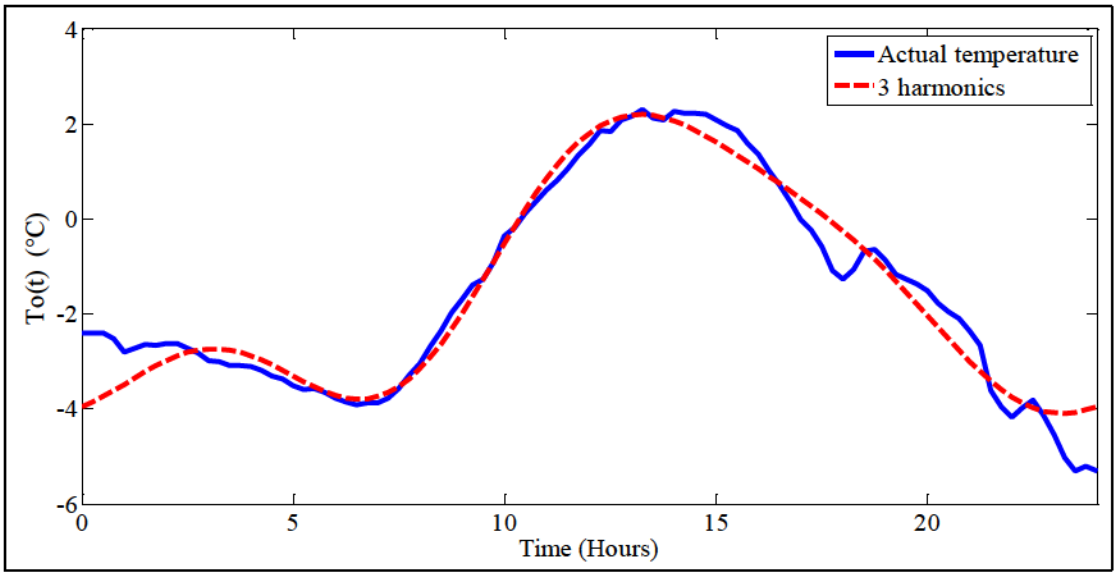

Figure 3.5. Actual To(t) and 3-harmonic discrete Fourier series fit

Other examples using different harmonics for an air setpoint profile and solar radiation profile are shown in Figure 3.6 and Figure 3.7:

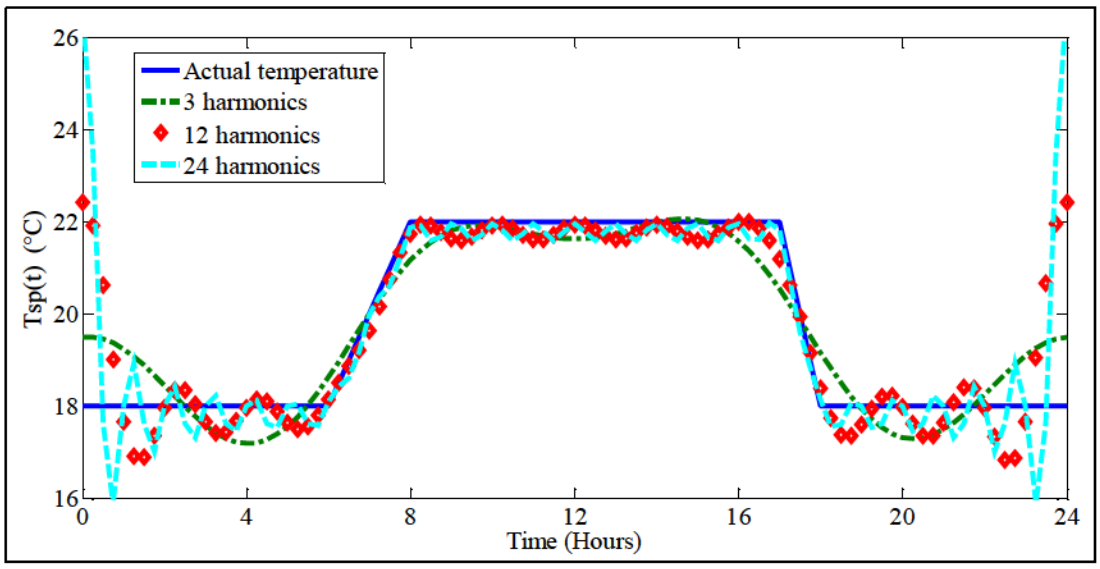

Figure 3.6 Actual setpoint temperature, Tsp(t), vs. discrete Fourier series fit with different harmonics

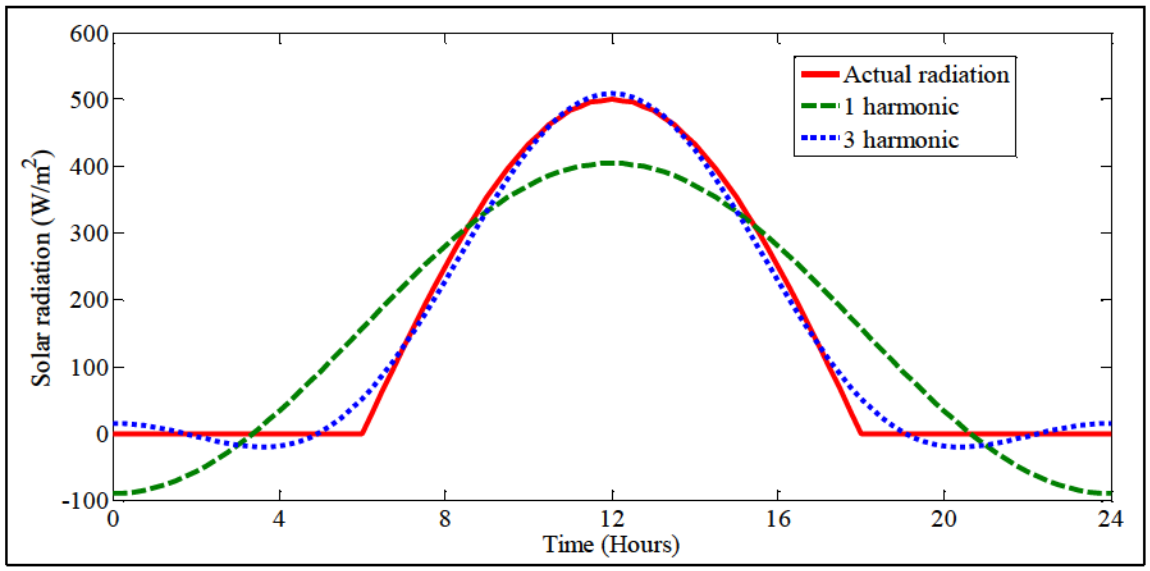

Figure 3.7. Actual solar radiation vs. discrete Fourier series fit with different harmonics

4 CASE STUDIES AND RESULTS

4.1 Solar Simulator / Environmental Chamber (SSEC)

As introduced in the Chapter 1, Solar Simulator/Environmental Chamber is a test facility located in Concordia University. This facility allows testing building models and technologies under controlled conditions.

In the following sections, the results of different modeling approaches applied for the building are described. First of all, a relatively detailed finite-difference model is developed to be used as a tool to estimate the auxiliary load for which the data was not empirically available. Then a detailed frequency domain model is developed from the application of first-principle heat transfer equations to study the thermal characteristics of the system. The thermal response of the system is obtained over a range of discrete frequencies and then analytical equations are obtained for building transfer functions using the fitting technique described in the Chapter 3.

4.1.1 Experiment description

To calibrate the model created for the chamber, an experiment has been set up. The Environmental Chamber has the following dimensions of 8.9m × 4.4m × 7.12m, corresponding to floor area of about 39.16 m^2, as shown in Figure 4.1 . The window area for the chamber is 10 m^2 which consists of 10 double-glazed windows with the U-value of around 2.9 $W/m^2.°C$ .The floor is made of 15-cm (6-in) thick concrete which is the main thermal mass in the chamber. Polyisocyanurate insulation is installed between the interior

surfaces and the exterior siding of the walls and ceiling. The walls and ceiling have the U-value of 0.19 W/m^2.°C .The air handling unit (AHU) providing cooling or heating is shown in Figure 4.1 . Sensors were attached to the interior surfaces of the chamber to measure temperature on each surface. Additional sensors were left hanging to measure the air temperature inside the chamber. These sensors were shielded so that their temperature would not be affected directly by the solar radiation coming from the mobile solar simulator. The temperature variation inside the environmental chamber was programmed to be cyclic as shown in Figure 4.3. The outdoor air temperature for the Chamber was room temperature in the lab and considered to be constant, 22°C.

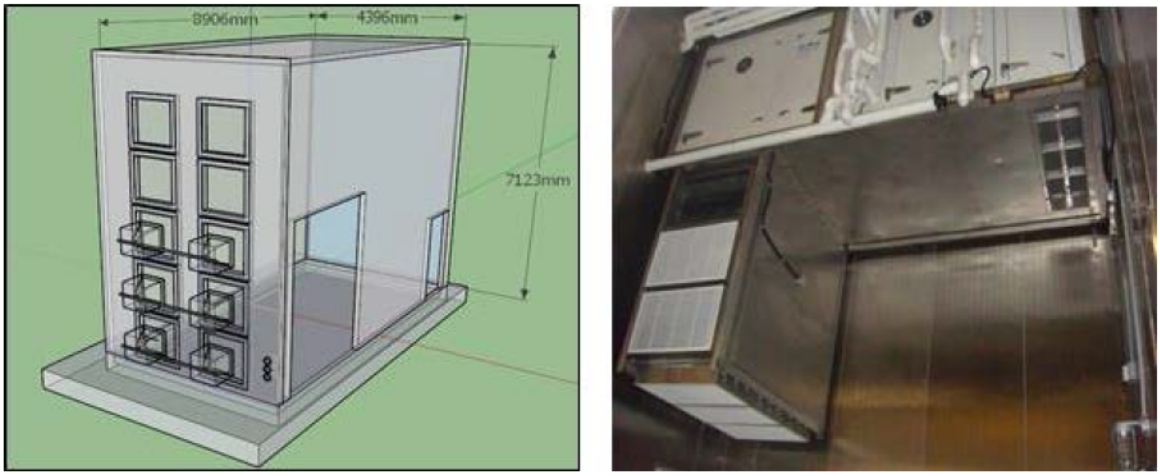

Figure 4.1. Schematic of environmental chamber (left, drawing courtesy of Jiwu Rao), air handling unit (AHU) (right).

4.1.2 Finite difference model

The auxiliary cooling/heating for the environmental chamber is supplied by the AHU which uses a PI controller designed specifically for the environmental chamber. One of the significant inputs in this case is the auxiliary load applied by the AHU. Conventionally, auxiliary cooling/heating can be calculated knowing the supply and return temperatures and the air flow rate of the AHU. But in this case, no sensor measuring the

return temperature was available (however, this could be estimated as the average temperature of the air in the chamber, which is measured). Also, information about the exact flowrate of the AHU was not available (new sensors are being installed for this purpose). A Lumped Parameter Finite Difference (LPFD) model was used to estimate the cooling/heating input and to study the detailed thermal dynamics of the space. A detailed lumped parameter finite difference model for environmental chamber has been created using the following thermal network shown in Figure 4.2. In this thermal network, radiative and convective conductances are treated separately.

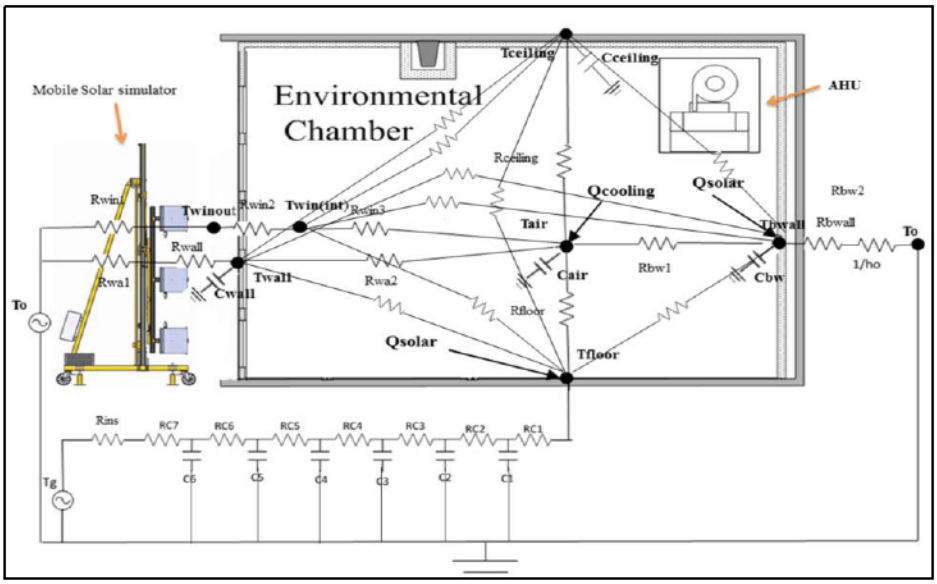

Figure 4.2. Thermal network for finite-difference model (convective and radiative resistances for the two side walls are not shown)

The auxiliary load, Q_{aux} , was calculated at each time step by applying proportional-integral(PI) control rule as explained in equation (4.2). The error function at each time step, *i,* is defined as:

$$e_i = (T_{setpoint})_i - (T_{air})_i \tag{4.1}$$

$$(Q_{\text{aux}})_i = K_{\text{p}} e_i + K_{\text{I}} \sum_{i=1}^{p} (e_i \cdot \Delta t) \tag{4.2}$$

K_{p} and K_{I} are considered the same value as the one in the controller of the environmental Chamber, which is 6000(W/ºC) for K_{p} and 10(W/ºC·S) for K_{I}. T_{setpoint} is the air setpoint temperature used in experiment and is shown on Figure 4.3:

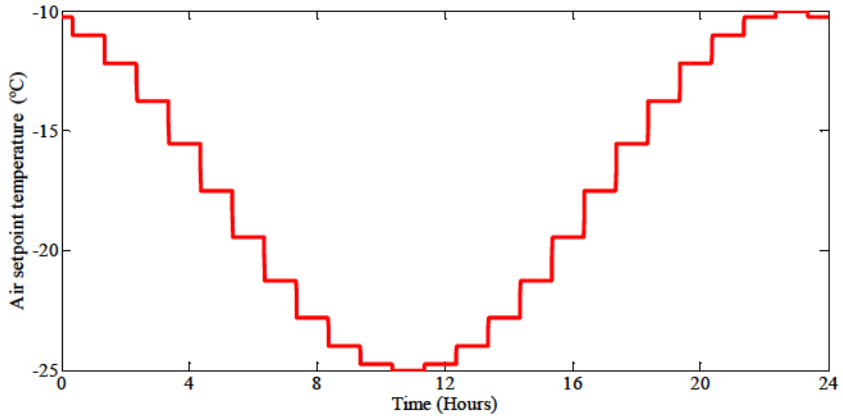

Figure 4.3. Experiment setpoint profile

The solar irradiance from the mobile solar simulator was 1000 W/m^2 (on average) for the period of two hours on the second day of the experiment. Considering windows area of about 6 m^2 and glass transmittance of 93%, Figure 4.4 shows solar gain profile:

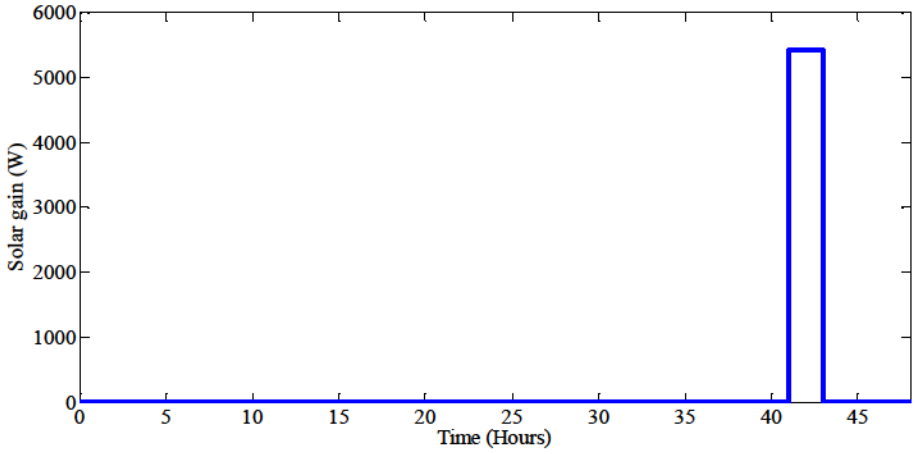

Figure 4.4. Solar gain profile; the width of rectangle is two hours

The energy balance equations for all the nodes and the auxiliary load were solved simultaneously considering time step of 30 seconds. The auxiliary load, calculated by finite difference model for the period of 48 hours is shown in Figure 4.5.

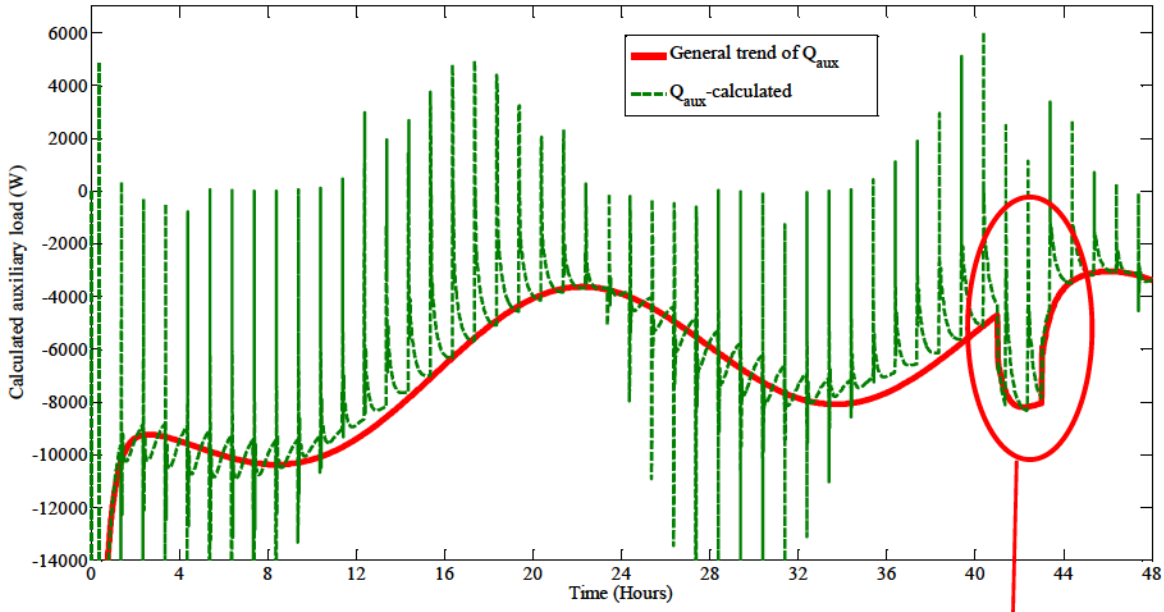

Figure 4.5. Auxiliary load profile calculated by LPFD method

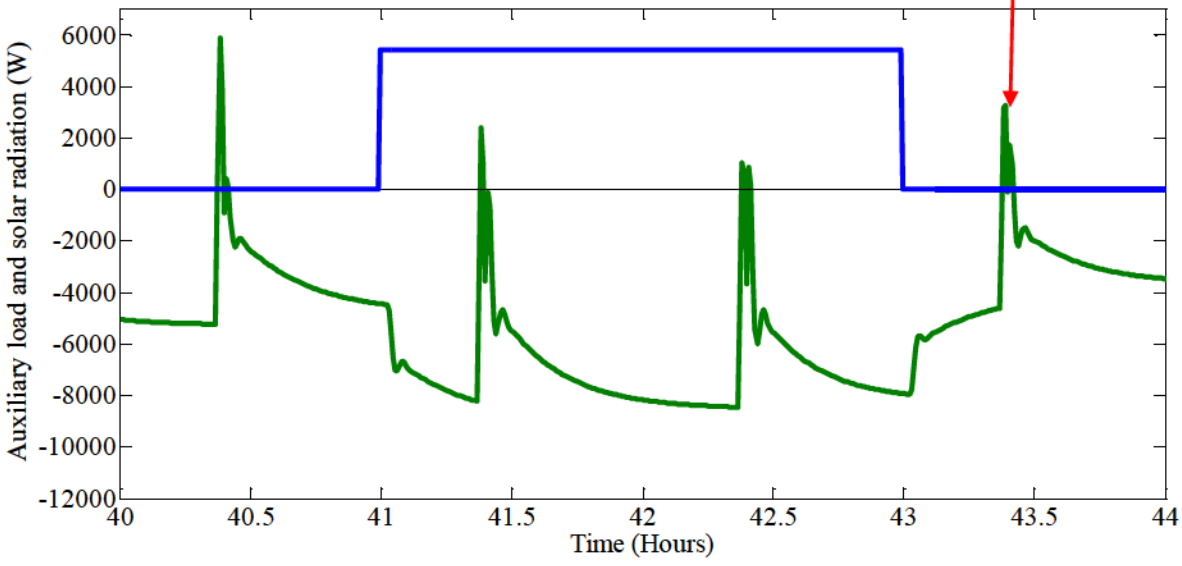

Figure 4.6. Auxiliary load during solar radiation time

As it can be observed, there is a sudden jump and increase in auxiliary load when temperature changes from one step to another and during certain periods of time heating is provided to the Chamber by air handling unit. The red dashed curve shows the *general trend* of the auxiliary load for more clear observation. Also, when the solar simulator gets turned on, the cooling load increases drastically (about 5KW). This is zoomed-in in Figure 4.6. (It should be noted that the total capacity of air handling unit is 4 refrigeration ton equal to 14.07 KW cooling and the heating coil is controlled by a pulse-width module in a proportional manner up to the capacity of 25 KW).

Also there is a good match between simulated air temperature and measured data:

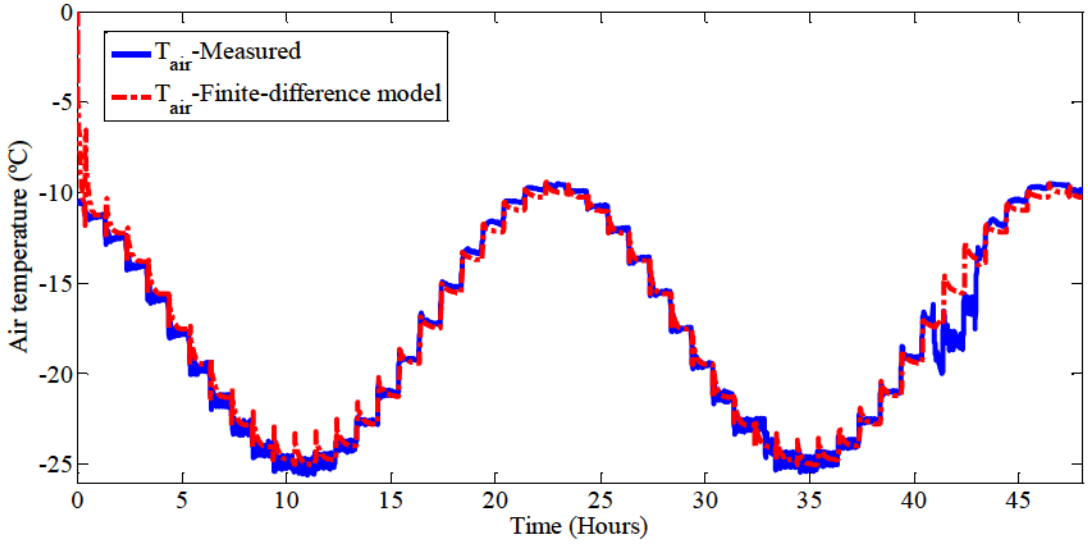

Figure 4.7. Comparison of air temperature profile obtained from finite difference model with measurements

4.1.3 Frequency domain model

Figure 4.8 shows the thermal network for the detailed frequency domain model for the environmental chamber. As described in the previous chapter, floor and each of the walls are represented by their Norton-equivalent network which consist of an equivalent

heat source, Q_{eq} , and a self-admittance, Y_{self} . The equivalent heat source equals to wall's transfer admittance, $Y_{transfer}$, times an equivalent exterior temperature (in this case outdoor air temperature, T_o). For example for node 1(air temperature), $Q_1 = Q_{aux} + U_o T_o ; \left(U_o = U_{inf} + U_{win}\right)$, or for node 3 (wall), $Q_3 = -Y_{transfer,3} \cdot T_o$.

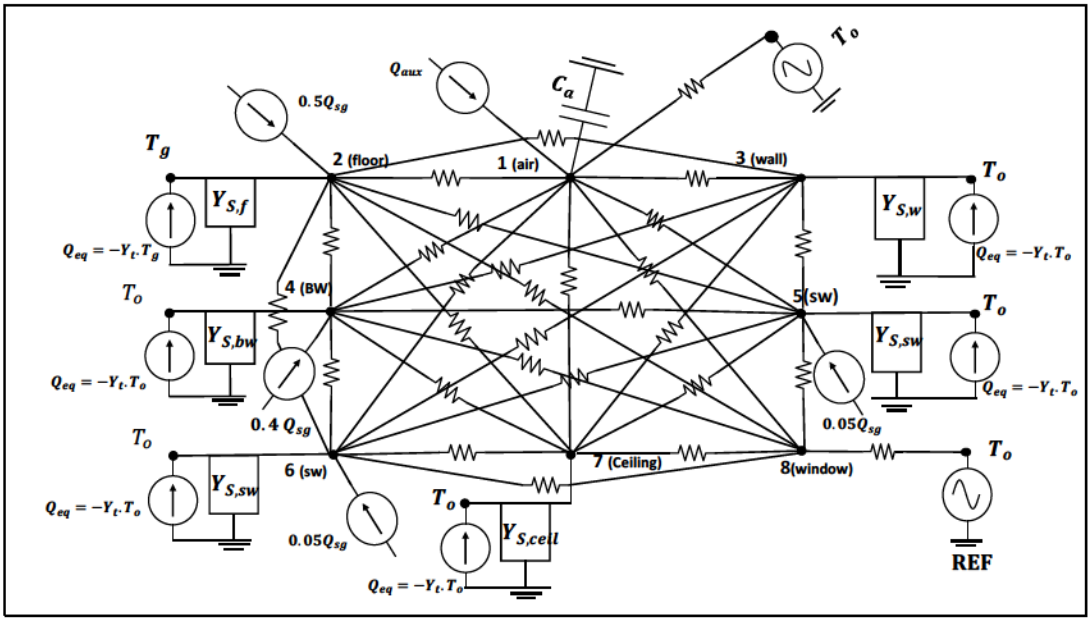

Figure 4.8. Detailed frequeny domain thermal network (nodes: 1:air, 2:floor, 3:wall, 4:backwall, 5:sidewall, 6:sidewall, 7:ceiling, 8:window)

Now considering all the nodes, the equation (3.6) for this case will be:

$$\begin{bmatrix}
sC_a + \sum_j U_{1j} + U_{inf} & -U_{12} & -U_{13} & -U_{14} & -U_{15} & -U_{16} & -U_{17} & -U_{18} \\
-U_{12} & Y_{Self,2} + \sum_j U_{2j} & -U_{23} & -U_{24} & -U_{25} & -U_{26} & -U_{27} & -U_{28} \\
-U_{13} & -U_{23} & Y_{Self,3} + \sum_j U_{3,j} & -U_{34} & -U_{35} & -U_{36} & -U_{37} & -U_{38} \\
-U_{14} & -U_{24} & -U_{34} & Y_{Self,4} + \sum_j U_{4,j} & -U_{45} & -U_{46} & -U_{47} & -U_{48} \\
-U_{15} & -U_{25} & -U_{35} & -U_{45} & Y_{Self,5} + \sum_j U_{5,j} & -U_{56} & -U_{57} & -U_{58} \\
-U_{16} & -U_{26} & -U_{36} & -U_{46} & -U_{56} & Y_{Self,6} + \sum_j U_{6,j} & -U_{67} & -U_{68} \\
-U_{17} & -U_{27} & -U_{37} & -U_{47} & -U_{57} & -U_{67} & Y_{Self,7} + \sum_j U_{7,j} & -U_{78} \\
-U_{18} & -U_{28} & -U_{38} & -U_{48} & -U_{58} & -U_{68} & -U_{78} & \sum_j U_{8,j}
\end{bmatrix}
\begin{bmatrix} T_1 \\ T_2 \\ T_3 \\ T_4 \\ T_5 \\ T_6 \\ T_7 \\ T_8 \end{bmatrix}
=
\begin{bmatrix} Q_1 \\ Q_2 \\ Q_3 \\ Q_4 \\ Q_5 \\ Q_6 \\ Q_7 \\ Q_8 \end{bmatrix}$$

Note that for node 8 (window) there is no admittance considered due to negligible thermal mass of the window. The view factors between the surfaces are calculated using the correlations introduced by Howell et al. (2010) ,(Appendix B). Then matrix **Z** is obtained by inverting the matrix **Y**.

4.1.3.1 Analysis of building transfer functions

The developed frequency domain model was calibrated by experimental data as shown in Figure 4.9. In the calibration process it was observed that thermal bridges (openings for pipes, door frames…) which exist in the chamber envelope have a significant effect and should be considered in the model. There is also a small heating system around the door frame in order to prevent the door from getting frozen and stuck on its frame when there is low-temperature inside.

Figures 4.9-4.12 show the result of frequency domain model for different harmonics versus experimental data. As we can see by increasing the number of harmonics, the model becomes closer to measured data.

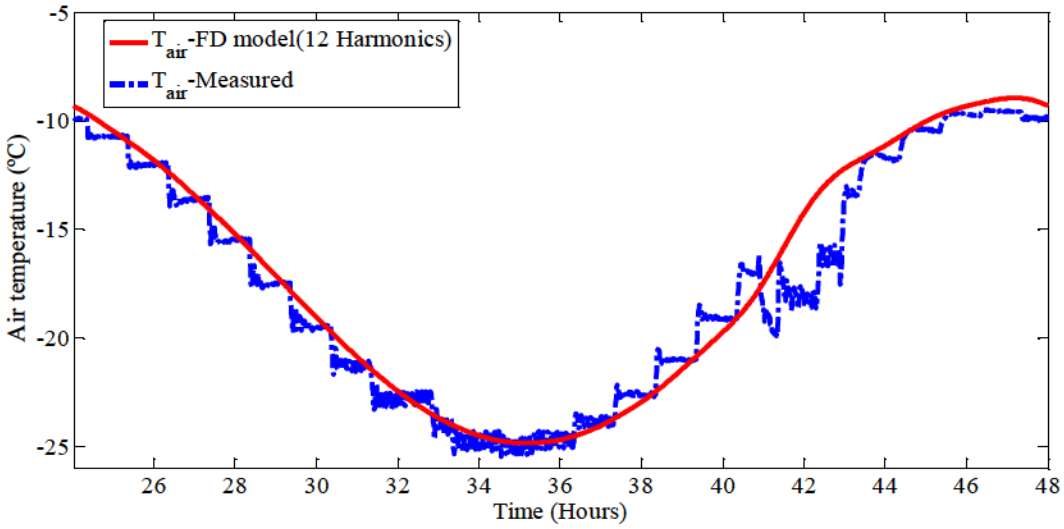

Figure 4.9. Air temperature, simulated (12 harmonics) vs. experimental

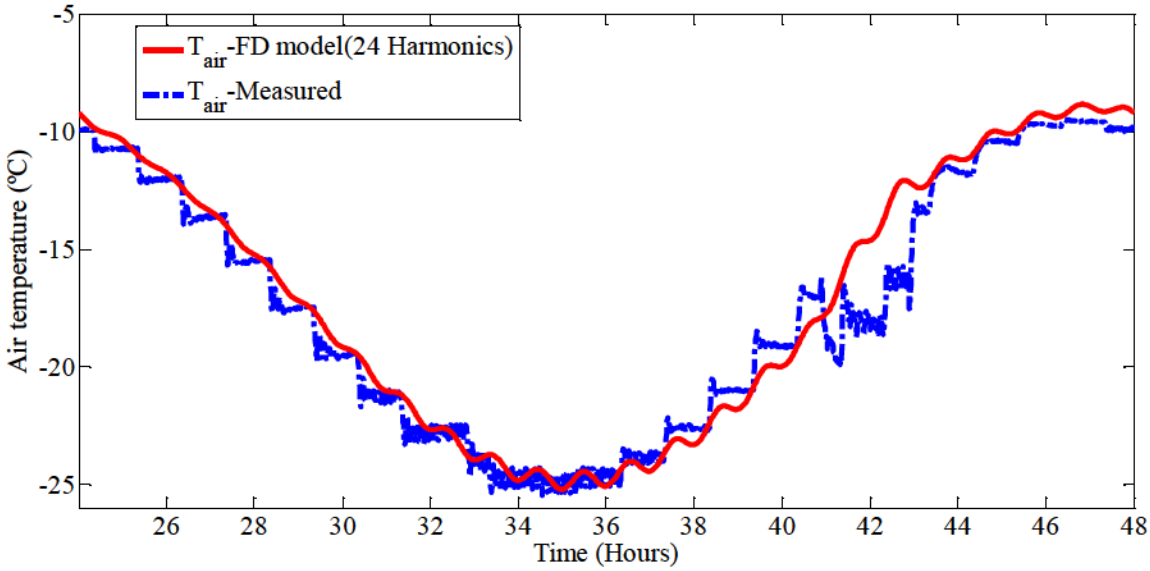

Figure 4.10.Air temperature, simulated (24 harmonics) vs. experimental

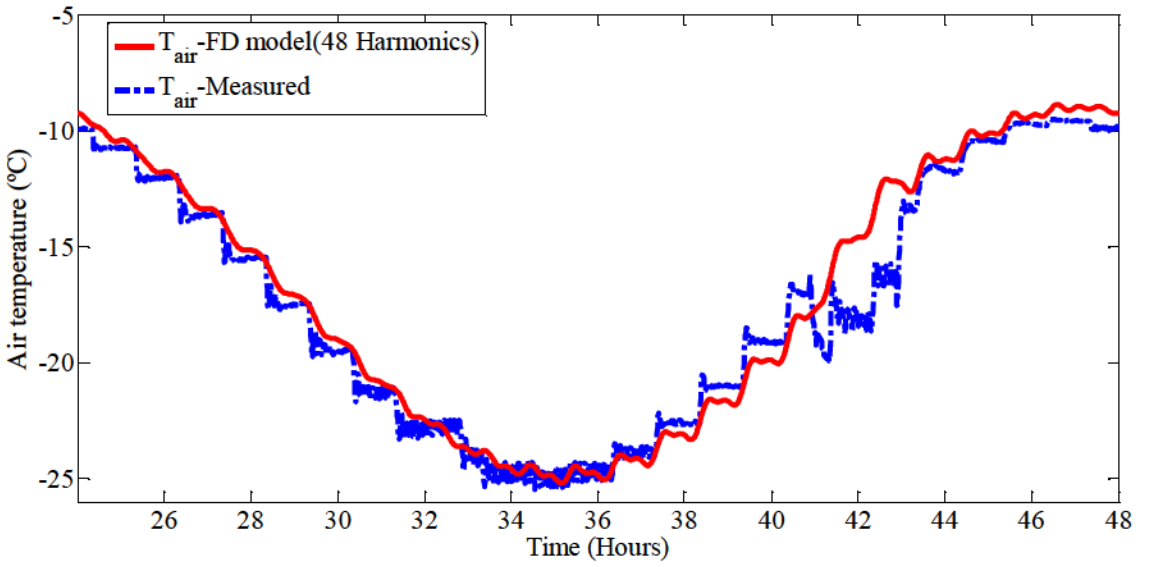

Figure 4.11.Air temperature, simulated (48 harmonics) vs. experimental

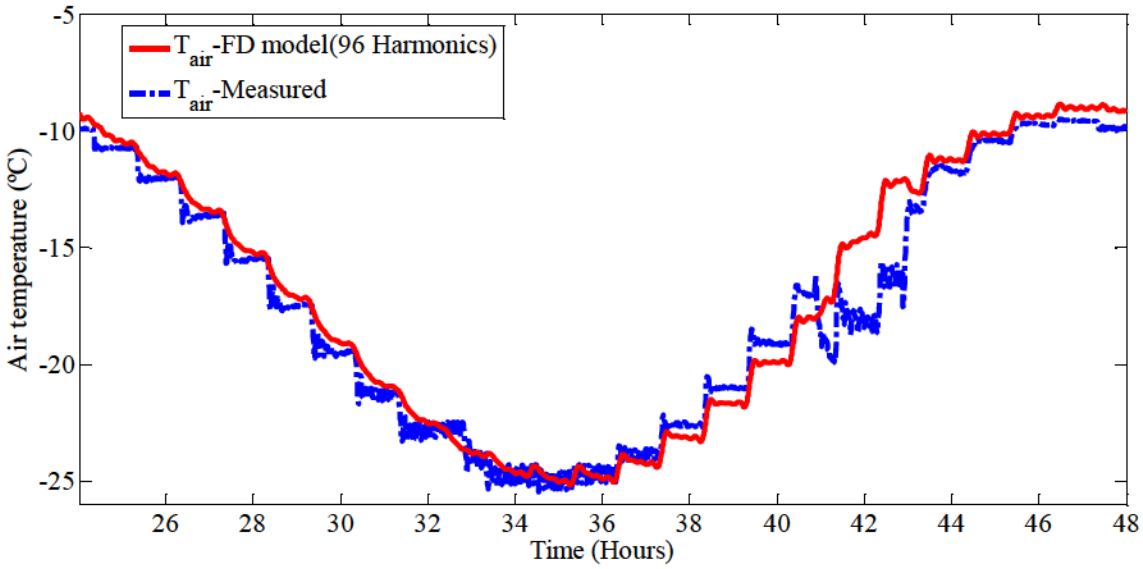

Figure 4.12.Air temperature, simulated (96 harmonics) vs. experimental

Building transfer functions are obtained by calculating matrix **Z** at discrete frequencies. One of the important transfer functions to study is $Z_{1,1}$, the transfer function between air temperature (T_1) and the source at node 1 (Q_1). A mathematical equation for this transfer function is obtained (equation (4.3)) by performing the modified least-squares fitting technique described in chapter 3:

$$Z_{1,1}(s) = \frac{0.005498 + (85.39)s + (9.078\times10^{4})s^{2} + (1.467\times10^{7})s^{3}}{1 + (3.883\times10^{4})s + (2.133\times10^{8})s^{2} + (8.216\times10^{10})s^{3}} \qquad (4.3)$$

The Bode plot (Figure 4.13) shows the fitted transfer function versus the exact response of the system.

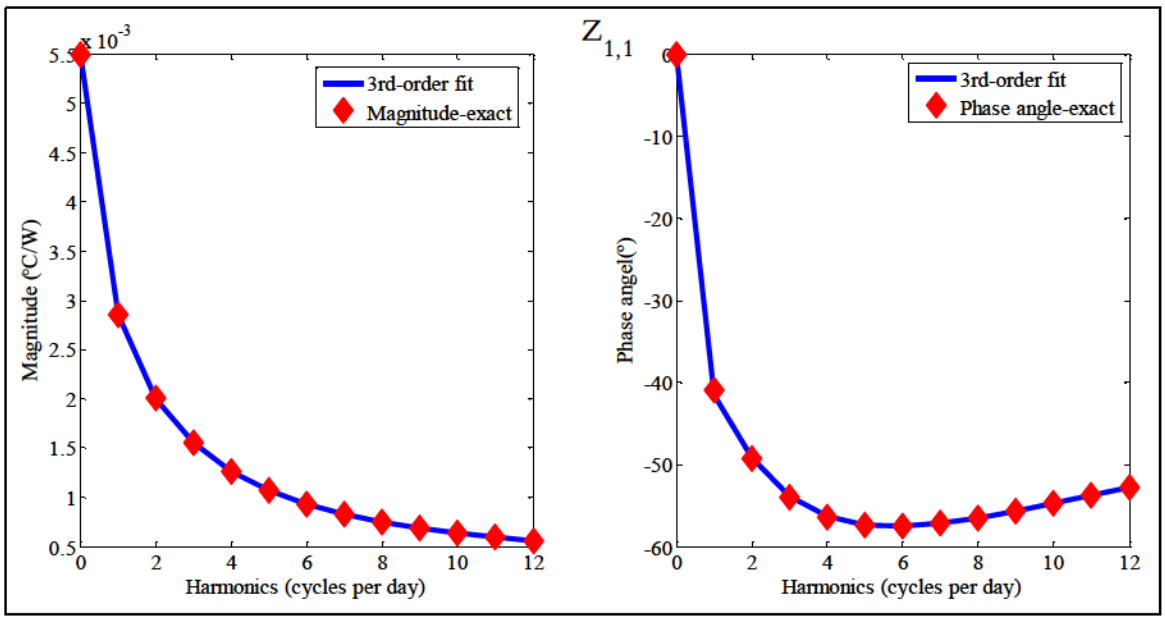

Figure 4.13. Bode plot for $Z_{1,1}$,discrete frequency responses vs fitted transfer function

In Figure 4.13 for *x*-axis, instead of frequency, ω_n, the harmonics, n, were used for easier interpretation. The plot shows a very good fit both in magnitude and phase, with the maximum error less than 2%. As can be seen from Figure 4.13, by increasing the frequency (cycles per day) the magnitude drops respectively. This phenomenon shows a low-pass filter effect that passes low-frequency signals and attenuates higher frequency ones.

It is important to consider that in the analysis of variables with a dominant diurnal harmonic (n=1) such as solar radiation and exterior temperature, the magnitude and phase angle of diurnal frequency is the most important to be studied (Athienitis and Santamouris 2002). It can be seen from the Bode plot on Figure 4.13, the first harmonic has the highest magnitude. One can determine the approximate delay in the response of the room temperature to Q_1, the auxiliary cooling load, by observing the phase angle of the first harmonic (Athienitis et al. 1990). From the phase angle plot in Figure 4.13, the phase angle, $\phi(\omega_1) = -40.89^{\circ}$. The minus sign indicates delay. Now considering 24 hours period, a

delay of: $-40.89^{\circ} \times \frac{24 \text{ hours}}{360^{\circ}} \cong 2.7 \text{ hours}$ in the room temperature response to the source Q_1 is expected. This result is verified by looking at the time plot of the variables shown on Figure 4.14:

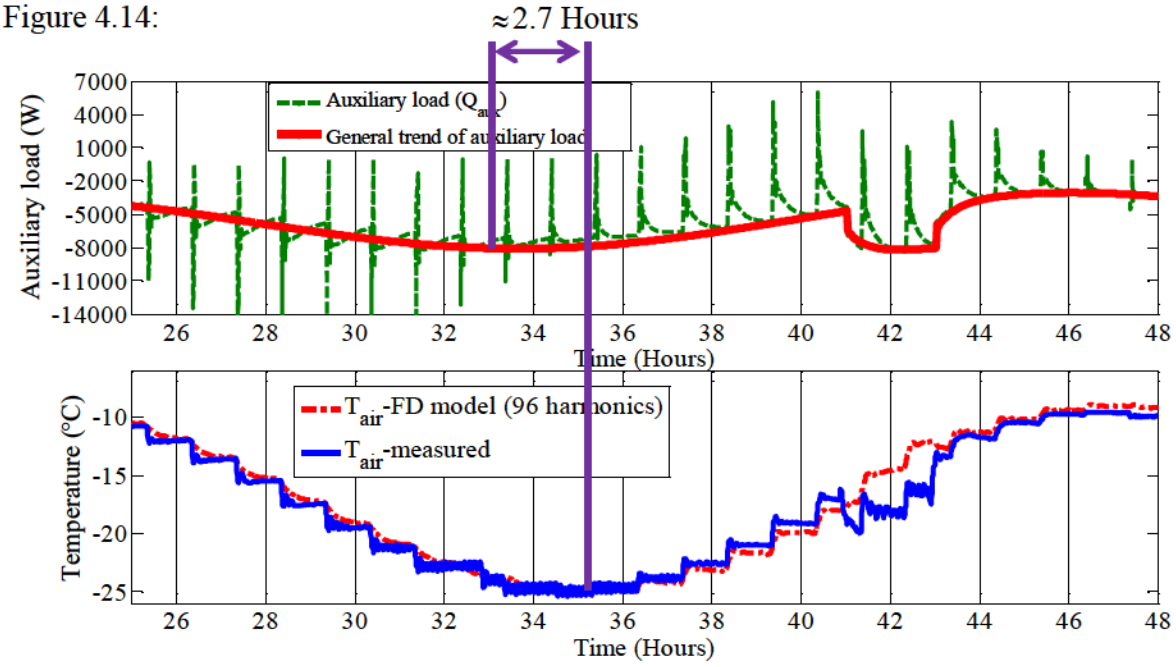

Figure 4.14. Delay in room temperature response to auxiliary cooling

Figure 4.14 shows an extremely important result. This means that there is an approximately 2.7 hours delay between the peak of air temperature and the cooling load.

Another important transfer function is $Z_{1,2}$, between the solar gain on the floor and air temperature. In this case the phase angle equals to -61.2°, which represents the delay of 4.08 hours in the room temperature response to the solar gain on the floor. This is reasonable because the concrete floor has a high thermal mass and it will take a while for it to release the absorbed heat.

Considering that the concrete floor is the largest thermal mass in the building, it is important to evaluate its thermal response. It has been verified that the delay in the floor

temperature response to Q_1 (cooling load) and Q_2 (solar gain on the floor) is 4.079 hours and 2.86 hours respectively.

4.1.4 Low-order, grey-box RC circuit model

This section presents the development of low-order, grey-box RC circuit for the Environmental Chamber (EC). As stated in chapter 3, first a thermal network configuration for the building is proposed and the parameters are calculated using the material physical properties (see Appendix A). The result of the simulation using the initially proposed values for circuit parameters will be used as the initial condition for the optimization routine. Here, three circuit configurations are proposed for the Environmental Chamber. Each of these RC circuits is described in the following section. It should be reminded that the models have three inputs: outdoor air temperature (T_o), solar gains (Q_{SG}) and auxiliary load (Q_{aux}).

Figure 4.15 shows the first proposed circuit for the EC. This circuit consists of two capacitances and three resistances. C_1 is considered to represent the total thermal capacitance of the floor and envelope walls and C_2 represents thermal capacitance of the interior space. Both nodes (1) and (2) are connected to outdoor air temperature (node (3)) by R_{13} and R_{23} respectively. The solar gains heat source is entered into node (1) and the auxiliary power into node (2). The circuit parameters are calculated from basic heat transfer equations considering the physical properties of the building and shown in Table 1:

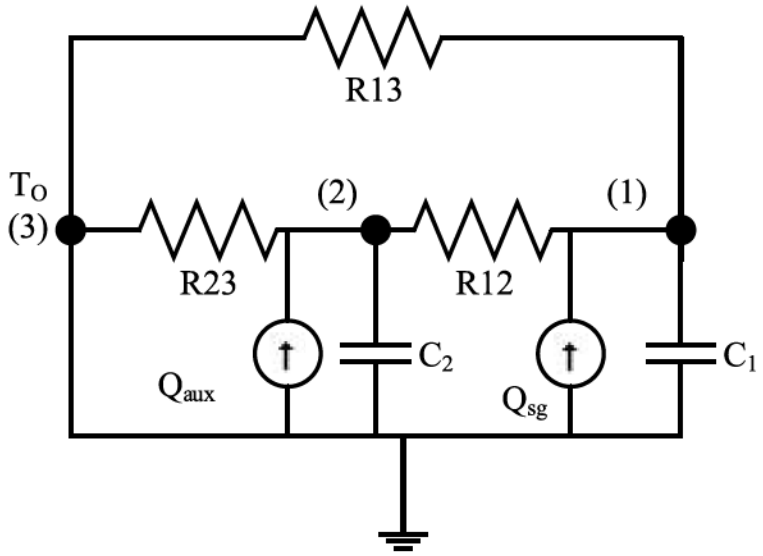

Figure 4.15. 2nd -order RC circuit model for EC

Circuit parameters	Calculated values
C_1 (J/K)	8,362,000
C_2 (J/K)	341,600
R_{12} (K/W)	0.00433
R_{13} (K/W)	0.023
R_{23} (K/W)	0.031

Table 1.initially proposed values for the 2nd-order circuit parameters

Air temperature (temperature of node 2) is the main output of interest. Figure 4.16 shows the simulation result with the initially proposed circuit values:

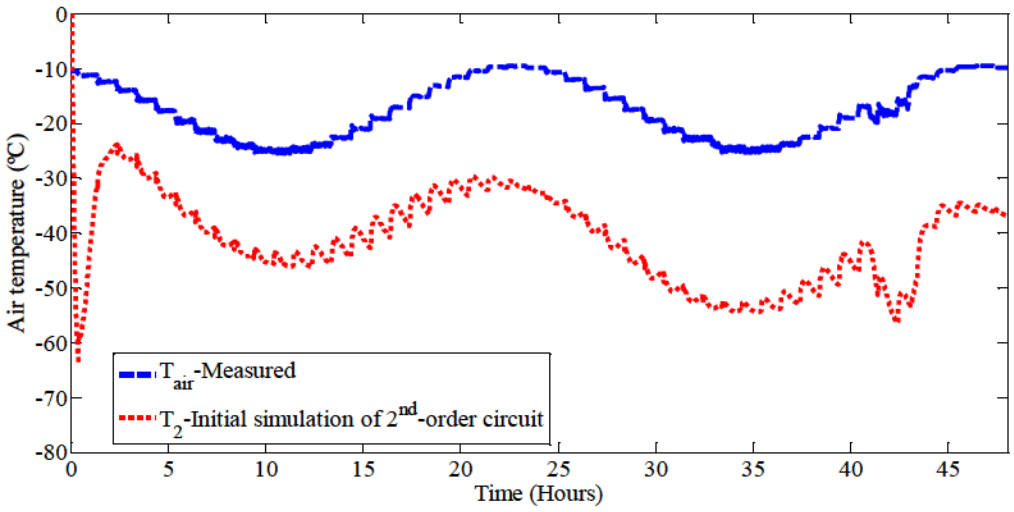

Figure 4.16. Air temperature profile; initial simulation vs. measured

As can be observed there is significant discrepancy between the temperature profile of node 2 (T_2) and the measured data. Thus, an optimization exercise of the R and C values of the circuit with respect to an objective function is performed. First of all, the RC circuit is described by the following convention as *a text file*: type of the element (R or C) followed by the nodes between which the element is situated and the value of the element (Candanedo et al. 2014). For the circuit shown on Figure 4.16 we have:

C	1	0	8362000
C	2	0	341600
R	1	4	0.00433
R	1	2	0.023
R	2	3	0.031

Table 2. Values of RC network as shown in a text file

The node #0 is the reference node or ground node. Here, the states of the system are defined by the temperature of the nodes with thermal capacitances connected to the ground. The "inputs" for the RC circuit are also provided in another text file as:

Q	1	1
Q	2	1
T	3	

Table 3. Inputs of the circuit as a text file

The letter (Q or T) shows the type of input (heat flux or temperature), the second element represents the entry node of the source and the third element (only for heat sources) shows the fraction of input that affects the entry node. Finally, the outputs are indicated in another text file. For example, the temperatures of the nodes 1 and 2 (which are the states) are expressed as outputs:

T	1
T	2

Table 4. Output of the RC network as shown in a text file

Then, after defining the RC circuit, the circuit is converted to an equivalent canonical state-space representation. For this purpose, a MATLAB function RCT2SS[2] is used which takes the RC circuit in the form described above and gives its state-space representation.

To perform optimization the MATLAB Optimization Toolbox™ is used. Here the objective function is defined as:

$$J = \left\| T_2 - \hat{T}_2 \right\| = \sqrt{\sum_{i=1}^{n} (T_{2_i} - \hat{T}_{2_i})^2} \tag{4.4}$$

by calculating J and running the optimization[3], the new R and C values are obtained for the circuit. Figure 4.17 shows the simulation result (for T_2) with the new circuit parameters obtained from optimization:

[2] Developed by José A. Candanedo and Vahid R. Dehkordi at CanmetENERGY, Varennes
[3] Optimization algorithm is explained in appendix D

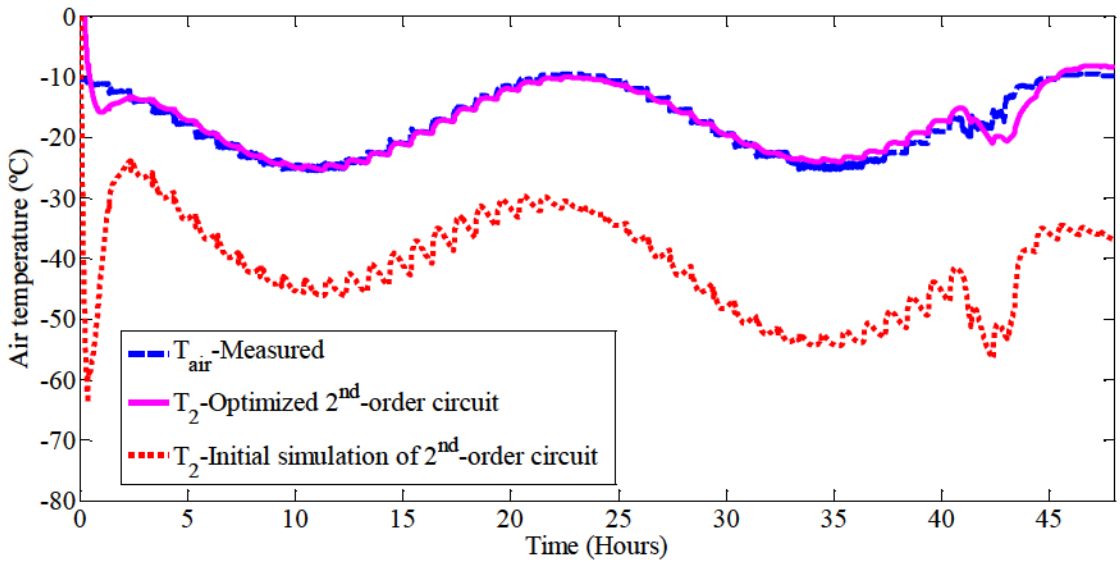

Figure 4.17. Air temperature profile with the new circuit parameters vs. initial profile

The new circuit values obtained are:

Parameters	New values obtained	Initial values
C_1 (J/K)	1,220,0136	8,362,000
C_2 (J/K)	1,357,352	341,600
R_{12} (K/W)	0.00338	0.00433
R_{13} (K/W)	0.006	0.023
R_{23} (K/W)	0.033	0.031

Table 5. Comparison of 2nd-order RC circuit parameters

Figure 4.18 shows the error of fit. It is observed that the fit error is typically less than 2ºC:

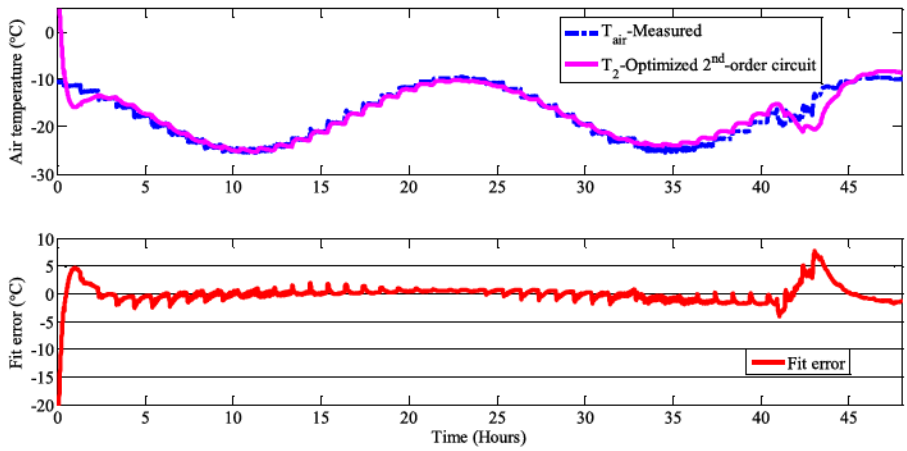

Figure 4.18. Error of fit for optimized 2nd-order RC circuit

The calibrated RC values provide a better fit to the measured air temperature both in phase and amplitude. However, it should be taken into consideration that this is only a second-order model and higher order models may further improve the fitting. Thus, two other circuit configurations are considered; one with three capacitances and four resistances (third-order model) and another one with four capacitances and 5 resistances (fourth-order model) as shown in Figure 4.19 and Figure 4.25.

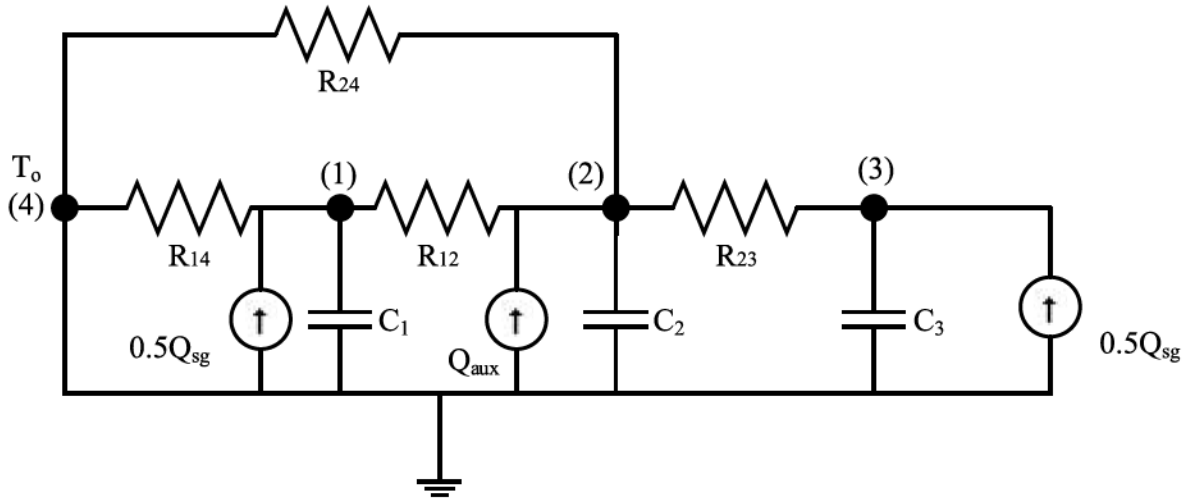

Figure 4.19. 3rd-order RC circuit model for EC

In the RC circuit shown in Figure 4.19 , C_1 represents the thermal capacitance of the envelope, C_2 represents the thermal capacitance of the interior space and C_3 represents

the thermal capacitance of the floor. Solar gains are assumed to be divided equally between the envelope and the floor. R_{24} is the resistance between indoor and outdoor air and accounts for the effect of infiltration, windows and doors. Figure 4.20 shows the simulation result using the initially proposed parameters:

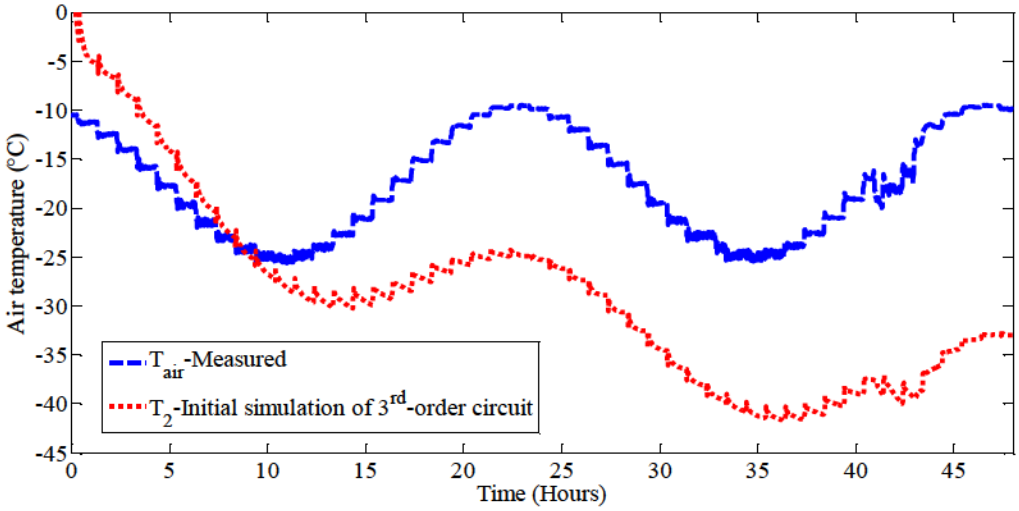

Figure 4.20. Result of initial simulation for the 3rd-order RC circuit

and Figure 4.21 shows the new curve for the air temperature after running the optimization:

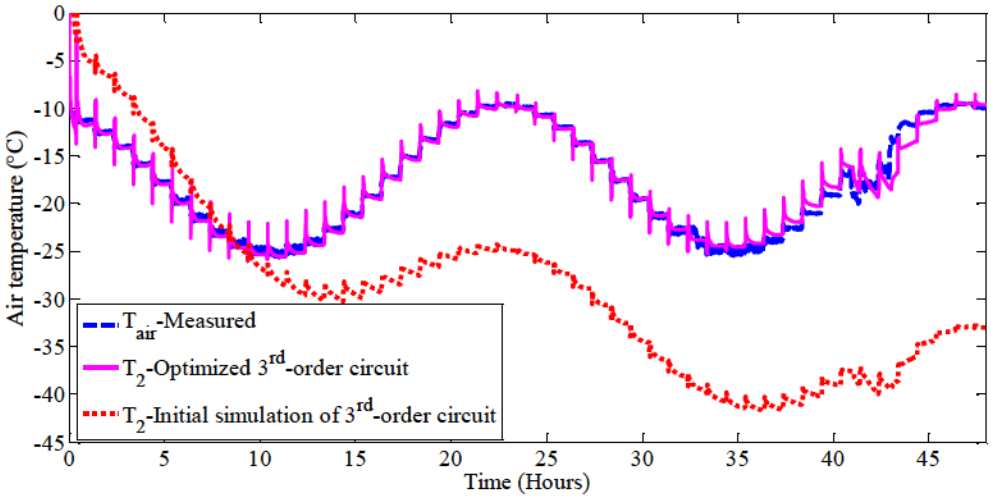

Figure 4.21. Comparison of the results for the 3rd-order RC circuit model

A better fit between modeled and measured air temperatures is observed. The optimized R and C values for the circuit are in the same order of magnitude as the originally proposed ones.

Parameters	Initially proposed values	New values obtained through optimization
C_1 (J/K)	1,783,000	1,577,415
C_2 (J/K)	341,600	110,473
C_3 (J/K)	6,579,000	5,406,491
R_{14} (K/W)	0.023	0.027
R_{12} (K/W)	0.0004095	0.000751
R_{23} (K/W)	0.003192	0.006294
R_{24} (K/W)	0.031	0.0103

Table 6. Comparison of the initially proposed values for circuit parameters with the ones obtained from optimization

The fit error is shown in Figure 4.22 :

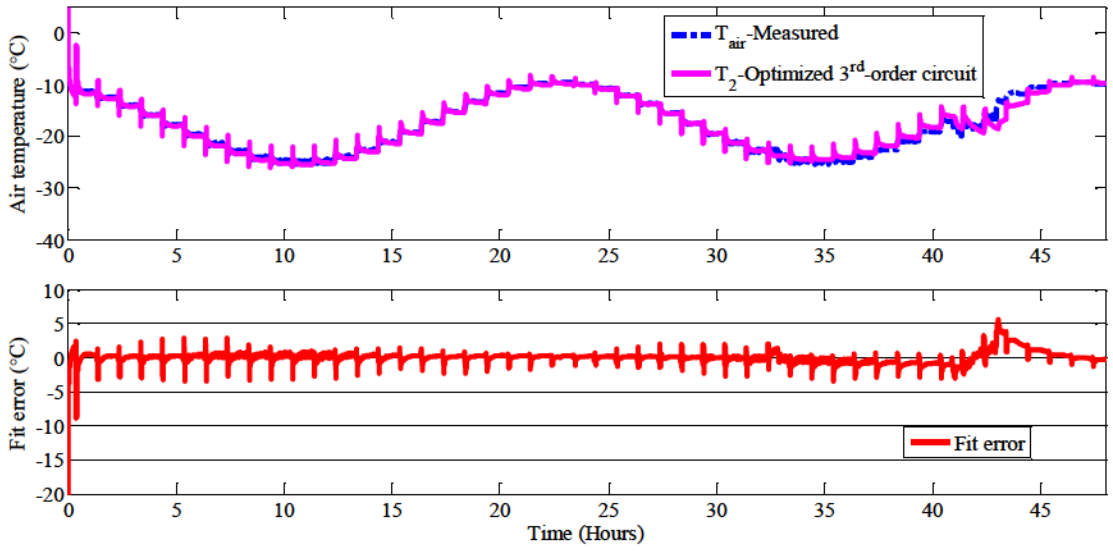

Figure 4.22. Fit error for the optimized 3rd-order RC circuit

Again the fit error is typically less than 2ºC. However, there has been a decrease in the value of C_2, which physically may not be realistic. Trying to get a more realistic value, the data is downsampled and the optimization is repeated. After running several cases, with a downsampling factor of 20 (taking every 20th number), the following results are obtained:

Parameters	Initially proposed values	New values obtained through optimization
C_1 (J/K)	1,783,000	1,149,698
C_2 (J/K)	341,600	616,706
C_3 (J/K)	6,579,000	5,337,767
R_{14} (K/W)	0.023	0.0105
R_{12} (K/W)	0.0004095	0.00126
R_{23} (K/W)	0.003192	0.00663
R_{24} (K/W)	0.031	0.0212

Table 7. 3rd-order optimized RC circuit with downsampled data

Now this circuit shows a more realistic value for the internal capacity of the chamber (C_2). However, it should reminded that these numbers are "equivalent" values rather than physical ones. Figure 4.23 shows simulation results using those circuit values:

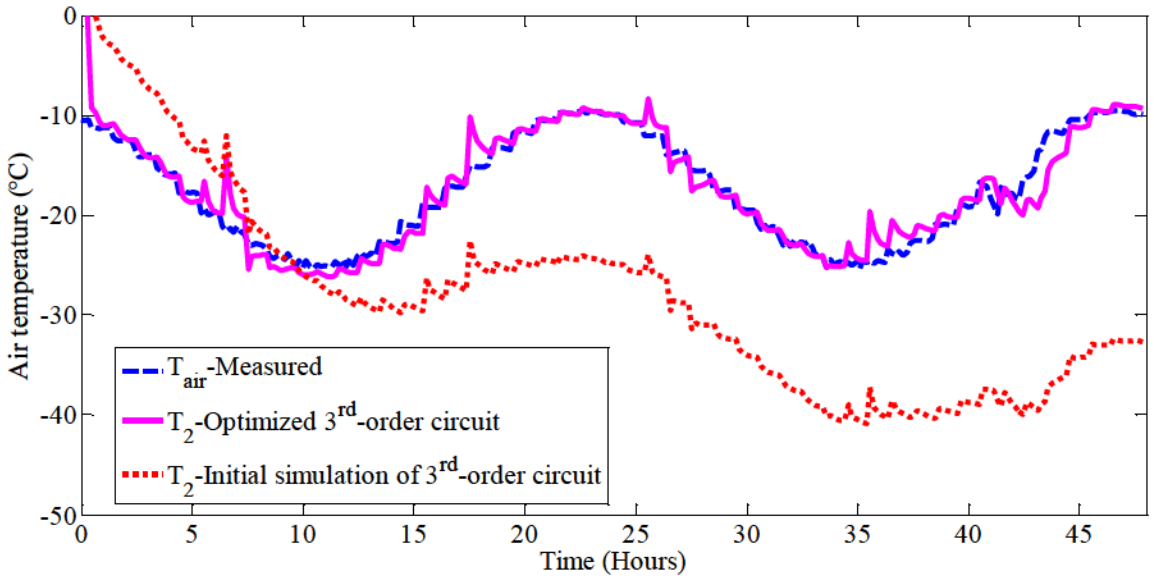

Figure 4.23.Result for 3rd-order RC circuit with downsampled data

The fit error is shown at the bottom of Figure 4.24:

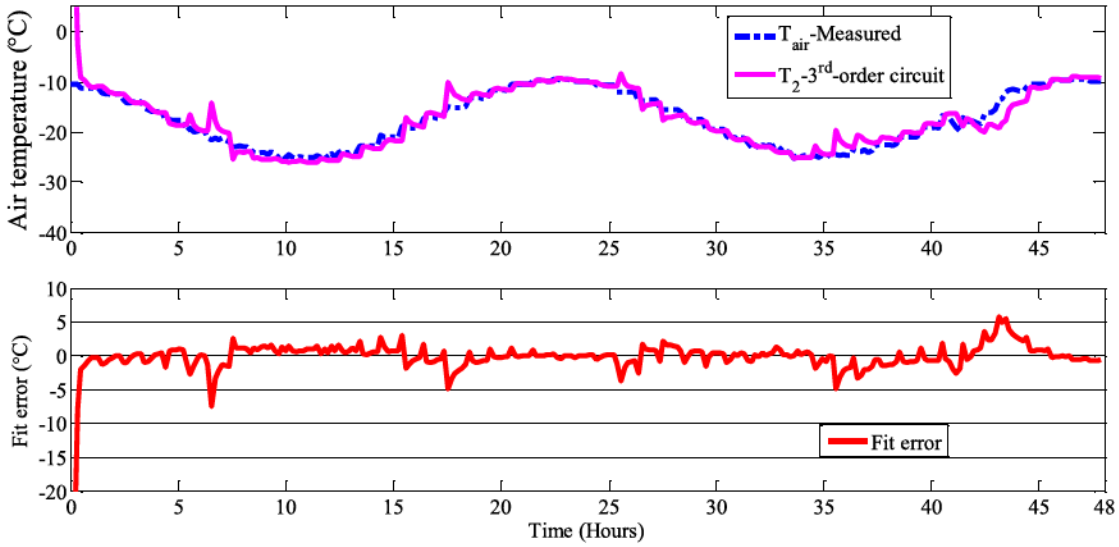

Figure 4.24. Fit error for 3rd-order optimized RC circuit with downsampled data

Now, let us consider the circuit configuration shown in Figure 4.25. In this RC circuit, C_1 is considered as the summation of the thermal capacitances of the front wall and back wall of the Environmental Chamber, C_2 as the internal space thermal capacitance, C_3 as the summation of thermal capacitances for two sidewalls and ceiling and C_4 is thermal capacitance of the floor.

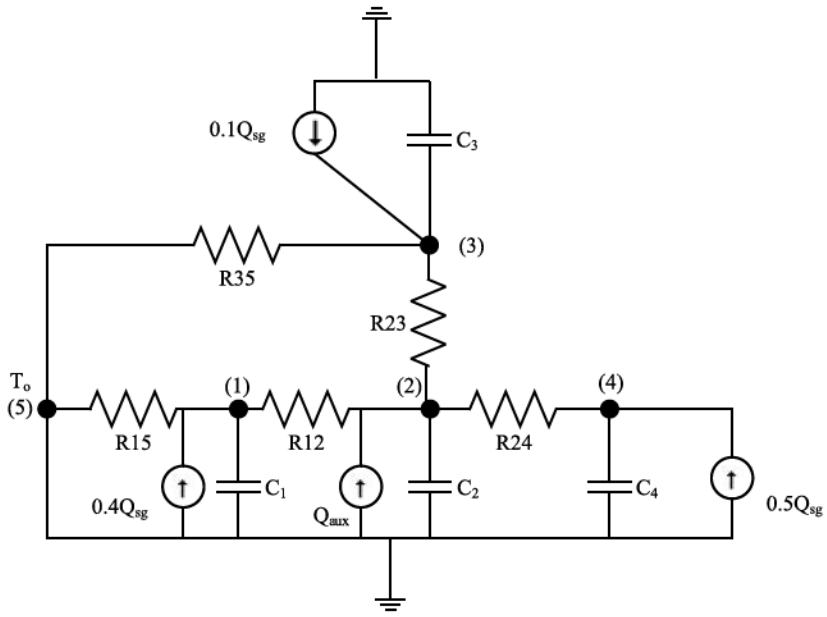

Figure 4.25. 4th-order RC circuit model for EC

For this configuration the data was downsampled by a factor of 25. Figure 4.26 shows the simulation results using the circuit parameter values before and after the optimization:

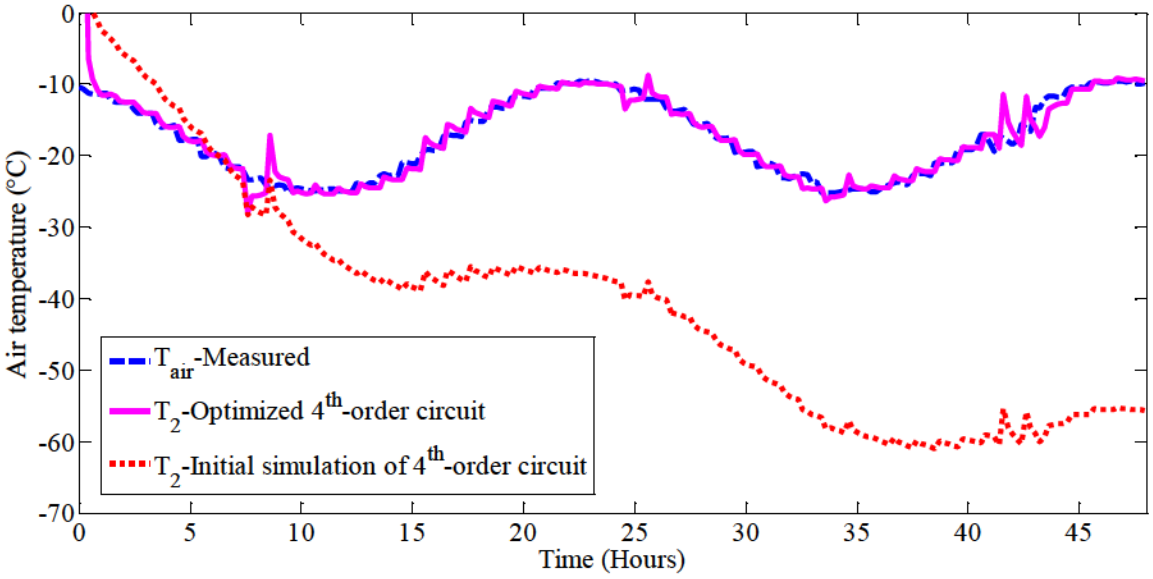

Figure 4.26. Results of simulation for the 4th-order RC circuit model for EC

Table 8 shows the circuit parameter values before and after optimization:

Parameters	Initially proposed values	New values obtained through optimization
C_1 (J/K)	456,600	321,410
C_2 (J/K)	341,600	306,683
C_3 (J/K)	1,327,000	955,168
C_4 (J/K)	6,579,000	5,477,601
R_{15} (K/W)	0.091	0.201
R_{12} (K/W)	0.001599	0.00516
R_{23} (K/W)	0.00055	0.00075
R_{24} (K/W)	0.003192	0.006271
R_{35} (K/W)	0.031	0.0071

Table 8. Comparison of the initially proposed values for 4th-order RC circuit parameters with the ones obtained from optimization

Fit error is shown in Figure 4.27:

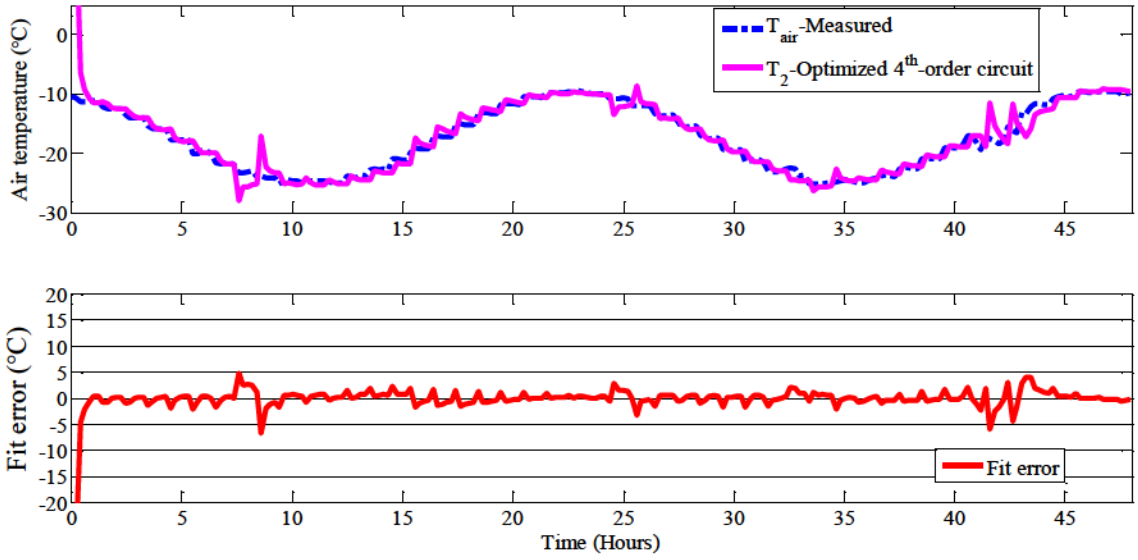

Figure 4.27. Fit error for 4th-order RC circuit

Although different assumptions can be made during the process of modeling a building, one should choose the model that works best for the desirable objective. It is also pointed out that higher order models are not necessarily more useful.

Here, the third-order RC circuit is chosen as the model to work with, since it is physically more reasonable and also the values obtained through optimization are in the same order of magnitude as the calculated physical values. In the next section, different setpoint strategies are studied using the third-order model.

4.1.5 Application of the RC circuit model for a control study

In this section, the third-order model is used for a control study for the Environmental Chamber. In this study, different temperature setpoint transition curves are investigated to evaluate the peak demand corresponding to each curve during the transition period.

As mentioned in the previous section, the main inputs of the third-order model are: outdoor air temperature (T_o), solar gains (Q_{SG}) and auxiliary load (Q_{aux}). Q_{aux} is calculated by the previously introduced detailed finite-difference model (section 4.1.2). Figure 4.28 shows the schematic of the model, inputs and outputs:

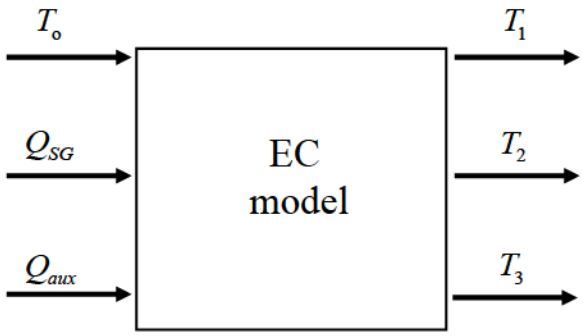

Figure 4.28. Schematic of modeling for EC

Figure 4.29 shows the Simulink representation of the EC model using the PI controller. Figure 4.30 shows that the controller works satisfactorily with the EC model and simulated air temperature matches the setpoint.

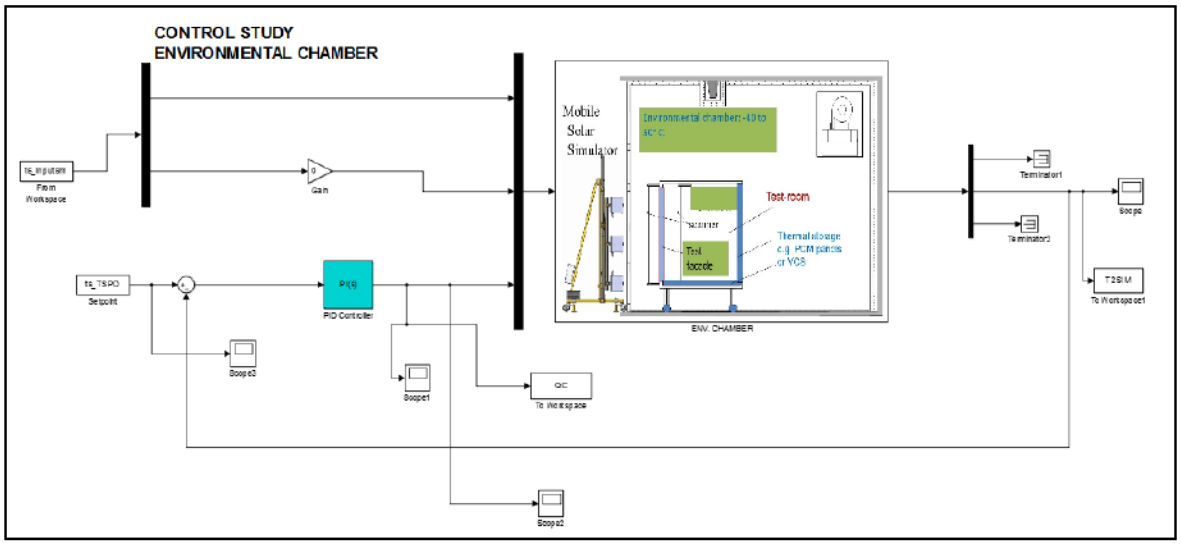

Figure 4.29. Simulink representation of the model for EC

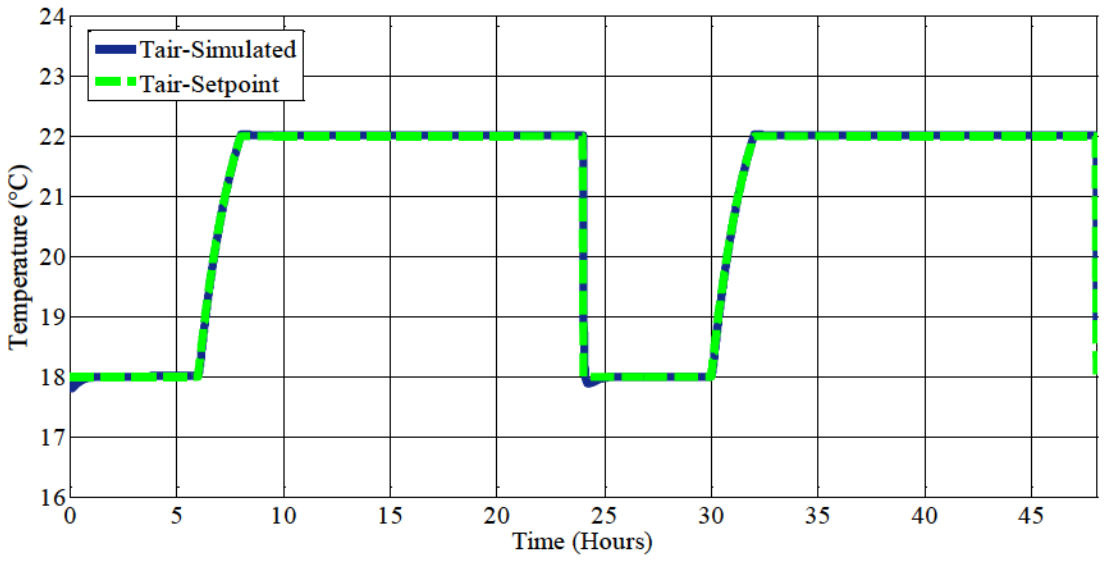

Figure 4.30. Example of setpoint and simulated air temperature using PI controller

To reduce energy consumption in residential buildings, it is common to apply a temperature setback during the night and then, as the day begins, the temperature setpoint is increased to maintain the occupant comfort. The sudden increase in the setpoint temperature and thus in the corresponding auxiliary load produces a heavy load on the grid and therefore it is necessary to reduce the peak load as much as possible. The transition between the two setpoint temperatures can happen in different ways, each producing a different load profile and peak load. Thus, the setpoint transition path is critical in mitigating the peak load.

Here, it is considered to set air temperature at 18°C during the night time and 22° C during the day time. The exterior temperature (T_o) is assumed to be constant and equal to -10ºC during the transition period. Also, it is assumed that there is negligible solar radiation during the transition period. Then, a number of setpoint profiles and their corresponding loads are studied. The first profile considered is the step change setpoint

profile. In this profile there is a sudden change in temperature profile over a very small period of time. Figure 4.31 shows the temperature profile and corresponding load for that:

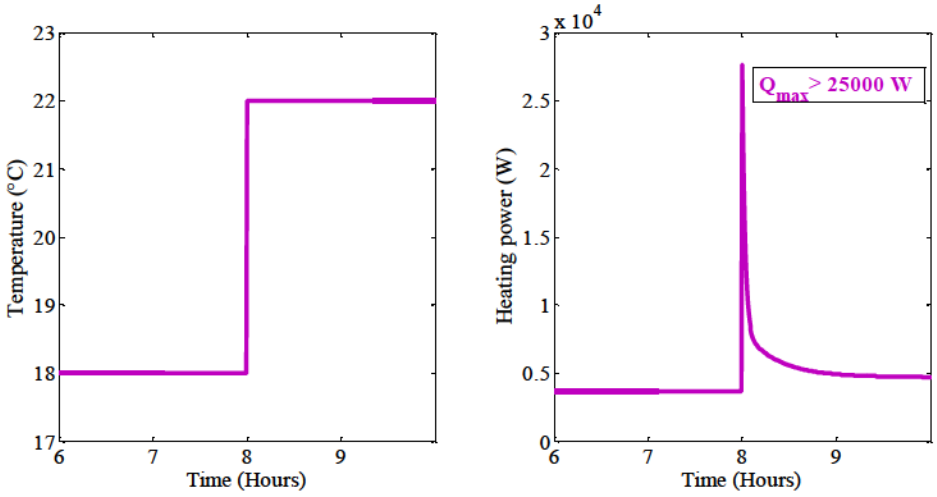

Figure 4.31. Step setpoint profile and the corresponding load

As it can be seen, there is a very significant, sudden increase in the auxiliary load profile. Thus, considering the peak load, this is not the suitable profile to be used in the building. Another profile considered is the linear ramp setpoint profile. Figure 4.32 shows the linear ramp setpoint profile (considering two hours transition time) and its corresponding load:

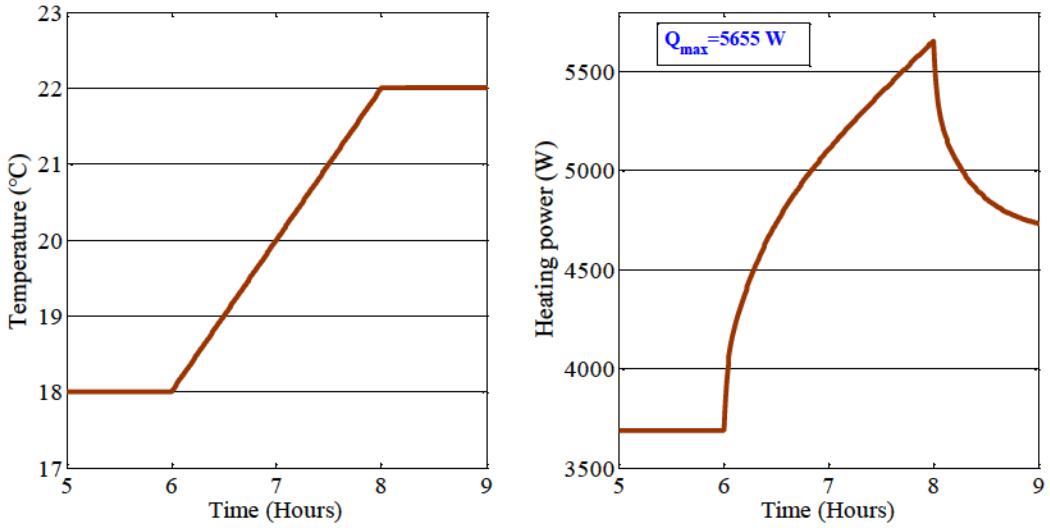

Figure 4.32. Ramp setpoint profile and the corresponding load

A much lower peak is observed for the linear ramp compared to the step setpoint. The maximum load in this case is 5655W. It should be emphasized that this profile corresponds to a two hour transition time and it will have different values by considering other transition times. Linear ramp is also relatively easy to program and implement. We can see that the transition setpoint profile is an important consideration in sizing the equipment and power supplies.

Now here a family of exponential profiles and their corresponding load is considered to be studied. The following equation is proposed and used to create exponential curves:

$$\Delta\theta(t) = \kappa \cdot B\left[1 - B^{-\frac{t}{\Delta t_{transition}}}\right], B = 1 + \frac{\Delta\theta_{total}}{\kappa}, \tag{4.5}$$

where $\Delta t_{transition}$ represents the transition period between the setpoints and $\Delta\theta_{total}$ is the total temperature rise. In equation (4.5) κ is a parameter corresponding to the curvature of the exponential curve and it defines the shape of the curve. Equation (4.5) is function of κ, transition time ($\Delta t_{transition}$) and total temperature rise ($\Delta\theta_{total}$). Figure 4.33 shows the setpoint profiles between 18ºC and 22ºC ($\Delta\theta_{total} = 4°C$) considering different κ values and the corresponding load profiles:

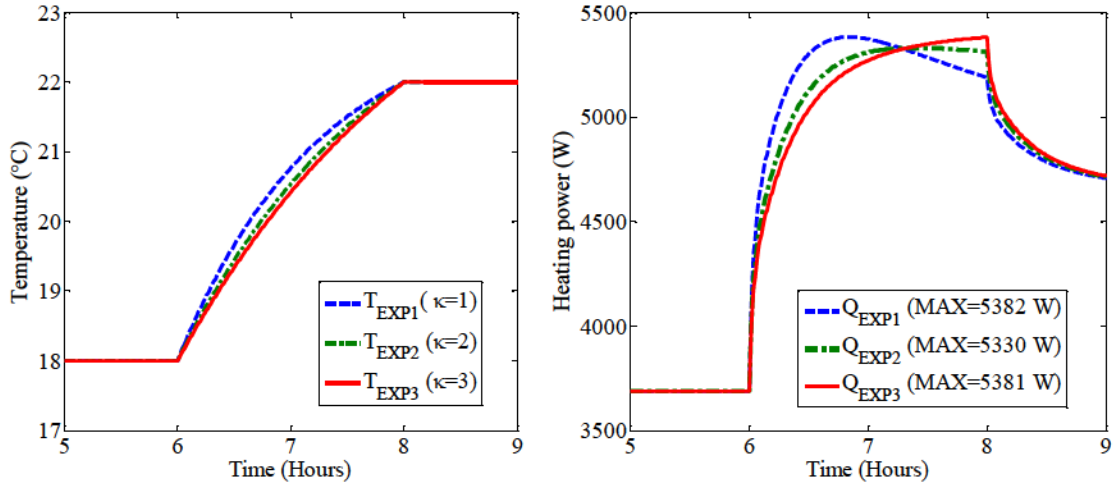

Figure 4.33. Temperature profile with different curvatures (on the left) and the corresponding load (on the right)

In order to be clearer, the above figure is zoomed-in and shown in Figure 4.34:

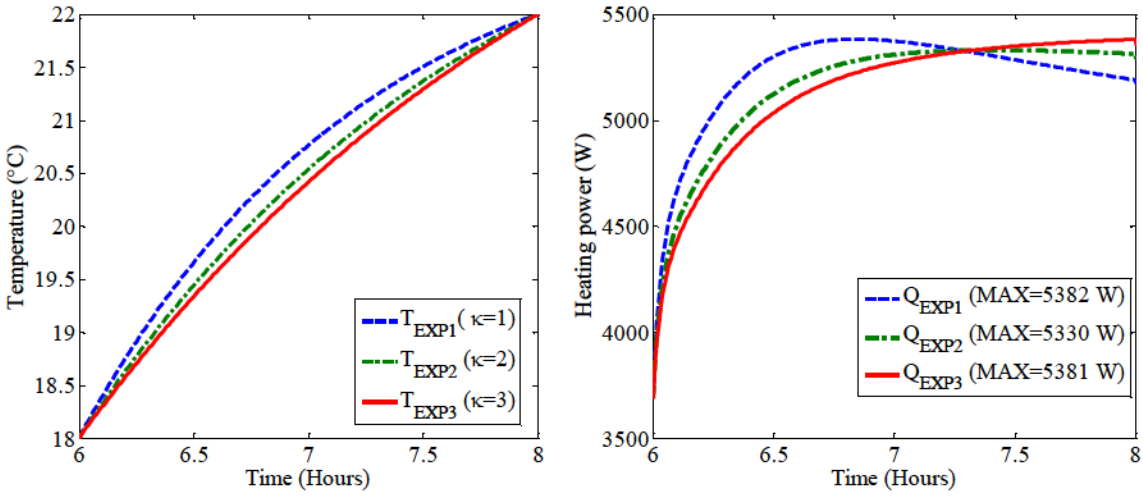

Figure 4.34. Comparison of different exponential curves and their corresponding load

As it can be seen the load profile corresponding to $\kappa = 2$ has the lowest peak equal to 5330W. In fact, an optimization can be performed to obtain the value of κ that corresponds to the minimum peak. This optimization is performed and the value of κ corresponding to minimum peak was found to be 1.87. The peak load in this case is 5329W. This optimal curve is compared with the ramp setpoint profile as shown in Figure 4.35 :

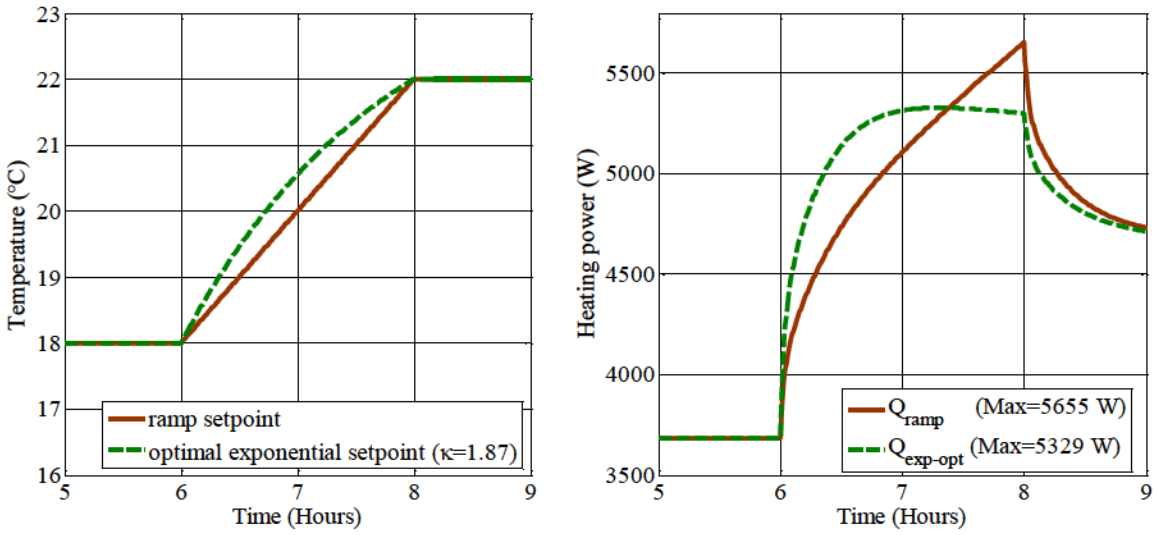

Figure 4.35. Comparison of load profile for linear ramp and exponential setpoints

By comparing the two load profiles, we can see that there is a reduction of 326 W (about 6%) in the peak load.

4.1.6 Effect of transition time on the peak load

Figure 4.36 shows the effect of transition time on the peak loads considering the optimal exponential curve ($\kappa = 1.87$). We can see that by increasing the transition time the peak load gets lower and lower so this is an important consideration to keep in mind.

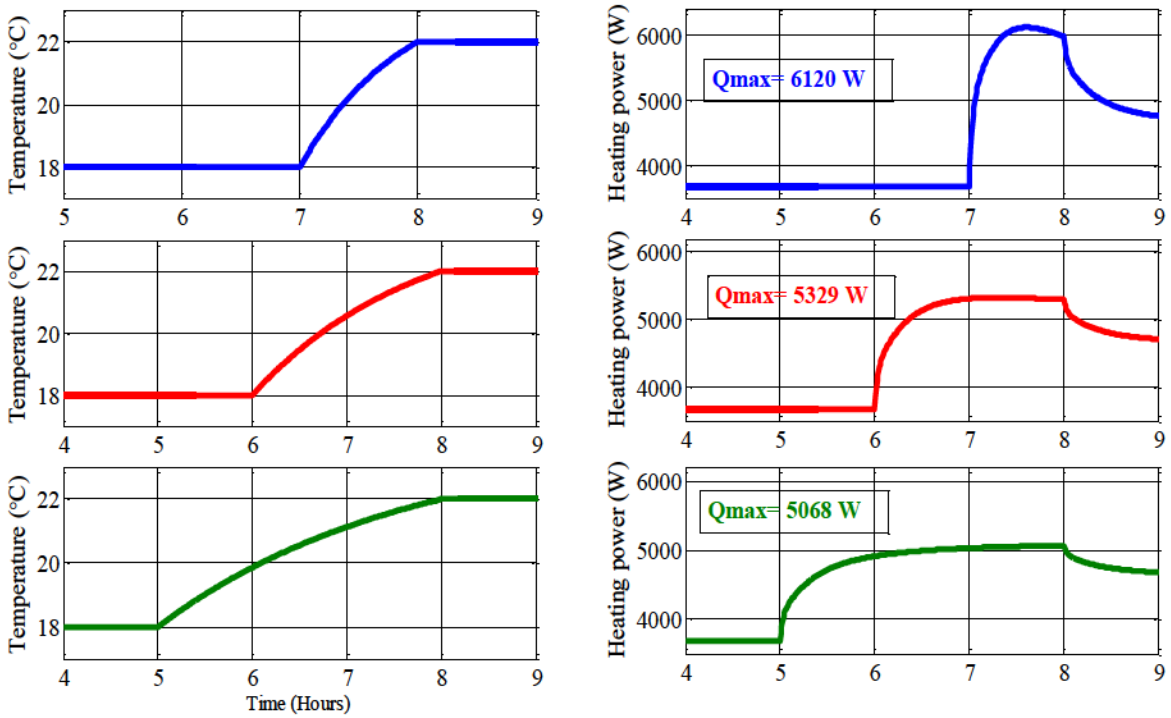

Figure 4.36. Effect of transition time on the peak load

Figure 4.37 show them all in one graph:

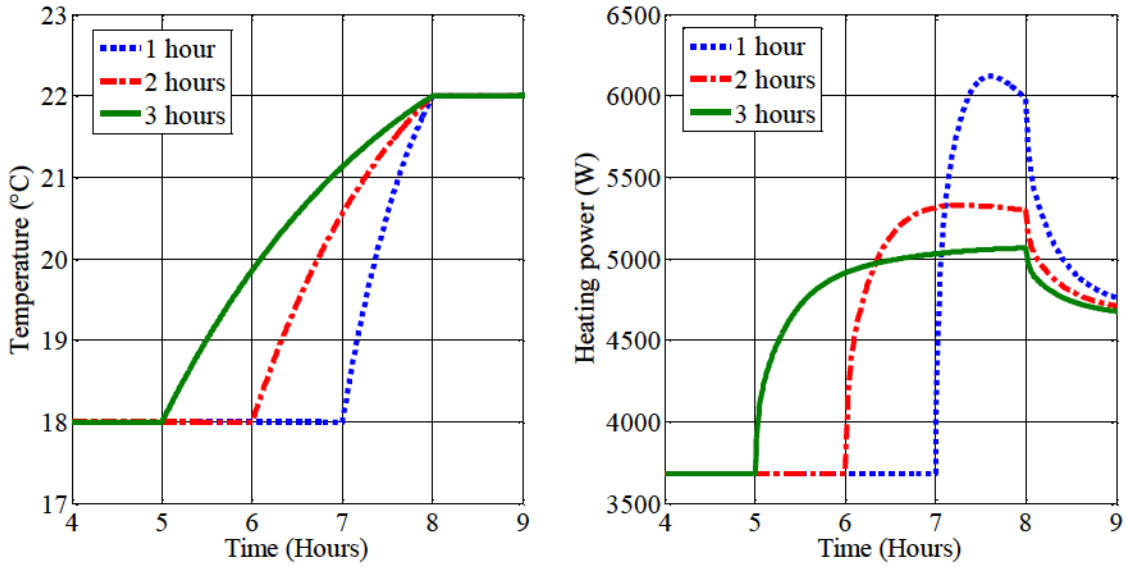

Figure 4.37.effect of transition time (all in a same plot)

Conclusion

Section 4.1.6 demonstrated an application of a low-order RC circuit model. By means of the developed model, different setpoint profiles were studied. The study has shown a considerable potential in peak load reduction in buildings in a relatively inexpensive way. More extensive study on this topic is under completion[4] and the ultimate goal is to find a generalized formula for the optimal setpoint transition profile that can be used for any type of building.

[4] Under a collaborative work on this topic with CanmetENERGY, a paper has been submitted to the journal of Energy and Buildings under the title "Near-optimal Transition between Temperature Setpoints for Peak Load Reduction in Small Buildings".

4.2 EHBE test facility of Hydro-Québec LTE in Shawinigan

In order to ensure its occupant comfort at minimum cost, Hydro-Québec is interested in performing studies on the building energy efficiency and demand management (Lafont 2013). EHBE (Experimentation Houses for Building Energetics), shown on Figure 4.38 and Figure 4.39, is a set of two similar houses built on the site of Hydro-Québec's LTE (Laboratoire des technologies de l'énergie) in Shawinigan and used for building energy studies. The houses have been designed according to the Quebec's standard to be representative of the Quebec's residential buildings and they are highly-instrumented to compare thermal models with reality. Figure 4.40 shows the floor plan and the studied zone.

Each one of the houses consists of several thermal zones. Here, one of the zones are considered to be studied. A frequency domain model is developed for the zone and by means of the model, the effect of different floor coverings on the thermal response of the zone is investigated. Also, the advantage of frequency domain model to evaluate design options for effective thermal performance of the thermal zone is discussed.

Figure 4.38. Twin houses test facility at Shawinigan

Figure 4.39. Twin houses test facility in Shawinigan (Photo courtesy of Jennifer Date)

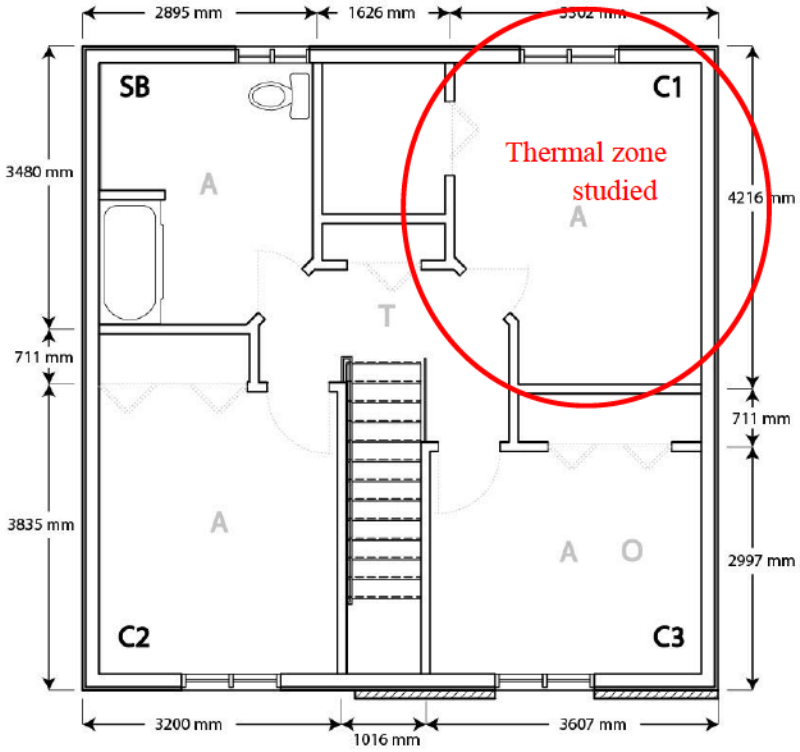

Figure 4.40. Floor plan and the considered thermal zone

4.2.1 Frequency domain model for one zone

The thermal network for the developed frequency domain model is shown in Figure 4.41. All the walls and elements with thermal mass are modeled with a two-port equivalent network. The exterior walls (East and North) are made of gypsum board with a layer of insulation, while the interior walls (South and West) are made of gypsum board with wood framing. The R-value for the exterior walls is 4.6 (m^2 °C/W), for ceiling is 5.6 (m^2 °C/W) and for interior walls is 0.65(m^2 °C/W). The east and west walls are 4.2m×2.5m and the south and north walls are 3.3m×2.5m. The floor area is 13.9m^2 and is made of plywood with a layer of gypsum board underneath. The zone temperature is controlled by means of a 1250W baseboard heater.

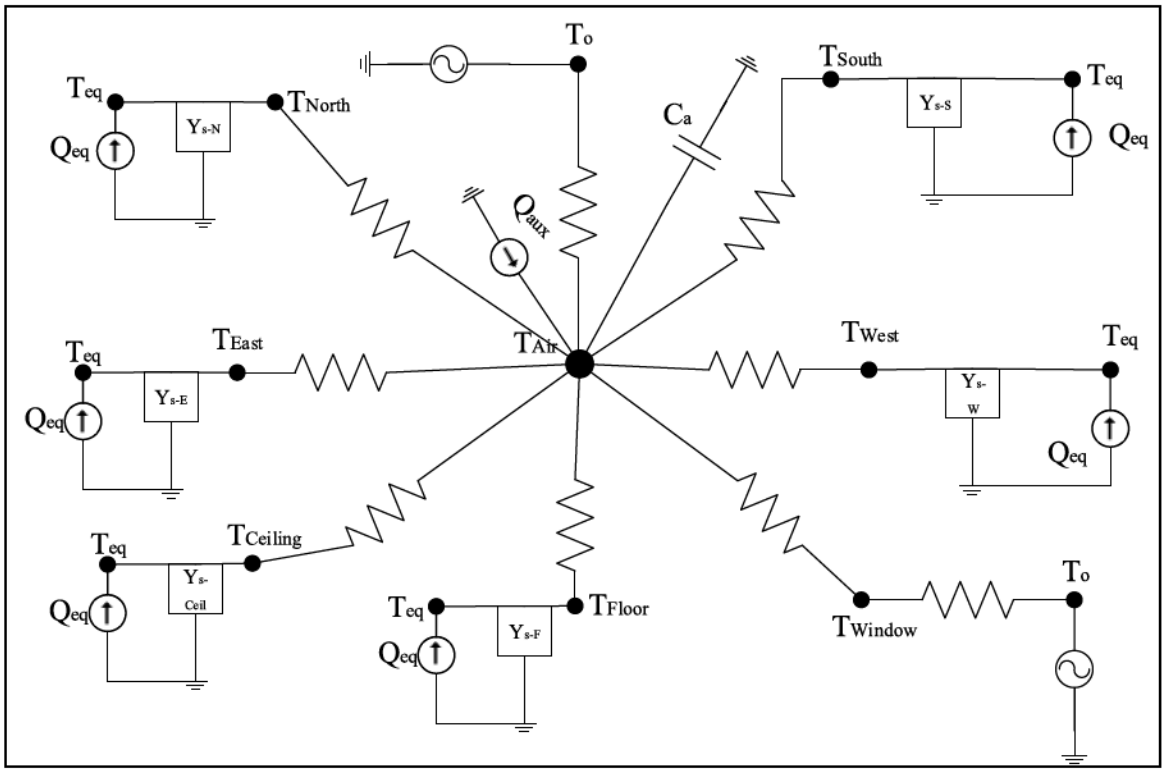

Figure 4.41. Thermal network for frequency domain model of the zone

Wall self-admittances and transfer-admittances are calculated using the formula introduced in Chapter 3. Here, a variable called zone admittance (Y_z) is introduced and defined by equation(4.6) (Athienitis 1994). Zone admittance is the effective dynamic U value of the zone. Several observation are obtained by studying the magnitude and phase angle of the zone admittance (or its invers which is called zone impedance $Z_z = Y_z^{-1}$) at important dominant harmonics that are up to 12-24 harmonics most of the time. Effective thermal storage and fluctuation in room temperature can be evaluated by studying the zone admittance in the dominant harmonics range:

$$Y_z = U_{inf} + \sum U_{wd} + \sum_i Y_{n,i} \tag{4.6}$$

where:

$\sum U_{wd}$ = summation of windows and doors U-values

$$\sum_i Y_{n,i} = Y_{self_{n,i}} \frac{U_i}{Y_{self_{n,i}} + U_i} \quad , \quad U_i = A_i h_i, \text{ i=surface, n=frequency}$$

all the self-admittances and other U-values are transferred to the air node. Then, by writing the energy balance equation (Athienitis 1994):

$$Y_z \cdot T_{Air} = \sum_i Q_{eq,i} + Q_{aux} \tag{4.7}$$

in the equation (4.7) Q_{aux} is the auxiliary load from a baseboard heater.

4.2.2 Effect of floor covering on zone thermal response

Air temperature inside the thermal zone can be determined using equation (4.7) is determined. Two floor coverings are considered here: tile and carpet. It is assumed that the base board heater has a sinusoidal profile with the dominant harmonic of 1 cycle/days as shown in Figure 4.42:

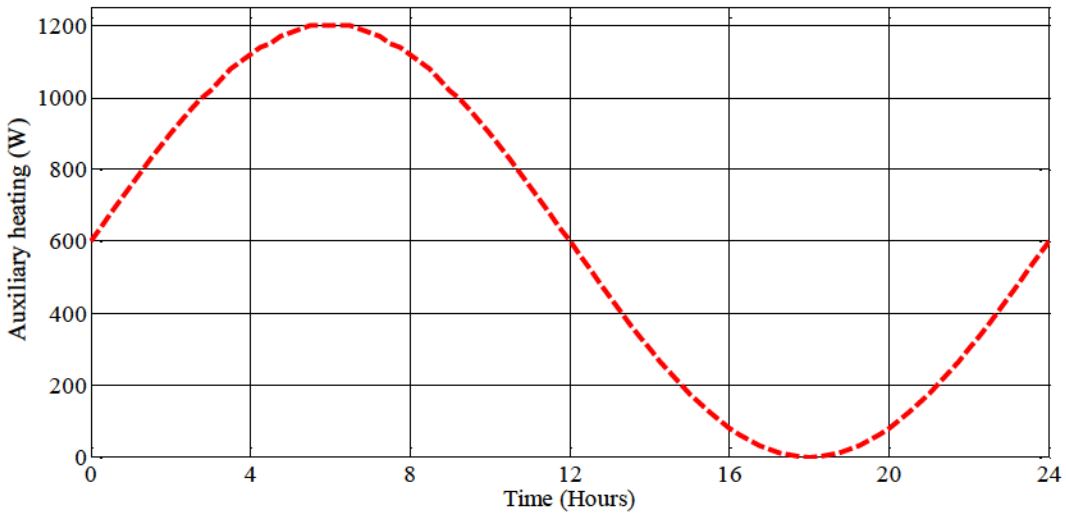

Figure 4.42. Sinusoidal profile for the baseboard heater

It is assumed that no other variables affect the air temperature. That is the auxiliary load from the baseboard heater is the only input that affects the air temperature of the zone. The delay in the response of the air temperature to the auxiliary source can be found by looking at the phase angle of the first harmonic for the zone impedance in each case:

$$\varphi(\omega_1)_{\text{carpet}} = -25.12° = -25.12° \frac{24\text{hrs}}{360°} = 1.67\text{hrs}$$

$$\varphi(\omega_1)_{\text{tile}} = -35.43° = -35.43° \frac{24\text{hrs}}{360°} = 2.36\text{hrs}$$

this is investigated by looking at time plot of the variables. Figure 4.43 shows the temperature profiles and the corresponding delay in each case:

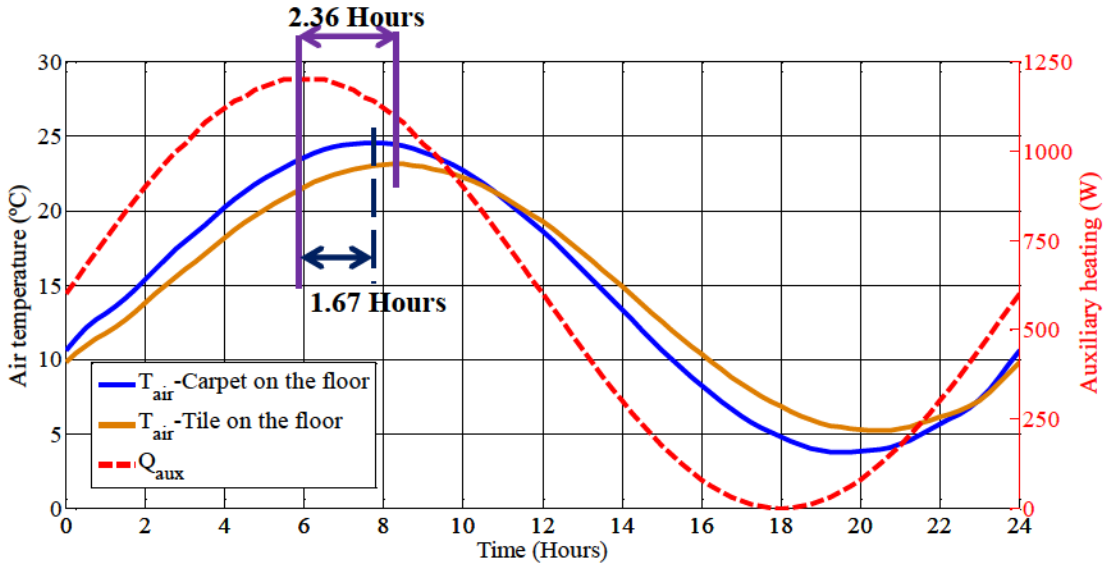

Figure 4.43. Room temperature response to a sinusoidal heat input

As can be observed there is a longer delay in the air temperature response when there is tile on the floor compared to carpet. This is mainly due to higher thermal mass of the tile compared to carpet as calculated in Table 9 :

Material	Density ρ (Kg/m^3)	Specific heat C_p (J/Kg.K)	Conductivity K (W/m.K)	Thickness L (mm)	Total thermal capacity $\rho \times C_p \times L \times A_{floor}$ (J/K)
Tile	2300	840	1.5	9.5	2.556×10^5
Carpet	200	1300	0.06	9.5	3.439×10^4

Table 9. Material properties of the floor coverings

this is an important consideration to take while designing control strategies and setpoint profiles for a house.

4.2.3 Analysis of zone impedance for effective thermal storage

Zone impedance is an important characteristic of a thermal zone. Here, an analysis of zone impedance for the effective thermal storage in the zone and thermal response of the zone is presented.

First, the effect of increasing the thermal mass of the building on the thermal response of the zone is considered. This is investigated by increasing the thickness of gypsum board twice as before. In this case the phase angle is: $-39.516° \approx 2.64$ hours.

Figure 4.44 shows the results:

Material	Density ρ (Kg/m^3)	Specific heat C_p (J/Kg.K)	Conductivity K (W/m.K)	Thickness L (mm)
Gypsum board	800	750	0.16	12.7

Table 10. Physical properties and thickness of gypsum board

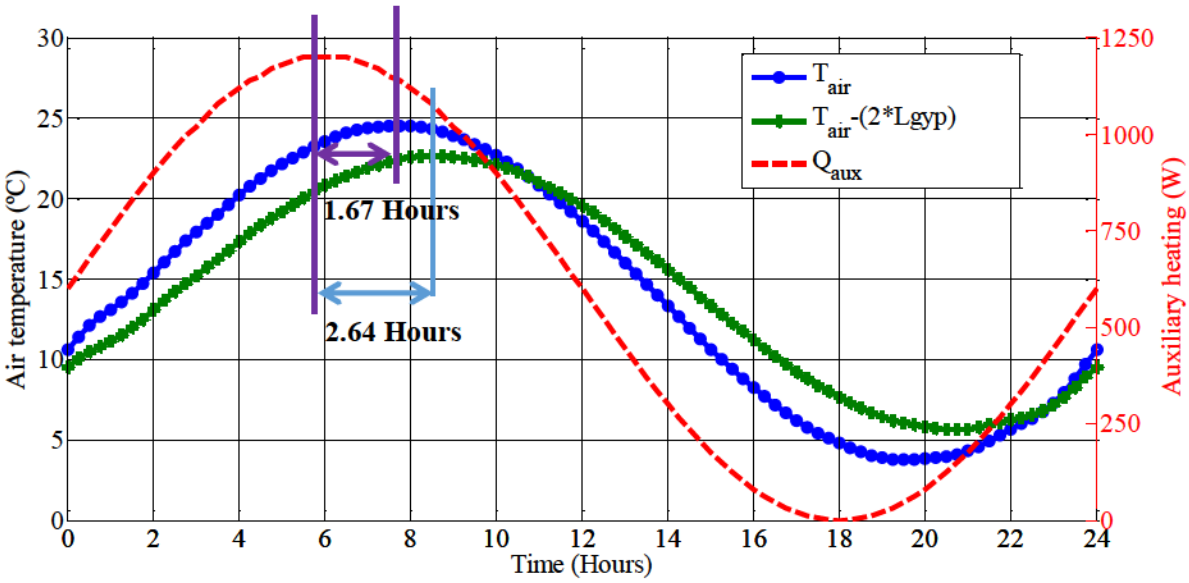

Figure 4.44. Effect of increasing thermal mass on the room thermal response

Another important parameter that affects the room thermal response is the conductivity (k) of the thermal mass of the walls. Since the main thermal mass here is gypsum board, the effect of increasing k value of the gypsum board is studied by evaluating the magnitude of the zone impedance at different frequencies. Figure 4.45 shows the magnitude plot for the zone impedance:

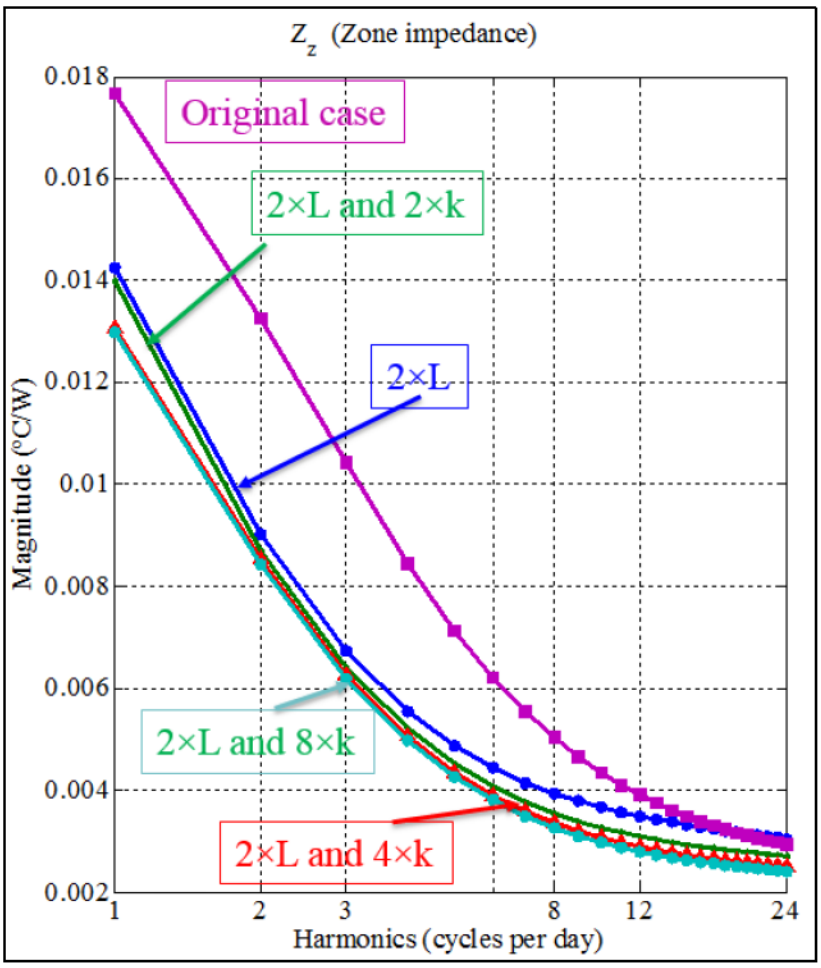

Figure 4.45. Magnitude of zone impedance considering different values of *k* and *L* for gypsum board

By increasing the thickness and conductivity, significant difference in the magnitude of zone impedance is observed. Table 11 shows the magnitude of the zone impedance for each case:

Change in properties	Magnitude of the 1st harmonic of the zone impedance (°C/W)
$L_{gyp}=2\times L_{initial}$, $k_{gyp}=k_{initial}$	0.0143
$L_{gyp}=2\times L_{initial}$, $k_{gyp}=2\times k_{initial}$	0.0139
$L_{gyp}=2\times L_{initial}$, $k_{gyp}=4\times k_{initial}$	0.0131
$L_{gyp}=2\times L_{initial}$, $k_{gyp}=8\times k_{initial}$	0.0129
$L_{gyp}=L_{initial}$, $k_{gyp}=k_{initial}$ (Original)	0.0177

Table 11. Magnitude of the 1st harmonic of the zone impedance considering different change in material properties

By increasing the thermal conductivity, magnitude of the zone impedance decreases. Also by increasing the thickness of the gypsum board, the magnitude of zone impedance decreases and since zone impedance, $Z_z = \frac{T_{Air}}{Q} \Rightarrow Q = \frac{T_{Air}}{Z_z}$, this means that for specific value of Q, there will be less fluctuations in air temperature of the zone. This was also shown in Figure 4.44.

Figure 4.45 also shows another important result. It should be pointed out that in residential buildings it is common to have a setpoint profile with a ramp of 1-2 hours. As an example a setpoint profile with a two-hour ramp in the morning and 1-hour ramp in the afternoon along with its amplitude at a frequency range are shown in Figure 4.46 :

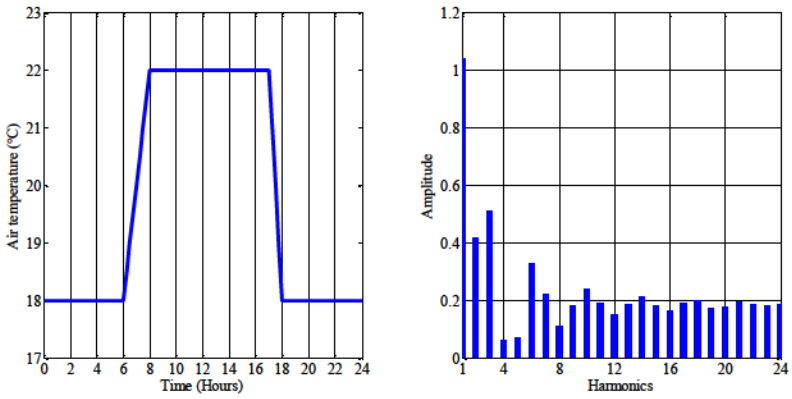

Figure 4.46. Air temperature setpoint profile with one hour (between 17 and 18 hours) and two hours (between 6 and 8 hours) ramp (left) and Amplitude spectrum at discrete harmonics (right)

The 1-2 hours setpoint change in a ramp form corresponds to the frequency range of 12-24 cycles per day. Thus, lower value of zone impedance (higher zone admittance) at this frequency range results in lower fluctuations in room air temperature which results in better thermal comfort and also that means more effective thermal storage and thermal

performance for the building. Thus, choosing the appropriate material is extremely important in enhancing the building's thermal performance.

4.2.4 Conclusion

A frequency domain model is used to study the effect of different materials on the zone air temperature response and zone thermal storage performance. Frequency domain modeling is shown to be very useful and informative for this type of analysis on the energy performance of the building. The design options can be evaluated by means of the frequency domain model on a relative basis without any need to perform simulation. The magnitude and phase angle of the zone impedance at a range of low and high frequencies are the important characteristics of a thermal zone and give the direction in choosing the right material for optimal thermal performance and energy storage in a thermal zone.

5 CONCLUSION

This thesis has investigated different time domain and frequency domain modeling approaches to be used in the development of model-based control strategies in buildings. The theoretical background behind each of the modeling approaches was explained.

The Environmental Chamber of Concordia University was used as a case study. A detailed frequency domain model was developed for the Environmental Chamber. In this model, both the distributed elements and lumped elements were considered. The model included radiant heat exchanges between the surfaces. The model had three inputs: solar gains, auxiliary load from air-handling unit (a finite-difference model was used to calculate the auxiliary load) and the exterior temperature. The main output of interest was the air temperature inside the building. The model was calibrated using experimental data. Building transfer functions were obtained at discrete frequencies from the model. A modified least-squares fitting technique was presented and used to obtain the continuous form of the building Laplace transfer functions. The delay in the response of the room temperature to the auxiliary loads was determined by studying the phase angle of the corresponding transfer function.

In the section 4.1.5, low-order RC circuit models (of 2^{nd}, 3^{rd} and 4^{th} order) were developed for the Environmental Chamber. The optimization routine applied to obtain equivalent circuit parameters was explained. The third-order model was used to study different temperature setpoint profiles and the corresponding peak load in each case. It was observed that low-order models optimized for a specific objective work satisfactorily and also give insight into the physical aspect of the building while, in detailed models

information may not be available about some details of the model and this may cause complexity in the studying control strategies.

In the section 4.2 a thermal zone in one of the Hydro-Québec's EHBE buildings was studied. A frequency domain model was used to investigate the effect of different floor coverings on the thermal response of the zone. Also by means of the zone impedance obtained from the frequency domain model, the effect of increasing the thickness and conductivity of materials on the thermal response of the zone and effective thermal storage in the zone was studied. It was concluded that choosing the material with high thermal capacity and conductivity results in less fluctuation in room air temperature and effective thermal storage in the zone.

Based on the models developed and the work done, the following conclusions can be drawn:

1. Frequency domain modeling techniques give a great deal of insight on the thermal characteristics of the building. By increasing the number of harmonics, the results have a better fit with reality. Frequency domain modeling is a convenient tool to do the steady-periodic analysis and to evaluate design options in buildings. Since the superposition rule is applied into the frequency domain model, the effect of different variables on the thermal response of a building can be studied separately. The delay in the response of an output to an input can be observed by studying the phase angle of their corresponding transfer function obtained from the frequency domain model. The magnitude of the zone impedance (or the zone admittance) is a substantial characteristic of a thermal zone in a desirable frequency range and different design options aimed at

enhancing the thermal performance of a building can be evaluated by studying the magnitude of the zone impedance and for this no simulation is required.

2. The modified least-squares complex curve fitting technique is an efficient tool to obtain low-order building Laplace transfer functions for the frequency range of interest.

3. Optimized low-order, grey-box RC circuit models can be used efficiently for control applications and it is important to choose the order of the model carefully considering the desired objective of the problem.

4. Models are the key tool for evaluating the effect of different control strategies and design options (such as different indoor thermal storage layers) in buildings. Control-oriented modeling is highly beneficial for design of control strategies in buildings. The developed model can be used in the future experiments.

5.1 Summary of contributions

The main contributions of this thesis are as follows:

- Comparison of two modeling approaches for a case study and verification of the models with experimental data.

- Application of frequency domain modeling to study the effect of floor coverings on the response of the zone to different loads and evaluation of the effect of choosing different materials (with different level of thermal storage) for a thermal zone on the thermal response of the zone and effective thermal storage in the zone by

studying the magnitude of the zone impedance at a desirable frequency range. The relevance of dominant harmonics to the thermal response of the zone to a sinusoidal heat input is evaluated and discussed and it is concluded that the magnitude of the zone impedance is an important characteristic of the zone and thus using the proper material in the zone enhances the thermal performance and thermal comfort (less fluctuations in the air temperature) in the zone.

- Modification of Levy method for complex curve fitting of transfer functions for the case of a known steady state response and use that to obtain low-order building Laplace transfer functions for a frequency range of interest.

- Development of low-order grey-box RC circuit models with parameter optimization which are suited for further MPC studies. The application of a low-order RC circuit model for a control study is demonstrated and a contribution is made to a collaborative project on the determination of an optimal thermostat setpoint profile by using the Environmental Chamber low-order (third-order) model developed under this thesis.

5.2 Recommendations for future work

- Study system identification of grey-box RC models with different objective functions. This study can be done for different buildings. Different objective functions can be defined based on the variables that can be measured empirically (for example electric power or heating/cooling load).

- Continue studies on model-based control strategies. Develop MPC model for buildings to optimize their energy efficiency.

- Study the application of different control strategies and different setpoint strategies by using a frequency domain model in a frequency range of interest.

- Find a general solution for the optimal setpoint trajectory during transition time that can be applied to residential buildings. This solution should be practical to be implemented easily.

- Study the integration and control of active solar systems in buildings by using control-oriented models. The optimized operation of active solar systems can be highly beneficial in reducing building energy consumption and in reducing peak loads.

REFERENCES

Allard, A. (2013). *A linear data-driven system identification methodology for an active/passive solar thermal storage system and application to a solar house*. master of applied science thesis,Concordia.

Antonopoulos, K. A. and Koronaki, E. (1998). *Apparent and effective thermal capacitance of buildings.* Energy 23(3): 183-192.

ASHRAE (2005). *ASHRAE Handbook Fundamentals*. Atlanta, GA.

Athienitis, A. K. and Santamouris, M. (2002). *Thermal analysis and design of passive solar buildings*. London, UK, James & James.

Athienitis, A.K. (1994). *Building thermal analysis*. Boston,MA, USA, MathSoft Inc.

Athienitis, A.K. (1997). *Investigation of thermal performance of a passive solar building with floor radiant heating.* Solar Energy 61(5): 337-345.

Athienitis, A.K., Chandrashekar, M. and Sullivan, H.F. (1985). *Modelling and analysis of thermal networks through subnetworks for multizone passive solar buildings.* Applied Mathematical Modeling.

Athienitis, A.K. and Chen, Y. (2000). *The effect of solar radiation on dynamic thermal performance of floor heating systems.* Solar Energy 69(3): 229-237.

Athienitis, A.K., Hollands, K.G.T. and Sullivan, H.F. (1986). *Anlytical model, sensitivity analysis and algorithm for temperature swings in direct gain rooms.* Solar Energy 36(4): 303-312.

Athienitis, A.K. and O'Brien, W., Eds. (2014). *Modelling, design and optimization of net-zero energy buildings,* Solar heating and cooling, Berlin Ernst, Wilhelm & Sohn 2014.

Athienitis, A.K., Stylianou, M. and Shou, J. (1990). *A methodology for building thermal dynamics studies and control applications.* ASHRAE Transactions 96(2).

Athienitis, A.K., Sullivan, H.F. and Hollands, K.G.T. (1987). *Discrete Fourier series models for building auxiliary energy loads based on network formulation techniques.* Solar Energy 39(3): 203-210.

Bacher, P. and Madsen, H. (2011). *Identifying suitable models for the heat dynamics of buildings.* Energy and Buildings 43(7): 1511-1522.

Borresen, B.A. (1981). *Thermal room models for control analysis.* ASHRAE Transactions 87: 251-261.

Braun, J. E. (1990). *Reducing energy costs and peak electrical demand through optimal control of building thermal storage.* ASHRAE Transactions 96(2): 876-887.

Braun, J. E. and Chaturvedi, N. (2011). *An inverse gray-box model for transient building load prediction.* HVAC & R Research 8(1): 73-99.

Braun, J. E. and Lee, K. (2006). *Assessment of demand limiting using building thermal mass in small commercial buildings.* ASHRAE Transactions 110(1).

Candanedo, J and Athienitis, A.K. (2010). *Simplified linear models for predictive control of advanced solar homes with passive and active thermal storage*. Internationl High Performance Building Conference, Purdue Univeristy ,West Lafayette, Indiana.

Candanedo, J., Allard, A. and Athienitis, A.K. (2011). *Predictive control of radiant floor heating and transmitted irradiance in a room with high solar gains*. ASHRAE Transactions 117(2): 652-665.

Candanedo, J., Dehkordi, V. and Lopez, Ph. (2013). *A control-oriented simplified building modeling strategy*. IBPSA Chambery , France.

Candanedo, J., Dehkordi, V. and Lopez, Ph. (2014). *A multi-level architecture to facilitate MPC implementation in commercial buildings: basic principles and case study*. esim 2014, Ottawa, Canada.

Carslaw, H.S. and Jaeger, J.C. (1959). *Conduction of heat in solids*, Oxford,:Clarendon Press.

Chen, Y., Athienitis, A.K. and Galal, Kh. (2013). *Frequency domain and finite-difference modeling of ventialted concrete slabs and comparison with field measurements: Part 1, modeling methodology*. Heat and Mass Transfer 66: 948-956.

Chen, Y., Athienitis, A.K. and Galal, Khaled (2012). *Thermal modeling for ventilated structural components using frequency response and finite difference methods and comparison with experimental data*. esim, Halifax, Nova Scotia.

Chen, Y. and Wang, Sh. (2005). *A new procedure for calculating response factors based on frequency domain regression method.* Thermal sciences 44(4): 382-392.

Crawley, D. B., Hand, J. W., Kummert, M. and Griffith, B. T. (2008). *Contrasting the capabilities of building energy performance simulation programs.* Building and Environment 43(4): 661-673.

Dewson, T., Day, B. and Irving, A. D. (1993). *Least squares parameter estimation of a reduced order thermal model of an experimental building.* Building and Environment 28(2): 127-137.

Duffie, J. A. and Beckman, W. A. (2006). Solar engineering of thermal processes. U.S.A, John Wiley & Sons, inc.

Edwards, D.K. (1981). *Radiation heat transfer notes*. New York, Hemisphere.

EnergyPlus.(2013).www.eere.energy.gov/buildings/energyplus.

Fournier, M. and Leduc, M. (2014). *Study of electrical heating setpoint modulation strategies for residential demand response*. esim 2014, IBPSA Canada National conference, Ottawa, ON.

Fraisse, G., Viardot, C., Lafabrie, O. and Achard, G. (2002). *Development of a simplified and accurate building model based on electrical analogy.* Energy and Buildings 34(10): 1017-1031.

Gordon, J.M., Ed. (2001). *Solar Energy: The State of the Art* London, James & James.

Gouda, M. , Danaher, S. and Underwood, C. P. (2002). *Building thermal model reduction using nonlinear constrained optimization*. Building and Environment 37(12): 1255-1265.

Haghighat, F. and Athienitis, A.K. (1988). *Comparison between time domain and frequency domain computer program for building energy analysis*. Computer-aided design 20(9): 525-532.

Haghighat, F., Fazio, P. and Zmeureanu, R. (1988). *A systematic approach for derivation of transfer function coefficients of buildings from experimental data* Energy and Buildings 12(2): 101-111.

Howell, J. R., Siegel, R. and Menguc, M.P. (2010). *Thermal Radiation Heat Transfer*, CRC Press.

Hydro-Québec, 2013, Annual report 2012, http://www.hydroquebec.com/publications

Incropera, F.P., DeWitt, D.P., Bergman, T.L. and Lavine, A.S. (2006). *Fundamentals of heat and mass transfer*, John Wiley & Sons Canada, Ltd.

Kim, D. and Braun, J. E. (2012). *Reduced-order building modeling for application to madel-based predictive control*. Fifth National Conference of IBPSA-USA, Madison, Winsconsin.

Kim, D., Braun, J. E., Zuo, W. and Wetter, M. (2013). *Comparison of building system modeling approaches for control system design*. IBPSA 2013, Chambéry, France.

Kimura, K. (1977). *Scientific basis for air-conditioning*. London, UK, Applied Science Publishers Ltd.

Kummert, M., André, Ph. and Argiriou, A. A. (2005). *Performance comparison of heating control strategies, combining simulation and experimental results*. Ninth International IBPSA Conference, Montreal, Canada.

Kummert, M., André, Ph. and Nicolas, J. (2001). *Optimal heating control in a passive solar commercial building*. Solar Energy 69: 103-116.

Lafont, A., 2013, MEEB TRNsys: calibration 2013 and inclusion of TRNFlow,

Lee, K. and Braun, J.E. (2008a). *Development of methods for determining demand-limiting setpoint trajectories in buildings using short-term measurements*. Building and Environment 43(10): 1755-1768.

Lee, K. and Braun, J.E. (2008b). *evaluation of methods for determining demand limiting setpoint trajectories in commercial buildings using short term measurements*. Building and Environment 43(10): 1769-1783.

Levy, E.C. (1959). *Complex curve fitting*. IRE Transactions on Automatic Control: 37-43.

Lin, Y., Middelkoop, T. and Barooah, P. (2012). *Issues in identification of control-oriented thermal models of zones in multi-zone buildings*. 51st IEEE Conference on Decision and Control, Maui, Hawaii, USA.

Ljung, L. (1987). *System identification; Theory for the user*. USA, Prentice-Hall.

Marszal, A.J., Heiselberg, P., Bourrelle, J.S., Musall, E., Voss, K., Sartori, I. and Napolitano, A. (2011). *Zero Energy Building – A review of definitions and calculation methodologies*. Energy and Buildings 43: 971-979.

Nise, N.S. (2011). *Control Systems Engineering*, Wiley.

Ogata, K. (2009). *Modern control engineering*, Prentice Hall.

Saberi Derakhtenjani, A., Athienitis , A. K., Candanedo, J. and Dehkordi, V. (2014). *Thermal response characterization of an Environmental Test Chamber by means of dynamic thermal models*. esim 2014, Ottawa, ON.

Shou, J.G. (1991). *A computer technique for heating control analysis and application to radiant heating*. Master of applied science Thesis,Concordia.

TRNSYS, Website.(2014).www.trnsys.com , http://sel.me.wisc.edu/trnsys/.

Vlach, J. and Singhal, K. (1983). *Computer methods for circuit analysis and design*. New York, Van Nostrand Reinhold Co.

Wang, Sh. and Chen, Y. (2002). *Transient heat flow calculation for multilayer constructions using a frequency-domain regression method.* Building and Environment 38: 45-61.

Wang, Sh. and Xu, X. (2006). *Parameter estimation of internal thermal mass of building dynamic models using genetic algorithm*. Energy Conversion & Management 47: 1921-1941.

Xu, X., Wang, Sh. and Chen, Y. (2007). *An improvement to frequency-domain regression method for calculating conduction transfer functions of building walls.* Applied Thermal Engineering 28(7): 661-667.

APPENDICES

Appendix A:

Example of Mathcad code for initial calculation of RC circuit parameters

CALCULATION OF PARAMETERS FOR SIMPLIFIED THIRD-ORDER RC CIRCUIT MODELS FOR ENVIRONMENTAL CHAMBER

3rd order RC circuit

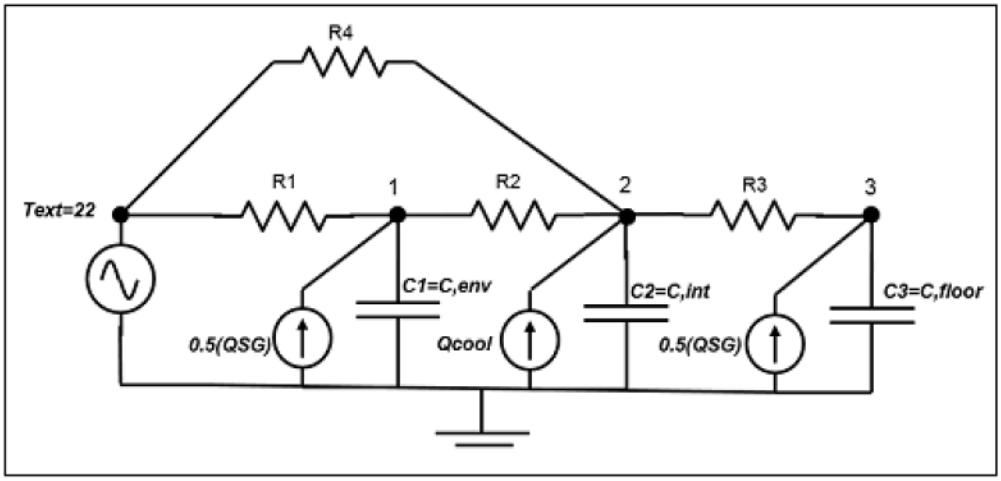

It should be noted that since Mathcad does not recognize temperature units (degC, K,..), it is considered that degC=1 , so then all the resistance units are calculated by Mathcad as 1/W instead of K/W and capacitances as J instead of J/K.

Surface areas:

$degC \equiv 1$

$Awin := 5.821m^2$ $Aw := 25.5m^2$ $Af := 39.16m^2$ $Abw := 31.35m^2$ $Asw := 63m^2$

$Vchamber := 280m^3$ $Aceiling := Af$

Air properties:

$cpair := 1000\frac{joule}{kg \cdot degC}$ $\rho air := 1.22\frac{kg}{m^3}$

Concrete Properties:

$c := 800 \frac{joule}{kg \cdot degC}$ $k := 0.51 \frac{watt}{m \cdot degC}$ $\rho := 1400 \frac{kg}{m^3}$

$Lf := 0.15m$ thickness ....

$Rcon := \frac{Lf}{k \cdot Af} = 7.511 \times 10^{-3} \frac{1}{W}$

$\alpha_{con} := 0.6$ solar absorbtance....

Wall properties(stainless steel) :

$Lw := 0.003m$ ..Thickness $\rho ssteel := 8000 \frac{kg}{m^3}$

$Cpw := 502 \frac{joule}{kg \cdot degC}$ $\alpha ssteel := 0.6$

Exteior surface heat transfer coefficient:

$ho := 5 \frac{watt}{m^2 \cdot degC}$

Interior surfaces heat transfer coefficients:

$hf := 8 \frac{watt}{m^2 \cdot degC}$ $hw := 11 \frac{watt}{m^2 \cdot degC}$

$hbw := hw$ $hsw := hw$

Envelope walls thermal resistances:

$Rinsulation := 5m^2 \cdot \frac{degC}{watt}$

Windows properties and thermal resistance:

$\tau win := 0.93$ $\alpha win := 0.07$ *..Transmittance and absorptance*

$Rwin := 0.34 m^2 \frac{degC}{W}$ So $uwin := \frac{1}{Rwin}$

$Uwin := uwin \cdot Awin = 17.121 W$

$$UTwin := \frac{1}{\frac{1}{Uwin} + \frac{1}{ho \cdot Awin} + \frac{1}{hw \cdot Awin}} = 9.226 W$$

Infiltration:

$ach := 0.245$ $Uinf := \frac{ach \cdot Vchamber}{3600 sec} \cdot (\rho air \cdot cpair)$

$Ueq := Uinf$ (This Ueq is to consider for infiltration and thermal bridges of the chamber components, thermal bridge is considered as a multiplier of the infiltration conductance.)

Proposed values for the circuit resistances:

$$R14 := \frac{\frac{1}{ho} + Rinsulation}{Aw + Abw + 2 \cdot Asw + Aceiling} = 0.023 \frac{1}{W}$$

$$R12 := \frac{1}{hw \cdot (Aw + Abw + 2 \cdot Asw + Aceiling)} = 4.095 \times 10^{-4} \frac{1}{W}$$

$$R23 := \frac{1}{hf \cdot Af} = 3.192 \times 10^{-3} \frac{1}{W}$$

$$R24 := \frac{1}{Ueq + UTwin} = 0.031 \frac{1}{W}$$

Proposed values for circuit capacitances:

$$Cenv := \rho ssteel \cdot Cpw \cdot Lw \cdot (Aw + Abw + 2 \cdot Asw + Aceiling) = 1.783 \times 10^{6}\, J$$

$$C1 := Cenv$$

$$Cair := cpair \cdot \rho air \cdot Vchamber = 3.416 \times 10^{5}\, J$$

$$C2 := Cair$$

$$Cfloor := \rho \cdot c \cdot Lf \cdot Af = 6.579 \times 10^{6}\, J$$

$$C3 := Cfloor$$

Appendix B:

View factor correlations

This section presents the correlations used to calculate view factors between the surfaces of the Environmental Chamber. The following pictures and formula are taken from the book "Thermal Radiation Heat Transfer" by Howell et al (2010). The pictures and formulas are also available online at:

http://www.thermalradiation.net/tablecon.html

1. Two rectangles in two perpendicular planes.

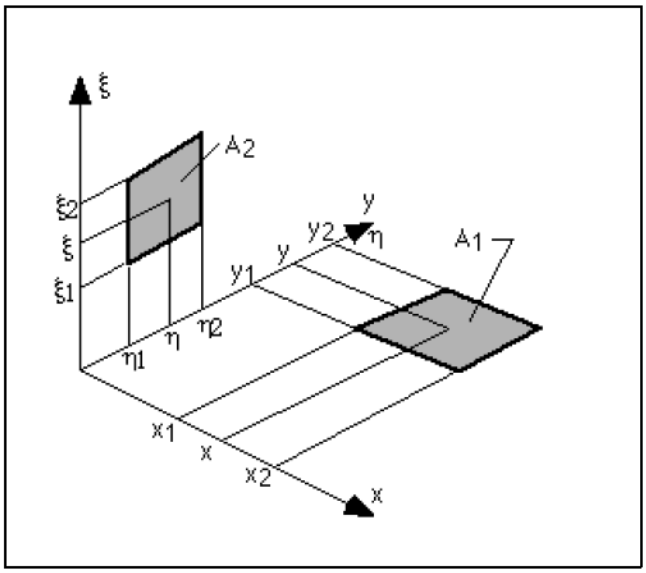

$$F_{1-2} = \frac{1}{(x_2 - x_1)(y_2 - y_1)} \sum_{l=1}^{2} \sum_{k=1}^{2} \sum_{j=1}^{2} \sum_{i=1}^{2} \left[(-1)^{(i+j+k+l)} G(x_i, y_j, \eta_k, \xi_l) \right]$$

$$G = \frac{1}{2\pi} \left\{ (y-\eta)(x^2+\xi^2)^{1/2} \tan^{-1}(K) - \frac{1}{4} \left[(x^2+\xi^2) \ln(1+K^2) - (y-\eta)^2 \ln\left(1+\frac{1}{K^2}\right) \right] \right\}$$

where: $K \equiv (y-\eta)/(x^2+\xi^2)^{1/2}$

Note that the equation above is not valid if the two surfaces share a common edge. The above correlation was used to calculate view factors from surfaces to window

2. Two rectangles in parallel planes.

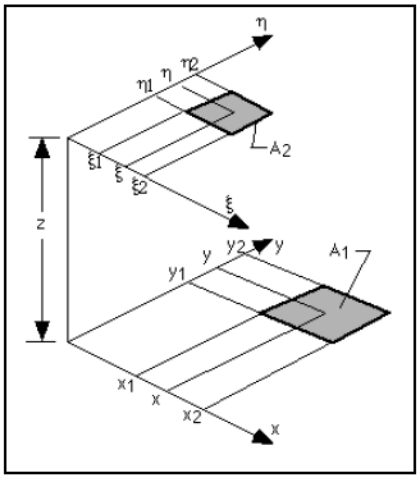

$$F_{1-2} = \frac{1}{(x_2 - x_1)(y_2 - y_1)} \sum_{l=1}^{2} \sum_{k=1}^{2} \sum_{j=1}^{2} \sum_{i=1}^{2} (-1)^{(i+j+k+l)} G(x_i, y_j, \eta_k, \xi_l)$$

$$G = \frac{1}{2\pi} \left(\begin{array}{l} (y-\eta)\left[(x-\xi)^2 + z^2\right]^{1/2} \tan^{-1}\left\{ \dfrac{y-\eta}{\left[(x-\xi)^2 + z^2\right]^{1/2}} \right\} \\ \quad + (x-\xi)\left[(y-\eta)^2 + z^2\right]^{1/2} \tan^{-1}\left\{ \dfrac{x-\xi}{\left[(y-\eta)^2 + z^2\right]^{1/2}} \right\} \\ \quad - \dfrac{z^2}{2} \ln\left[(x-\xi)^2 + (y-\eta)^2 + z^2\right] \end{array} \right)$$

3. Two rectangles having one common edge and at an angle of 90° to eachother.

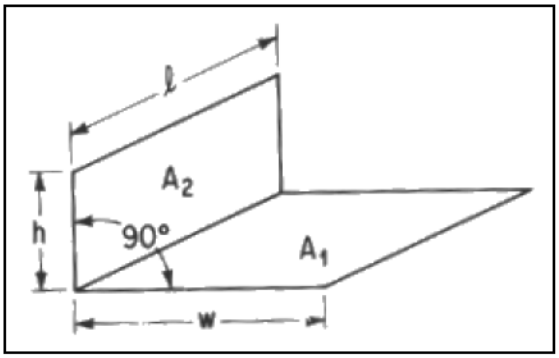

$$F_{1-2} = \frac{1}{W\pi}\left(W\tan^{-1}\frac{1}{W} + H\tan^{-1}\frac{1}{H} - \sqrt{H^2+W^2}\tan^{-1}\sqrt{\frac{1}{H^2+W^2}}\right.$$

$$\left. + \frac{1}{4}\ln\left\{\frac{\left(1+W^2\right)\left(1+H^2\right)}{1+W^2+H^2}\left[\frac{W^2\left(1+W^2+H^2\right)}{\left(1+W^2\right)\left(W^2+H^2\right)}\right]^{W^2}\left[\frac{H^2\left(1+H^2+W^2\right)}{\left(1+H^2\right)\left(H^2+W^2\right)}\right]^{H^2}\right\}\right)$$

Appendix C:

Admittance transfer function

Let's consider a slab and assume one dimensional transient heat conduction, with uniform properties, k (conductivity), ρ (density), c (specific heat), the 1-D heat conduction equation is (Athienitis and Santamouris 2002):

$$\alpha \frac{\partial^2 T}{\partial x^2} = \frac{\partial T}{\partial t}$$

Where thermal diffusivity $\alpha = k / \rho c$.

Then by applying Laplace transform:

$$\alpha \cdot \frac{\partial^2 T}{\partial x^2} = sT$$

Now our equation has been transformed from partial differential equation into an ordinary differential equation. By solving the equation for *T(x)* with keeping "*s*" as a constant and initial condition as $T(x, t=0) = 0$:

$$T(x,s) = c_1 e^{\gamma x} + c_2 e^{-\gamma x}, \qquad \text{where} \quad \gamma = \sqrt{s/\alpha}$$

The above equation can be written as:

$$T(x,s) = M\cosh(\gamma x) + N\sinh(\gamma \mathrm{x})$$

The heat flux can be calculated by:

$$q = -k\,dT/dx \;\Rightarrow\; \mathrm{q}(x,s) = -Mk\gamma\sinh(\gamma x) - Nk\gamma\cosh(\gamma \mathrm{x})$$

Considering the thickness *l* for the wall, then at the each surface temperatures and heat fluxes are obtained as:

$T_1(x=0,s) = M$

$$q_1(x=0,s) = -Nk\gamma$$
$$T_2(x=l,s) = M\cosh(\gamma L) + N\sinh(\gamma L)$$
$$q_2(x=l,s) = -\left[Mk\gamma\sinh(\gamma L) + N\cosh(\gamma \text{ xL})\right]$$

The above equations can be written in the form of the so-called cascade matrix form (Carslaw and Jaeger 1959) as:

$$\begin{bmatrix} T_1 \\ q_1 \end{bmatrix} = \begin{bmatrix} \cosh(\gamma L) & \sinh(\gamma L)/k\gamma \\ k\gamma\sinh(\gamma L) & \cosh(\gamma L) \end{bmatrix} \cdot \begin{bmatrix} T_2 \\ -q_2 \end{bmatrix}$$

In the equation above it was assumed that q is positive into the slab. k is the thermal conductivity, γ is equal to $\sqrt{s/\alpha}$, while s is the Laplace transform and α is thermal diffusivity. For frequency domain calculations, $s = j\omega$, where $j = \sqrt{-1}$ and $\omega = 2\pi/P$. To perform diurnal (day-length) analysis, P is set to 86400 sec.

A wall usually consists of more than one layer. If that is the case, an equivalent cascade matrix can be obtained by multiplying the cascade matrices for each of the layers. Thus, all the intermediate nodes will be eliminated without any necessary discretization:

$$\begin{bmatrix} T_1 \\ q_1 \end{bmatrix} = \begin{bmatrix} A_1 & B_1 \\ C_1 & D_1 \end{bmatrix} \cdot \begin{bmatrix} A_2 & B_2 \\ C_2 & D_2 \end{bmatrix} \cdots \begin{bmatrix} A_N & B_N \\ C_N & D_N \end{bmatrix} \cdot \begin{bmatrix} T_N \\ -q_N \end{bmatrix}$$

And the wall effective cascade matrix is presented as:

$$\begin{bmatrix} T_1 \\ q_1 \end{bmatrix} = \begin{bmatrix} \overline{A} & \overline{B} \\ \overline{C} & \overline{D} \end{bmatrix} \cdot \begin{bmatrix} T_N \\ -q_N \end{bmatrix}$$

For example if a wall has a layer of insulation with negligible thermal capacitance on the external side, the cascade matrix for the layer of insulation with total conductance equal to u is:

$$\begin{bmatrix} 1 & 1/u \\ 0 & 1 \end{bmatrix}$$

Now combining this conductance the with exterior air film, the total wall cascade matrix is obtained as:

$$\begin{bmatrix} T_1 \\ q_1 \end{bmatrix} = \underbrace{\begin{bmatrix} D & B \\ C & D \end{bmatrix}}_{\substack{\text{Thermal mass} \\ \text{cascade matrix}}} \cdot \underbrace{\begin{bmatrix} 1 & 1/u_0 \\ 0 & 1 \end{bmatrix}}_{\substack{\text{insulation and air} \\ \text{cascade matrix}}} \cdot \begin{bmatrix} T_2 \\ -q_2 \end{bmatrix} = \underbrace{\begin{bmatrix} D & D/u_0 + B \\ C & C/u_0 + D \end{bmatrix}}_{\text{wall cascade matrix}} \cdot \begin{bmatrix} T_2 \\ -q_2 \end{bmatrix}$$

From the above matrix equation, admittance transfer functions are obtained. As stated by (Athienitis and Santamouris 2002): "By studying the magnitude and phase angle of the admittance transfer functions, significant insight into the thermal behavior of the wall is obtained.". For inputs with more than one harmonics, the total response is obtained by applying superposition to the response harmonics. The thermal admittance of the wall is useful for the analysis of the effects of cyclic variations in solar radiation, outdoor temperature and other heat flows under steady periodic conditions.

There are two admittance transfer functions of interest, self-admittance, Y_{self}, relating the effect of a heat source at a surface to the temperature of the surface and , the transfer admittance, Y_{transfer}, relating the effect of an outdoor temperature to the resulting heat flux at the interior surface. The equivalent thermal network for a wall using these transfer functions is shown on Figure 1. The procedure to obtain these two transfer functions is described below.

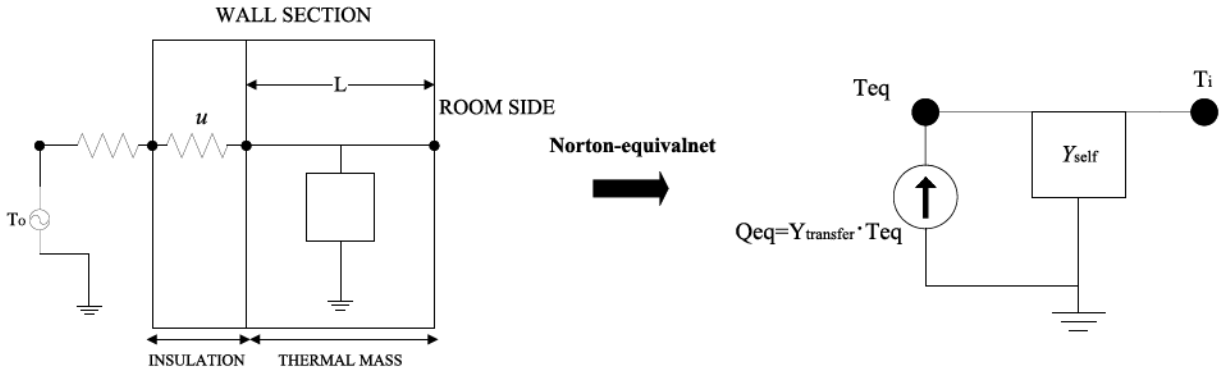

Based on the equation described, the cascade form of the conduction equation for the wall considering an exterior layer of insulation, is:

$$\begin{bmatrix} T_{\text{surfac}} \\ q_{\text{surface}} \end{bmatrix} = \begin{bmatrix} D & B \\ C & D \end{bmatrix} \cdot \begin{bmatrix} T_{\text{o}} \\ -q_{\text{o}} \end{bmatrix}$$

Where:

$T_{\text{surface}} = \text{surface temperature}$, $q_{\text{surface}} =$ surface heat source

$T_{\text{o}} = \text{outside temperature}$, $q_{\text{o}} =$ heat source on the exterior surface

,

$D = \cosh(\gamma \, \text{x})$

$B = \sinh(\gamma \, \text{x}) / k\gamma$

$c = k\gamma \sinh(\gamma x)$

After multiplication of matrices, by setting $T_{surface} = 0$ (short-circuit), the Norton-equivalent source is obtained as:

$$Q_{\text{eq}} = -Y_{\text{transfer}} \cdot T_{\text{o}}$$

Where the transfer admittance is given as (Kimura 1977) :

$$Y_{\text{transfer}} = \frac{-A}{\frac{A}{U}\cosh(\gamma l) + \frac{\sinh(\gamma l)}{k\gamma}}$$

Now, to obtain Y_{self}, we set $T_o = 0$ and will obtain the Y_{self} as:

$$Y_{\text{self}} = \frac{U + Ak\gamma \tanh(\gamma l)}{\frac{U}{Ak\gamma}\tanh(\gamma l) + 1}$$

Where A and l are respectively the area and the thickness of the wall. Generally, when there are i surfaces inside a room:

$$Y_{\text{self,i}} = \frac{U_{\text{i}} + A_{\text{i}} k_{\text{i}}\gamma_{\text{i}} \tanh(\gamma_{\text{i}} l_{\text{i}})}{\frac{U_{\text{i}}}{A_{\text{i}} k_{\text{i}}\gamma_{\text{i}}}\tanh(\gamma_{\text{i}} l_{\text{i}}) + 1}$$

$$Y_{\text{transfer,i}} = \frac{-A_{\text{i}}}{\frac{A_{\text{i}}}{U_{\text{i}}}\cosh(\gamma_{\text{i}} l_{\text{i}}) + \frac{\sinh(\gamma_{\text{i}} l_{\text{i}})}{k_{\text{i}}\gamma_{\text{i}}}}$$

It should be noted in the case that there is no thermal mass in the wall, $Y_{\text{self}} = -Y_{\text{transfer}} = U_o$

Appendix D:

Optimization algorithm

MATLAB optimization toolbox was used to run an optimization to find the equivalent low-order RC circuit parameters. The function "fminsearch" in the optimization toolbox uses the Nelder-Mead simplex algorithm. This algorithm is also known as the simplex algorithm.

If n is the length of x, a simplex in n-dimensional space is characterized by the n+1 distinct vectors that are its vertices. In two-space, a simplex is a triangle; in three-space, it is a pyramid. At each step of the search, a new point in or near the current simplex is generated. The function value at the new point is compared with the function's values at the vertices of the simplex and, usually, one of the vertices is replaced by the new point, giving a new simplex. This step is repeated until the diameter of the simplex is less than the specified tolerance. The figures below are taken from Wikipedia website:

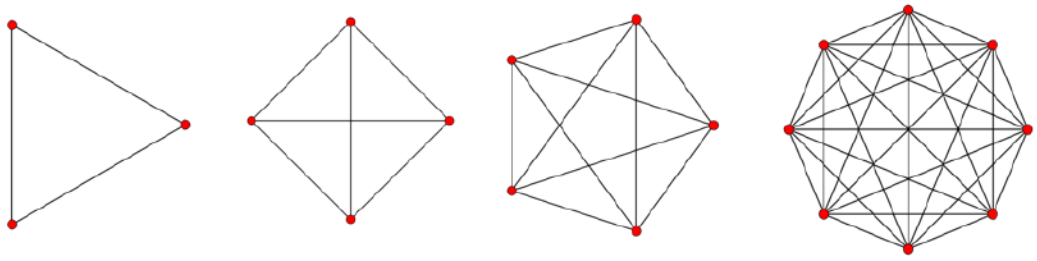

For more detailed information, the reader is referred to "fminsearch" documentation: http://www.mathworks.com/help/matlab/ref/fminsearch.html.